

INFORMATION TO USERS

This manuscript has been reproduced from the microfilm master. UMI films the text directly from the original or copy submitted. Thus, some thesis and dissertation copies are in typewriter face, while others may be from any type of computer printer.

The quality of this reproduction is dependent upon the quality of the copy submitted. Broken or indistinct print, colored or poor quality illustrations and photographs, print bleedthrough, substandard margins, and improper alignment can adversely affect reproduction.

In the unlikely event that the author did not send UMI a complete manuscript and there are missing pages, these will be noted. Also, if unauthorized copyright material had to be removed, a note will indicate the deletion.

Oversize materials (e.g., maps, drawings, charts) are reproduced by sectioning the original, beginning at the upper left-hand corner and continuing from left to right in equal sections with small overlaps. Each original is also photographed in one exposure and is included in reduced form at the back of the book.

Photographs included in the original manuscript have been reproduced xerographically in this copy. Higher quality 6" x 9" black and white photographic prints are available for any photographs or illustrations appearing in this copy for an additional charge. Contact UMI directly to order.

UMI

A Bell & Howell Information Company
300 North Zeeb Road, Ann Arbor MI 48106-1346 USA
313/761-4700 800/521-0600

The University of Alberta

Data acquisition and analysis system for power electronic circuits

by

Emanuel Bocancea



A thesis

submitted to the Faculty of Graduate Studies and Research in partial

fulfillment of the requirements for the degree of

Master of Science

Department of Electrical Engineering

Edmonton, Alberta

Fall 1997



National Library
of Canada

Acquisitions and
Bibliographic Services

395 Wellington Street
Ottawa ON K1A 0N4
Canada

Bibliothèque nationale
du Canada

Acquisitions et
services bibliographiques

395, rue Wellington
Ottawa ON K1A 0N4
Canada

Your file *Votre référence*

Our file *Notre référence*

The author has granted a non-exclusive licence allowing the National Library of Canada to reproduce, loan, distribute or sell copies of this thesis in microform, paper or electronic formats.

The author retains ownership of the copyright in this thesis. Neither the thesis nor substantial extracts from it may be printed or otherwise reproduced without the author's permission.

L'auteur a accordé une licence non exclusive permettant à la Bibliothèque nationale du Canada de reproduire, prêter, distribuer ou vendre des copies de cette thèse sous la forme de microfiche/film, de reproduction sur papier ou sur format électronique.

L'auteur conserve la propriété du droit d'auteur qui protège cette thèse. Ni la thèse ni des extraits substantiels de celle-ci ne doivent être imprimés ou autrement reproduits sans son autorisation.

0-612-22575-5

University of Alberta

RELEASE FORM

Name of author: Emanuel Bocancea

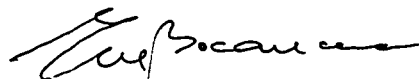
Title of thesis: Data acquisition and analysis system for
power electronic circuits.

Degree: Master of Science

Year this degree is granted: 1997

Permission is hereby granted to the University of Alberta Library to reproduce single copies of this thesis and to lend or sell such copies for private, scholarly or scientific research purposes only.

The author reserves other publication rights, and neither the thesis nor extensive extracts from it may be printed or otherwise reproduced without the author's written permission.



9042 - 50 Street
Edmonton, Alberta
T5R 1E9

Date: July 03, 1997

University of Alberta

Faculty of Graduate Studies and Research

The undersigned certify that they have read, and recommend to the Faculty of Graduate Studies and Research for acceptance, a thesis entitled "Data acquisition and analysis system for power electronics circuits" submitted by Emanuel Bocancea in partial fulfillment of the requirements for the degree of Master of Science

John C. Salmon

Dr. John C. Salmon

Don Koval

Dr. Don Koval

Ken R. Fyfe

Dr. Ken R. Fyfe

Date: 30/6/97

To my parents Gheorghe and Sânziana Bocancea

Abstract

A LabVIEW based virtual instrument for data acquisition and analysis for power electronic circuits is presented. The LabVIEW software defining this instrument is described in detail with reference to the instrument front panel and the program block diagram. The data acquisition system consists of a Power Macintosh 7100/66 running LabVIEW4 with an NI-488 card controlling a Tektronix TDS 420 oscilloscope via General Purpose Interface Bus (GPIB). Four channels of data can be acquired and saved in Matlab or Spreadsheet format. The program performs harmonic analysis and power factors calculations associated with power electronic circuits.

As an introduction to the subject harmonics, the major power system disturbances are briefly described. The "classical" harmonic producers are discussed and diode bridge rectifiers are reviewed with emphasis on current distortion and power factors.

The data acquisition system is employed in experiments including different rectifier circuits, voltage source inverter drives and novel topologies of rectifiers with resonant harmonic correction units. The performance of the virtual instrument is demonstrated by plots of acquired data, harmonic spectrums and calculated quality factors.

Acknowledgments

I would like to record out appreciation to:

- Dr. John C. Salmon for his assistance and advice I have received throughout my work
- Michael D. Markey from Lockheed Martin Astro Space for his kindness and patience with all my LabVIEW related questions
- My office fellow Rajat Bhargava who was an ideal partner in many projects
- My friends Carin and David Thomas for their review of the text and constant encouragement all the way long
- My loving daughters Emanuela and Bianca for their understanding for my long working hours
- My loving wife Romela who inspired me and overloaded herself to ease my work

Table of Contents

List of Tables

List of Figures

List of Abbreviations

1	Introduction	1
1.1	Power measurement methods.....	2
1.2	Digital filtering and Fast Fourier Transform.....	3
1.3	Digital technique for power measurement.....	6
1.4	Organization of the thesis.....	9
2	Introduction to Power Quality	14
2.1	Introduction.....	14
2.2	Power Quality Concept and Definition.....	15
2.3	Types of Electrical Disturbances.....	16
2.3.1	Voltage Disturbances.....	17
2.3.2	Interruptions.....	22
2.3.3	Frequency Variations.....	23
2.3.4	Voltage imbalance.....	24
2.3.5	Electrical Noise.....	24
2.3.6	Harmonics.....	26
3	Harmonics sources	27
3.1	Introduction.....	27
3.2	Transformer associated harmonics.....	28

3.2.1	Magnetization non-linearities.....	28
3.2.2	Symmetrical overexcitation.....	29
3.2.3	Inrush current harmonics.....	30
3.3	Rotating Machine Harmonics.....	31
3.4	Arc-furnaces Harmonics.....	32
3.5	Fluorescent Lighting Harmonics.....	33
4	Solid-state power conversion harmonics and performance factors	34
4.1	Introduction.....	34
4.2	Single-phase diode bridge rectifier.....	35
4.3	Three-phase full-bridge rectifier.....	40
4.4	Harmonic correction circuits.....	47
4.4.1	Current harmonics and power factor.....	47
4.4.2	Harmonic Standards and Recommended Practices.....	49
4.4.3	Improved utility interface.....	52
5	Data Acquisition Viturtual Instrument	57
5.1	The digitizing oscilloscope.....	58
5.2	LabVIEW overview.....	60
5.3	DAQ and analysis system.....	62
6	Experimental Results - Rectifier Circuits	73
6.1	Single phase diode bridge rectifier.....	73
6.1.1	Single-phase diode bridge rectifier with C output filter.....	74
6.1.2	Single-phase diode bridge rectifier with LC filter.....	76
6.2	Three-phase diode bridge rectifier.....	78

6.2.1	Three-phase diode bridge rectifier with C filter.....	79
6.2.2	Three-phase diode bridge rectifier with LC filter.....	81
6.3	12-Pulse diode rectifier.....	83
7	Data Acquisition from Variable Speed Drives	90
7.1	Square Wave Inverter Drive.....	92
7.1.1	VSD front-end: Semi-controlled Rectifier.....	92
7.1.2	VSD output stage: Square Wave Inverter.....	98
7.2	PWM Inverter Drive.....	101
7.2.1	Drive front-end: Diode Rectifier.....	102
7.2.2	PWM inverter.....	105
8	Passive Circuits for Harmonic Correction	111
8.1	Harmonic Correction for 3-phase Diode Bridge Rectifiers.....	111
8.2	Harmonic Correction for 12-Pulse Rectifiers.....	115
9	Conclusions	121
9.1	Author's contribution and general conclusions.....	121
9.2	Suggestions for further work.....	123
	Bibliography	125
Appendix A:	Example of Harmonic Current Limits.....	130
Appendix B:	LabVIEW environment and tools.....	132
Appendix C:	Data Acquisition and Analysis Program.....	140
Appendix D:	Virtual Instrument Documentation.....	161
Appendix E:	Electrical Machines Nameplate Data.....	174

List of Tables

Table 7.1	PWM inverter output data - VI readings.....	108
Table 7.2	PWM inverter output data- Fluke39 meter readings.....	108

List of Figures

2.1	Example of impulsive transients.....	18
2.2	Example of oscillatory transient.....	18
2.3	Example of voltage swell.....	20
2.4	Example of undervoltage.....	21
2.5	Example of voltage sag.....	22
2.6	Frequency variation.....	23
3.1	Transformer magnetization (hysteresis curve, flux and magnetization current waveforms).....	29
3.2	Flux density in a transformer at energization with both remnant flux B_R and zero remnant flux density.....	30
4.1	Single-phase diode bridge rectifier with capacitor output filter.....	36
4.2	Single-phase diode bridge rectifier waveforms (C filter).....	36
4.3	Three-phase diode-bridge rectifier with LC dc-link filter.....	41
4.4	The influence of the dc-link inductor size on the dc output voltage [14].....	42
4.5	Effect of L_d on power factor [14].....	43
4.6	Input V_{LL} and I_S for three-phase diode bridge with C filter and R load.....	44
4.7	Input V_{LL} and I_S for three-phase diode bridge with LC filter and R load.....	44
4.8	Three phase rectifiers and input waveforms: (a) diode bridge with a dc inductor; (b) diode bridge with ac inductor.....	46
4.9	Block diagram of utility interface.....	48
4.10	DC-link boost converter used as harmonic filter and PF correction unit.....	53
4.11	Three-phase diode bridge utility interface using a 3-phase Y-switch network with resonant capacitors for harmonic correction.....	54
4.12	SPICE Simulated waveforms for the resonant mode 3-phase Y-switch rectifier:.....	55
5.1	Developed data acquisition and analysis system: general arrangement.....	57
5.2	Oscilloscope sample averaging in High Resolution mode.....	59
5.3	Virtual Instrument Front Panel.....	63
5.4	Virtual Instrument Block Diagram.....	64

5.4	Virtual Instrument Block Diagram.....	64
5.5	Virtual Instrument's Hierarchy.....	65
5.6	Data acquisition sequence structure frames.....	68
5.7	Three-phase circuit diagram for power calculation.....	69
6.1	Voltage and current scale constants associated with data acquisition from single phase diode rectifier (virtual instrument front panel controls and indicators).....	74
6.2	Single-phase diode bridge rectifier with C dc-link filter and R load.....	75
6.3	Single-phase diode bridge rectifier with LC dc-link filter and R load.....	77
6.4	Three-phase diode bridge rectifier with C dc-link filter and R load.....	80
6.5	Three-phase diode bridge rectifier with LC dc-link filter and R load.....	82
6.6	Block diagram of a 12-pulse rectifier with L dc-link filter.....	83
6.7	12-pulse diode bridge rectifier with L dc-link filter and R load.....	85
6.8	Δ/Δ transformer of the 12-pulse rectifier.....	86
6.9	Δ/Y transformer of the 12-pulse rectifier.....	87
6.10	12-pulse rectifier output voltage (V_{dc}) and input line-line voltage (V_{ab}) acquired at 250V/div.....	88
7.1	Block-diagram of variable frequency drive for induction motor applications.	90
7.2	VSD experimental setup for data acquisition and analysis.....	91
7.3	Square wave inverter drive with semi-converter input stage.....	92
7.4	Square wave inverter drive input power and performance factors for 60Hz output frequency.....	93
7.5	Square wave inverter drive input-stage waveforms at 60 Hz output frequency.....	93
7.6	Harmonic spectrum of semi-converter input current for 60 Hz drive output	94
7.7	Square wave inverter drive input at 40 Hz output frequency.....	95
7.8	Square wave inverter drive input at 20 Hz output frequency.....	97
7.9	Square wave inverter output waveforms.....	99
7.10	Harmonic spectrum of the square wave inverter output waveforms	

7.11	PWM inverter drive.....	102
7.12	PWM drive input current, phase voltage and dc-link voltage.....	103
7.13	Input current harmonic spectrum and THD _i of the PWM drive	104
7.14	Virtual instrument data acquisition based calculations: PWM drive input line-line voltage, input current, input apparent power, input active power, total power factor and fundamental power factor.....	105
7.15	PWM drive output current, output phase voltage and line-line voltage.....	106
7.16	60 Hz PWM inverter drive output.....	107
8.1	Resonant harmonic correction circuit for 3-phase diode bridge.....	112
8.2	Diode bridge with harmonic correction unit.....	113
8.3	Harmonic correction unit waveforms.....	114
8.4	12-pulse rectifier with resonant-mode harmonic correction circuits.....	116
8.5	Input waveforms and harmonic spectrum for the 12-pulse rectifier with harmonic correction unit.....	117
8.6	Resonant action of the Δ connected capacitors of the Δ - Δ -fed rectifier.....	118
8.7	Resonant action of the Δ connected capacitors of the Δ -Y-fed rectifier.....	119
B.1	Front panel toolbar.....	133
B.2	Example of front panel: ChooseFileType.VI.....	134
B.3	Block diagram of ChooseFileType.VI.....	135
B.4	Icon of ChooseFileType.VI.....	136
B.5	LabVIEW 4.0 Tools Palette.....	137
B.6	LabVIEW floating palettes.....	138
C.1	The graph and its legend.....	141
C.2	Main front panel controls.....	141
C.3	Data acquisition indicators.....	142

C.4	Channels controls and indicators.....	143
C.5	Scale-prompt front panels.....	144
C.6	Initialization subVI.....	145
C.7	Data Acquisition: Frame 0 with True set Case structures.....	147
C.8	Frame 1: channel 1 data acquisition and constants display.....	149
C.9	Standard probe and voltage probe Case structure in Fig. C.6.....	150
C.10	Frame 5: Writing data to the Graph.....	151
C.11	Frame 6: Save Data subroutine- Spreadsheet format.....	153
C.12	Front panel for ChooseFileType.VI.....	154
C.13	Choose File Type.VI.....	155
C.14	Front panel: Harmonic Analyzer. power calculation and performance factor.	157
C.15	Harmonic Analyzer block diagram.....	159

List of Abbreviations

a	phase-a of the 3-phase system
ac	alternating current
A/D	analog to digital
C_{ab}	resonant capacitor connected from line a to line b
C_d	dc-link capacitor
CDF	Current Distortion Factor
CF	Crest Factor
chl	channel 1 of the oscilloscope
DAQ	data acquisition
dc	direct current
DFT	Discrete Fourier Transform
DPF	displacement power factor
EMI	electromagnetic interference
f	frequency
FFT	Fast Fourier Transform
FPF	fundamental power factor
GPIB	General Purpose Interface Bus
h	harmonic order
Hi Res	high resolution
I_a	effective value of the current in phase-a
IEEE	Institute of Electrical and Electronics Engineers
I_d	dc-link current
I_H	harmonics current
I_L	load current
i_R	resonant current
I_S	source current
I_{S1}	fundamental component of the source current
I_{SC}	short circuit current
L	inductance
LabVIEW	Laboratory Virtual Instrument Engineering Workbench

LC	inductive-capacitive filter
L_d	dc-link inductor
L_s	supply inductance
NI	National Instruments
P	active power (W)
PCC	point of common coupling
PWM	Pulse Width Modulation
RE	resolution enhancement
rms	root-mean-square
S	apparent power (VA)
subVI	subprogram in LabVIEW programming
TDD	Total Demand Distortion
THD	Total Harmonic Distortion
TVS	transient voltage surge
VI	virtual instrument
V_{an}	phase-a voltage (line-a to neuter voltage)
V_{dc}	dc-link voltage
V_{LL}	line-line voltage
Φ	magnetic flux
Φ_1	displacement angle between fundamental current and voltage
ω	angular frequency

“He had to move forward even if he could not see where and how”

Irving Stone. *The Agony and the Ecstasy*

Chapter 1

Introduction

During the last several years the electric utilities have experienced an unprecedented increase in the levels of different power disturbances on the electrical delivery system. The most prominent disturbance is the harmonic pollution that has become of primary interest due to the large amount of power being processed by power electronic equipment.

With the development and increasing proliferation of systems that produce electric power with highly distorted waveforms, there is a need for accurate instruments to measure high frequency power signals. Electronically measured waveforms in many applications contain far more information than can be fully extracted by human users. Also, the large volume of data will make it very difficult if not impossible for human users to obtain the desired information in a reasonable amount of time. Computer-aided, interactive, and fully automated techniques have been developed for data processing.

The waveforms are digitized before processing can be performed by the digital computer. The digitization (i.e., sampling) of a continuous waveform is performed by analog to digital (A/D) converters at a sampling rate that is at least twice the highest significant frequency of the waveform, as emphasized in the following discussions.

This chapter provides an overview of the sampling theory employed in digital instruments and summarizes the content of this work.

1.1 Power measurement methods

Traditional analog instruments have been used in the past for measuring power, voltage and current. The bandwidth of these instruments is limited to power frequencies and they are unsuitable for high frequency switched-waveforms such as PWM inverter output voltages. Beside that, they can not be incorporated into automated processes [1].

There are several distinct principals that may be employed for the measurement of ac power. In purely thermal methods, such as the calorimetric method, the power absorbed by the load causes a measurable rise in temperature or the temperature is maintained constant by the controlled reduction of some more readily measurable form of power. Considering the investigation of the power input of a motor, the electric machine is placed in a carefully sealed and thermally insulated chamber with controlled airflow into and out of the chamber. By using a calibration curve constructed for the particular chamber, the total losses incurred by the motor for any kind of electrical input can be measured. The thermal loss is proportional with the input power. The principal disadvantages of this technique are that the measurement can only be made once thermal stabilization is achieved (i.e. 6-8 hours for a 10 hp motor) and the need to construct various sizes of chambers for different sizes of machines or equipment [1].

Another non-sampling and non-electronic type of wattmeter is the precision reflecting electro-dynamometer. This instrument contains sensitive mechanical components, it is inconvenient to use and, by not providing automated process integration capabilities, it is not considered a viable alternative to the digital sampling technique discussed in the following sections [2].

1.2 Digital filtering and Fast Fourier Transform

An important class of processing operation in digital instruments is the filtering of the data to minimize the effect of instrumentation noise or to constrain the data to a specific frequency range. This can be done in both analog and digital form. Digital filtering has gained much acceptance because of its flexibility and high performance. Another important class of processing operations is the spectral analysis of waveforms. In addition to time-domain analysis of the data, frequency domain analysis is essential in waveform study. Quite often both time-domain and frequency-domain processing are needed to derive certain desired information like amplitude variations and harmonic content [3].

Analog filters are constructed by combining conventional circuit elements to provide the desired response. Such filters are liable to variations in performance due to different factors such as component aging, drift, long term stability and thermal effects. To maintain full performance, they consequently require careful implementation, regular checking and recalibration.

A recursive digital filter receives continuous sample data at its input which is then subject to a sequence of digital processing to produce an output which has been filtered with respect to the input. As the data is continuous with an output value obtained for each input data point, the operation of the digital filter is comparable with the action of an analogue filter. Many digital filters have properties equivalent to those of virtually any practical analog filter and they can be designed to display characteristics which are not realizable in analogue form [4].

The digital filtering is based on the Z transform, which is defined as

$$F(z) = \sum_{n=-\infty}^{\infty} f(n\Delta t)z^{-n} \quad (1.1)$$

where z is a complex variable. This is of the same form as the sampled time function transform when

$$z = e^{j2\pi f\Delta t} \quad (1.2)$$

Here, a delay corresponds to an integration and consequently by inserting multiple delay circuits, multiple pole filters can be constructed.

One of the main advantages of a digital filter is that the same hardware can be used to generate virtually any filter shape just by changing the filter coefficients used in the calculations. Once established, the filter coefficients completely determine the filter properties. As these coefficients are in numeric form, they do not change with time and the filter never requires trimming.

The Fourier transform assumes a continuous signal, with averaging taking place over infinite time. In practice this is not possible, and a finite measuring time must be used, the effect of which is to introduce a ripple into the frequency domain solution. This error is compensated for with different averaging techniques [5].

If the Discrete Fourier Transform (DFT) is computed without using the Fast Fourier Transform (FFT) algorithm, the number of arithmetic operations involved with N samples is proportional with N^2 . With use of the FFT algorithm, the number of operations is proportional to $N\log_2 N$. The factor of improvement is therefore

$$N^2/N\log_2 N = N/\log_2 N. \quad (1.3)$$

With large data sizes, a significant improvement in computation time can be achieved [4,5].

The sampling theorem, also known as Nyquist theorem, states that the sampling frequency must be at least twice the highest frequency contained in the original signal for a correct transfer of information to the sampled system. The frequency component at half the sampling frequency is referred to as the Nyquist frequency. The representation of frequencies above the Nyquist frequency as negative frequencies means that, if the sample frequency is less than twice the highest frequency present in the sampled waveform, these higher frequency components can mimic components below the Nyquist frequency, introducing errors into the analysis. It is possible for high frequency components to complete many revolutions between samplings but since they are only sampled at discrete points in time, this information is lost. This misinterpretation of frequencies above the Nyquist frequency, as being lower frequencies, is called "aliasing". To prevent aliasing it is necessary to pass the analog time domain signal through a band-limited low pass filter. The cut-off frequency must be ideally equal to the Nyquist frequency. In practice this is limited to about 80% of the Nyquist frequency due to the non-linear characteristics of a practical filter [6].

The application of a window function has the effect of multiplying each point of a time domain signal by the corresponding time point of the window function. The combination of the DFT and window function produces a response equivalent to filtering the time domain signal through a series of filters with centre frequencies at integer multiples of $1/T$, where T is the sampling period. The filter characteristic and the associated leakage is determined by the particular window function chosen. The effect

of spectral leakage can be reduced by changing the form of the window function. In particular, if the magnitude of the window function is reduced towards zero at the boundaries, any discontinuity in the original waveform is weighted to a very small value and thus the signal is effectively continuous at the boundaries. In practice a compromise is made between mainlobe width compression and sidelobe level reduction. There are different window functions available in the software employed in this work, such as: rectangular, triangular, cosine squared (Hanning), Hamming, Gaussian, Dolph-Chebyshev [3-6].

1.3 Digital technique for power measurement

The average electric power absorbed by a single phase load is given by:

$$P = \frac{1}{T} \int_0^T [v(t)][i(t)]dt \quad (1.4)$$

where $v(t)$ and $i(t)$ are the instantaneous values of the periodic voltage and current signals, with time period T . In the digital sampling technique, this is approximated by

$$P_d = \frac{1}{n} \sum_{k=0}^{n-1} [v(t_k)][i(t_k)] \quad (1.5)$$

with the following considerations [1,2,7,8]:

- The samples begin at $t=0$ and are taken at the rate of “ n ” times per period.

- The $v(t_k)$ and $i(t_k)$ are uniformly spaced, simultaneous, and instantaneous samples of the voltage and current signals, where $t_k=(kT/n)$ represents the sample times.
- The summation is carried out over a complete or integer multiple of cycles.

Since the $v(t)$ and $i(t)$ are assumed repetitive, the Fourier series of the power signal can be represented as

$$p(t) = [v(t)][i(t)] = P_0 + \sum_{\omega=1}^{\infty} P_{\omega} \sin[(2\pi\omega t / T) + \Theta_{\omega}] \quad (1.6)$$

where $P_0 = P$ is the true average power given by (1.1) and the oscillatory terms in (1.6) average to zero over the period T .

The Fourier series of the voltage and current signals are

$$v(t) = \sum_{u=0}^{\infty} V_u \sin[(2\pi u t / T) + \Theta_v] \quad (1.7)$$

$$i(t) = \sum_{c=0}^{\infty} I_c \sin[(2\pi c t / T) + \Theta_c] \quad (1.8)$$

Considering the trigonometric identity

$$2 \sin \alpha \sin \beta = \cos(\alpha - \beta) - \cos(\alpha + \beta) \quad (1.9)$$

the corresponding term in $p(t)$ due to the u -th voltage harmonic and the c -th current harmonic is given by the expression

$$\begin{aligned}
p_{u,c}(t) = \frac{1}{2} V_u I_c \{ & \cos[2\pi(u-c)\frac{t}{T} + (\Theta_u - \Theta_c)] \\
& - \cos[2\pi(u+c)\frac{t}{T} + (\Theta_u + \Theta_c)] \}
\end{aligned}
\tag{1.10}$$

For $u=c$, the first term of (1.10) becomes a constant ($0.5V_u I_u$) and represents a component of the total average power P_0 . The second term varies sinusoidally at twice this frequency and averages to zero. If $v \neq c$, there is no average power in any of the harmonics.

By substituting $t_k = kT/n$ in equation (1.5), the instantaneous power at t_k can be written as

$$p(t_k) = [u(t_k)][i(t_k)] \tag{1.11}$$

and the digital approximation to the true average power as

$$P_d = \frac{1}{n} \sum_{k=0}^{n-1} p(t_k) \tag{1.12}$$

It can be shown that the sampling error, which is the difference between P_0 and P_d , is given by

$$P_d - P_0 = \sum_{\omega > 0} *P_\omega \sin \Theta_\omega \tag{1.13}$$

where the starred summation is over only those terms for which ω/n is an integer [2].

An interesting result of this development is that the error in the digital sampling process is due to those product harmonics whose frequencies are integer multiples of the sampling frequency, i.e. for integer values of ω/n . By using the highest sampling frequency available, the error introduced in the power calculation by the digital method is minimized [2.7].

The focus of this thesis concerns the development of a virtual instrument (VI) for data acquisition (DAQ) and analysis for power electronic circuits. The instrument is a LabVIEW written program which controls a four channel digitizing oscilloscope via General Purpose Interface Bus (GPIB) cable. The DAQ system is an important research tool in the developing stage of new power electronic circuits enabling accurate measurements of different power quality factors. It can also be a teaching-aid tool since the data acquired can be saved on disk in Matlab or Excel format enabling further analysis of the waveforms under investigation.

1.4 Organization of the thesis

The thesis begins by introducing the “big picture” of power system disturbances. Forecasts performed in the early 1990s linked 28 percent of computer downtime to site and power problems and the figure is projected to grow to 47 percent by the year 2000 [30]. Each type of major disturbance is briefly described together with its most common causes (Chapter 2). Distorted waveforms and associated harmonics cause equipment and system problems. Electromagnetic equipment (such as transformers and motors) overheat because of high-frequency induced losses. Power

factor capacitors overheat, their fuses blow, or capacitor failure occurs. High harmonic content causes motors to pulsate and their bearings to fail. Other signs of harmonic distortion are random fuse blowing and nuisance tripping of circuit breakers. Electronic controls may operate erratically, especially where they depend on a clean sine wave for synchronization or control purposes. The discussion outlines the intrinsic harmonic sources which coexist in the power system since its inception (i.e. power transformers and rotating machines) as well as the “classical” harmonic polluters such as arc-furnaces and fluorescent lights (Chapter 3).

The major concern regarding harmonics comes from the proliferation of power electronic circuits. These are nonlinear loads in which the instantaneous current is not proportional with the applied voltage. An entire section is dedicated to the single-phase and three-phase diode rectifiers and introduces the basic power quality factors associated with harmonic analysis: current harmonic factor and total harmonic distortion. The 12-pulse series rectifier is presented as an effective mean for harmonic elimination and new topologies employing active resonant networks for harmonic control are discussed (Chapter 4).

Understanding power disturbances and particularly harmonics is essential to the engineer who wants to assess accurately performance factors associated with different electrical apparatuses. Moreover, for the researcher involved in developing new topologies of power electronic circuits with reduced harmonic content or harmonic correction units for existing power electronics loads, an accurate measurement tool is a necessity.

The LabVIEW program development used for creating a virtual instrument for waveform acquisitions and analysis is introduced prior to the description of the DAQ system. The main features of the graphical programming environment are explained

together with the basic programming tools specific to the instrument front panel and the program block diagram development.

The virtual instrument has three distinctive components: the virtual oscilloscope, the harmonic analyzer and the power factors and power calculations. The DAQ system consists of a Power Macintosh 7100/66 computer interconnected with a Tektronix-TDS-420 digitizing oscilloscope via GPIB cable. An NI-488 card from National Instruments is employed to interface the instrument with the computer. The signals to be acquired and analyzed are obtained via voltage and current probes. The virtual oscilloscope imitates the front panel of a real instrument and has the capability of acquiring four channels of data. When data is acquired, the user is prompted for constants regarding voltage and current probes employed. For saving waveforms to file, the virtual oscilloscope prompts the user to select the file format and data is saved in Amps or Volts. The front panel of the harmonic analyzer displays the harmonics spectrum of a selected signal and illustrates the harmonic amplitudes. The virtual instrument calculates the total harmonic distortion factor (THD) relative to the total RMS or relative to the fundamental of a selected signal as well as the current distortion factor (CDF). For three-phase power calculations, the program requires two voltages and two currents. Instructions regarding the measurement setup are given on front panel warning labels. The program calculates and displays the effective values of the line-line voltage and line current, the apparent power (S) and the active power (P), the power factor (PF), and fundamental power factor (FPF) (see Chapter 5).

The various features of the DAQ system are outlined by analyzing different power electronic circuits. Many experiments were conducted and different circuit topologies were investigated with the developed virtual instrument.

In most power electronic applications the power input is in the form of sine wave ac voltage provided by the utility which is first converted to dc voltage by means of rectifiers. The current trend is to convert the ac into dc in an uncontrolled manner employing rectifiers with diodes. This is the case of the majority switching dc power supplies, ac-motor drives, dc-servo drives. Experimental single-phase and three-phase diode bridges employing different filters are analyzed by means of data acquired and analyzed with the DAQ system. The line-current waveforms are appreciated with reference to the power quality factors calculated by the virtual instrument (Chapter 6).

Many rectifiers are employed in variable speed drives at different power levels. The most recent variable speed drives use various techniques to control the speed, torque or power output of squirrel-cage induction machines. Two different inverter drives are examined: the square-wave inverter drive and the PWM inverter drive. Acquired waveforms and processed data from both the utility interface and the motor-end of each drive are presented and insight regarding the nature of the harmonics and their effects is given (see Chapter 7).

One of the challenges facing the electric utilities and their customers in equal measure is harmonic control in conjunction with emerging quality standards. A great deal of effort is currently made by many researchers and engineers for designing economical switch-mode power supplies with improved utility interface. Part of the research undertaken by the power electronics group of the University of Alberta focuses on developing new, reliable utility interface circuits with reduced current distortion and unity power factor. The thesis presents novel circuit topologies investigated by means of the DAQ system developed. Resonant LC circuits are employed in conjunction with

three phase diode bridge rectifiers and the 12-pulse series rectifiers, and THD values less than 5 percent for the input current are obtained (see Chapter 8).

Chapter 2

Introduction to Power Quality

Diagnosing electrical power quality problems is a process that requires attention to details, careful planning and accurate instruments. The information presented in this chapter is intended to outline the most common power quality disturbances. Major causes of each type of disturbance are discussed and references to the power quality standards are given. The discussion creates the general context for the particular type of disturbance addressed in the following chapters. Data acquisition employed by the virtual instrument developed in this work is the state-of-the-art method for measuring power disturbances [9].

2.1 Introduction

Since its inception over a century ago, the electric utility industry has recognized the need to provide reliable electrical power. Standards for voltage regulation were implemented when the electric motor began to be used on a large scale in industry. The increase of public expectations for steady lighting intensity determined the adoption of stricter standards.

Customer equipment was early recognized by the utilities as a major factor for voltage disturbances on their lines. One of the first manifestation and the most annoying such disturbance was the visible flicker in incandescent lamps, caused by voltage fluctuations with a frequency range between 6 and 12 Hz. Research showed that this flicker could be perceived by many people, even if the pulsation on an incoming line was only one-third volt on a 120 V system. In the first half of this century, this type of

problem led to an increasing number of industry standards on end-use equipment to reduce voltage fluctuations sent back along a power line [10].

With the advent of air conditioners and their fast proliferation in the 1950s, electric utilities faced a different problem. The starting current required by the early models of air conditioners to start the compressor caused a temporary reduction in the incoming line voltage. As a result, other motors on the same grid often could not reach operating speed, ran poorly or even stalled. The problem was solved by adding power factor correction capacitors [10,11].

Today's power quality problems are far more complex due to a multitude of different causes and a wide range of susceptibility levels in electronic equipment. Because of the diversity of both the causes and the consequences of power quality problems, they can not be addressed by a single solution. There is a necessity for cooperative efforts among utilities, electronic product manufacturers, standard-setting organizations, electrical contractors and consumers to identify the various technical issues, conduct research, establish standards and implement solutions. A variety of power quality related research efforts are currently undertaken by the Power Electronics Group of the University of Alberta [11,12].

2.2 Power Quality Concept and Definition

In recent years increasing power quality concerns have attracted industry-wide attention on defining power quality in terms different from those used in the existing standards for electric power systems and equipment voltage ratings. The Guide for Applying harmonic limits on Power System [13] and IEEE 519-1992 Std.[14], specify steady-state voltage tolerances for the electric utility at the point of service to be within

5% for non-lighting loads (Appendix A). The standard also specifies the steady-state voltage tolerances at the end-use. Equipment utilizing electricity must be designed to give “satisfactory” performance throughout the range of +4 % to -10 %. This specification of steady-state voltage limits proves to be insufficient for today’s microelectronics technology. It is much more difficult to define what constitutes “acceptable performance” and “acceptable power quality” for computers. A comprehensive definition of power quality should encompass the following factors [9]:

- All types of power disturbances that occur.
- Quality of power necessary for successful operation of diverse electrical and electronic equipment.
- Practical limits to the capability of delivering power of high quality to diverse customers.
- Economics of the electric power distribution from both the utility and customer perspective.

The Institute of Electrical and Electronic Engineers (IEEE) proposed a definition that describes power quality as a concept of powering and grounding sensitive electronic equipment in a manner that is suitable to the operation of that equipment. In other words the power quality is not adequate when a change in the power line voltage, current or system grounding causes the equipment to malfunction or be damaged [11,14,15].

2.3 Types of Electrical Disturbances

The electrical disturbances can be categorized in a few types. They are described below together with a short listing of their most frequent causes.

2.3.1 Voltage Disturbances

Voltage disturbances can be categorized into short term, such as transients, long term, such as swells and sags and continuous, such as outages or harmonics.

Transients - A transient voltage surge (TVS) can occur on power lines or conductors, including telecommunications and data line links. It is a significant deviation from the normal alternating voltage sine wave, typically lasting from a fraction of a microsecond up to several milliseconds. A TVS can be categorized as a deviation generated from a natural occurrence (lightning) or through the switching of power equipment, either on-site or elsewhere. Irrespective of the cause of the TVS, the electric charge enters the power lines and conductors at some point and causes voltage there to rise in a manner determined by the system capacitance. The electric charge then spreads through the system in the form of traveling waves. Various forms of TVS are discussed below. [11.16].

- *Impulsive Transient* -An impulsive transient has the following characteristics: fast rise time (from several nanoseconds to tens of microseconds), fairly rapid decay, and high energy content. Its duration can be from a fraction of a microsecond up to several hundred microseconds. A typical impulsive transient is shown in Figure 2.1.[11]. The impulsive magnitude of this type of transient is measured from the point it occurs on the sine wave and not from zero voltage. Such a disturbance is called a spike if it adds to a sine wave, or a notch if it subtracts from the sine wave. Peak voltage can range up to about 6000V on a building distribution system. Possible causes include switching inductive loads on / off (e.g. motors, relays, transformers, x-rays equipment, lighting ballasts), consumers loads (computers, house appliances, light dimmers), capacitor switching, fault clearing. The operation of Uninterruptable Power Supplies (UPS) may cause notching.[11.17.18].

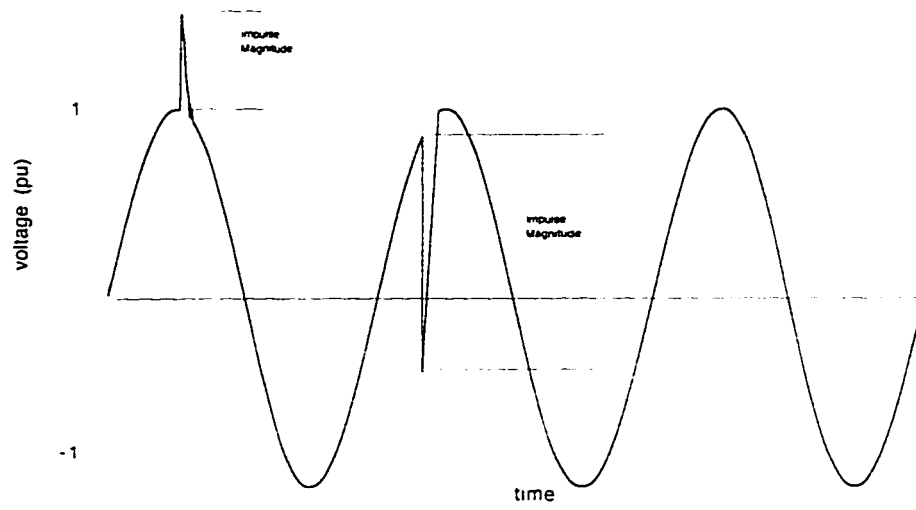


Figure 2.1 Example of impulsive transients.

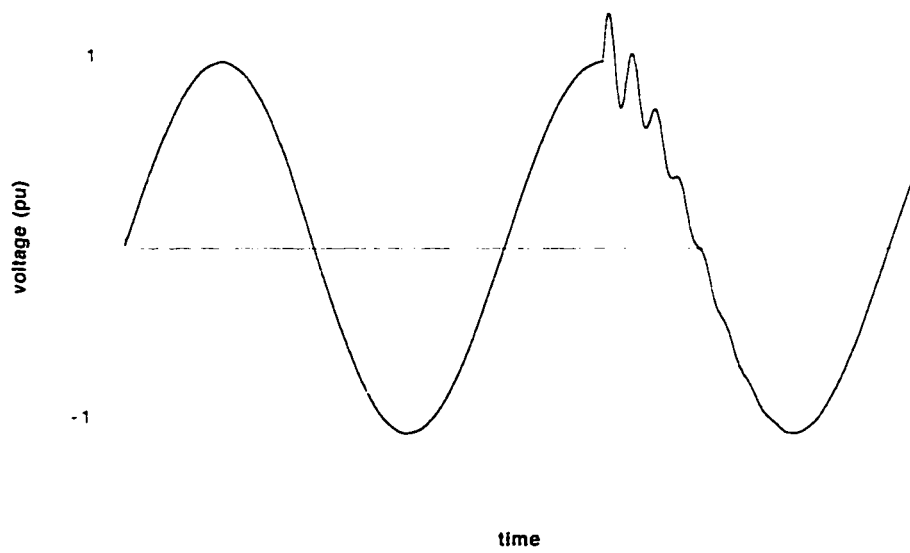


Figure 2.2 Example of oscillatory transient.

- *Oscillatory Transient* - An oscillatory transient rises in a short time and oscillates decaying exponentially, usually with a lower energy content than an impulsive transient. A typical oscillatory transient can last up to one cycle of the line voltage (16.67ms) and can have frequencies from a few hundred Hz to many MHz. Figure 2.2 shows a typical oscillatory transient.

-*Switching Transient* - When power equipment is switched on or off, transient voltages can be generated due to the energy stored in the circuit inductances (L) and capacitances (C). The size and duration of the transient depends on the waveform applied and the values of the reactive elements. Examples of switching transient generators are fault clearing, capacitor switching and switching on and off of large inductive loads.

The transient overvoltages can cause immediate or latent damage. By repeated transient overvoltage exposure the equipment's ability to withstand additional stress is reduced. At a later time it fails unexpectedly without apparent cause due to its weakened nature from previous transients. The same can occur to a component such as a diode or another power electronics switch when the corresponding snubbers are unable to "cut-off" the transients. The latent effect may not become apparent for some time.

The problems associated with transients are mainly due to the increased use of sensitive electronic equipment without regard for the realities of normal power system operation of the customer's facility. The source of a transient is very difficult to trace and there is general consensus that most transients get into computer logic and memory circuits by poor grounding or electromagnetic interference (EMI), not by conduction.[11,19].

Swell - A momentary overvoltage, or swell, is any change above the prescribed input voltage range for a duration of one half cycle to 2 minutes (Figure 2.3). If the increase in the line voltage is longer than 2 minutes, it is called a sustained swell. Most common causes for overvoltages are incorrect transformer tap settings and improper application of power factor correction capacitors. They can cause overheating and reduce the life of electrical equipment.

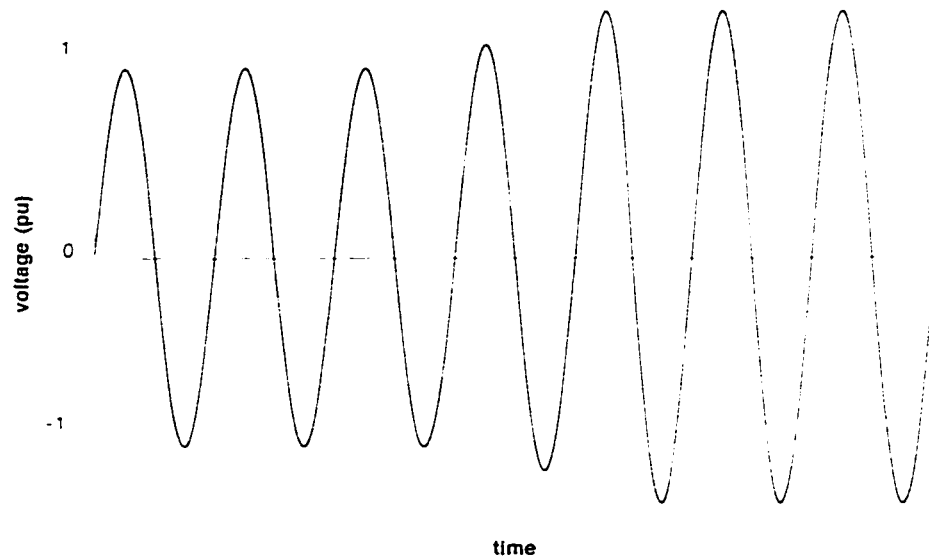


Figure 2.3 Example of voltage swell.

Undervoltage - Any change below the prescribed input voltage range for a given piece of equipment is called undervoltage (Figure 2.4). This type of disturbance can be caused by overloaded distribution systems or customer wiring, faulty connections or wiring, loose or corroded connections, incorrect transformer setting or unbalanced phase loading conditions. They cause problems ranging from errors in

sensitive equipment used in control and measurement to hardware damage, low efficiency and reduced life of electrical equipment (e.g. some heaters and motors).[11.19].

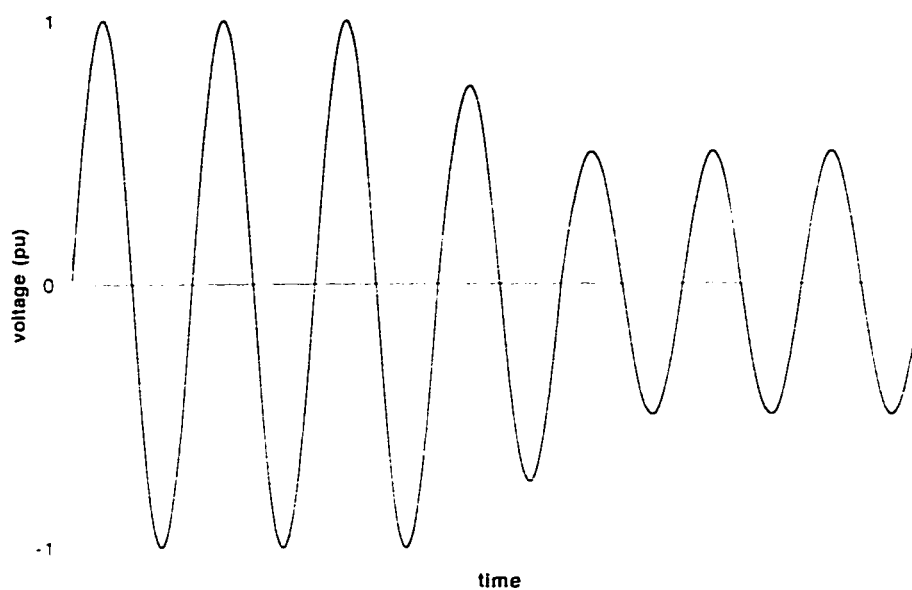


Figure 2.4 Example of undervoltage.

Sags- A sag is a momentary (0.5 - 120 cycles) reduction in voltage at the power frequency below a particular piece of equipment's utilization voltage tolerance (Figure 2.5). Sags can be caused by start-up of large loads (motors, air conditioners, etc.), overloaded or undersized wiring, faults on remote or adjacent feeders, utility switching failure and indirect lightning effects. They cause overheating of motors and electrically-driven equipment, motor stalling, and power-related computer system failures.

Flicker - A flicker is a small change in the line voltage that causes a perceptible change in the intensity of electric lights. In some situations people can perceive sags as

low as one third of a volt. Some of the sources known for causing voltage flicker are: large load (real and/or inductive) pick-up and load rejection, electric arc furnaces, electric welders, large wood chippers, strip mining electric drag lines, power oscillations...etc. A transient voltage drop, which causes light flicker is reduced almost instantaneously when series capacitors are used. To predict accurately the reduction in voltage flicker by series capacitors, the current and power factor of the sudden load increment causing the voltage dip must be known.[11.20].

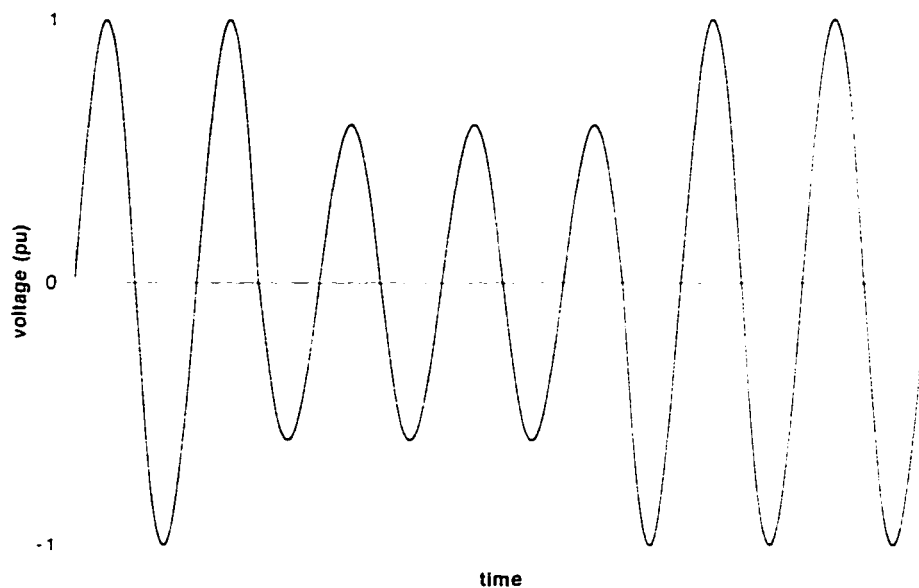


Figure 2.5 Example of voltage sag.

2.3.2 Interruptions

The complete loss of power lasting for cycles, seconds, minutes, hours or days is defined as power interruption. A variety of factors can cause power interruptions such as operation of protective devices in response to faults, tripping of the main fuse or circuit breaker due to a fault or malfunction of equipment. The effects of these

interruptions are loss of computer / controller memory, equipment shutdown or failure, hardware damage and productivity loss [11].

2.3.3 Frequency Variations

A frequency variation is a deviation from the specified system frequency such as 60 Hz (Figure 2.6). There are different causes for this type of disturbance such as sudden changes in load to the utility or generator, switching of power between utility companies, or generator malfunction. In large power systems typical frequency variations are only a few hundredths of one Hz. The effects of this disturbance are manifested in malfunctioning of timing circuits, ferroresonant transformers and motor speed in disks and tape drives. The equipment that measures the position of zero crossing of the 60 Hz waveform will interpret distortion of the waveform at zero crossing as change of frequency [11].

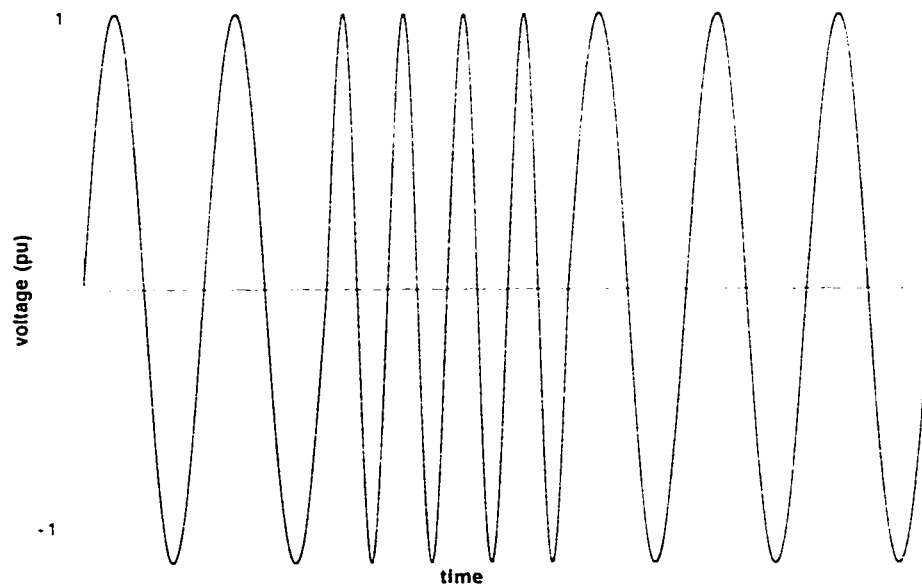


Figure 2.6 Frequency variation.

2.3.4 Voltage imbalance

A voltage imbalance is a long term, steady-state problem. It is expressed as a percent, i.e. the maximum deviation of voltage from the average of three-phase voltage multiplied by 100, divided by the average of the voltages.

Voltage imbalances are caused by unbalanced phase loading conditions such as large single phase loads, defective transformers and ground faults in undergrounded or resistive grounded systems. They cause premature failures of motors and transformers due to overheating. Only three-phase applications are affected by voltage imbalances [11].

2.3.5 Electrical Noise

Electrical noise is a low-voltage, high-frequency signal superimposed on the 60 Hz waveform. Its amplitude ranges from volts to many tens of a volt and occasionally more. Noise may be transient or repetitive, and frequency may range from a few kHz to many MHz. Some sources are: broadcast stations, opening and closing of switches, arching contacts, switch mode power supplies, pulse width modulation (PWM) drives and other power electronics. Noise can cause problems because its high frequency allows it to easily couple from wire to wire or through a power supply and into the circuitry it powers. If two wires are in contact for six metres, the capacitance between them will be about 400 pF and at 10 MHz this represents a 40 ohm impedance that will feed any noise present in one line directly into the other line. At higher frequencies these problems will be even worse as the coupling increases with the frequency [11]. There is normal-mode noise that occurs between line-to-neutral or line-to-line, and common

mode noise consisting of a potential difference between any or all current carrying conductors and the grounding conductor or earth.

Common-mode noise can be generated by a ground potential difference between elements of the computer or remote peripherals connected to the computer. This type of disturbance is influenced by several factors including the system configuration and the impedance of the grounding system and it can be suppressed by the use of a shielded isolation transformer. However, equalizing ground potential is often difficult due to the broad frequency band involved in wiring resonances [11].

Common-mode noise on the primary of the transformer that is converted to normal-mode noise on the secondary is referred to as transverse-mode noise, intercoupling noise or differential-mode noise.

A properly designed power grounding system has sufficiently low-impedance at 60 Hz to maintain enclosures and all grounded metals at the same voltage potential (ground reference). The 60 Hz ground system is unable to provide this equalization at higher frequencies because of the increased impedance caused by inductive resonance at higher frequencies: Skin effect - the tendency of high frequency currents to flow near the surface of the conductor, increases the ac resistance of the conductor and the inductive reactance of the conductor increases due to high frequency. At microprocessor switching speeds (e.g. 166 MHz), current penetration in the copper conductor is much less than at 60 Hz, with the result that the effective impedance between two points is much larger at high frequencies. Consequently, the long grounding conductors used in most grounding systems become ineffective for grounding of high frequency systems.

Short returns are always recommended for fast-rise circuits to provide effective signal returns at system signal frequencies. A signal Reference Grid, which is a dense

grid of grounding conductors, is the most effective form of grounding for a spread-out system [11].

2.3.6 Harmonics

Harmonics are voltages or currents at frequencies that are integer multiples of the supply frequency. They are caused by non-linear loads i.e. loads in which the current waveform is not the same shape as the waveform applied voltage. All equipment operating on the principle of ferromagnetic induction such as lighting ballasts, lifting magnets, solenoids, transformers and motors produce some degree of harmonics. An important example of a device that produces harmonics is a power converter (e.g. rectifier) that draws current in only a portion of each cycle. This type of disturbance is discussed in more detail in Chapter 3.

This investigation identifies major types of power quality problems encountered in power systems. The main sources for each particular disturbance are briefly listed together with some of their effects. Modern instruments use data acquisition techniques to accurately identify the disturbances and provide design information aimed to diminish their effects.

Chapter 3

Classical harmonics sources

Harmonics are created by nonlinear loads and devices on the power system. There is a wide variety of devices that generate harmonics and they can be connected to the power system at any voltage level. A description of the major harmonic sources follows. Understanding harmonics is the prime step for harmonics measurement and harmonics control.

3.1 Introduction

Before the advent of static power converters the main source of power system harmonics was associated with the design and operation of electric machines and transformers. The principal harmonic sources present in the power systems were the magnetizing currents of the power transformers. The main secondary sources were the electric power generators. This was due to the practical economic design considerations of the pole face, which allowed some departure from the ideal sinusoidal waveshape.

Modern transformer and rotating machines do not cause significant distortion under steady state operating conditions. However, their harmonic contribution increases considerably when operating outside their normal state range and during transient disturbances. Besides the static converter (which is separately treated in Chapter 4), two other non-linear loads have to be considered due to their harmonic contribution: arc furnaces and fluorescent lights.

3.2 Transformer associated harmonics

Transformer associated harmonics have different causes such as non-linear characteristics of the core material, overexcitation and in-rush current. A brief discussion of each of these causes follows:

3.2.1 Magnetization non-linearities

The primary voltage of a transformer at no-load is practically balanced by the back e.m.f. because at low currents the effect of winding resistance and leakage reactance is negligible. For a sinusoidal supply the impressed voltage v_1 at any instant is

$$v_1 = -e_1 = -E_m \sin \omega t = N_1 \frac{d\Phi}{dt}. \quad (3.1)$$

Consequently, the main flux is obtained:

$$\Phi = -\int \frac{e_1}{N_1} dt = \frac{E_m}{N_1 \omega} \cos \omega t = \Phi_m \cos \omega t \quad (3.2)$$

and its expression illustrates that sinusoidal primary voltage produces a sinusoidal flux at no load. The primary current will not be sinusoidal because the flux is not linearly proportional to the magnetizing current. The magnetization curve of the steel used in the core's laminations determines the relationship between the flux Φ and the magnetizing current i_m which is not linear. When the hysteresis effect is included as shown in Figure 3.1, the magnetizing current is no longer symmetrical about its maximum value.

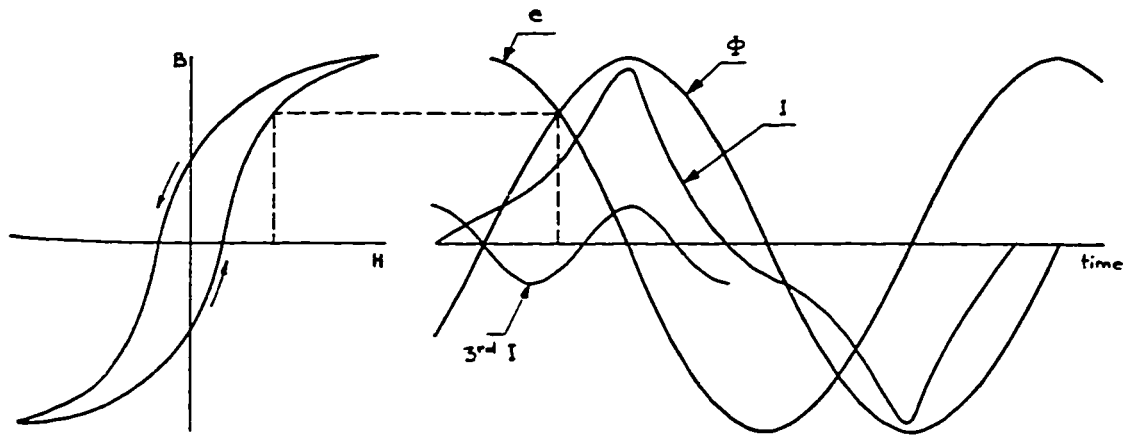


Figure 3.1 Transformer magnetization (hysteresis curve, flux and magnetization current waveforms).

The waveform distortion illustrated in Figure 3.1 is mainly caused by triple-n harmonics and particularly the third. In order to maintain a reasonably sinusoidal voltage supply, a path for the triple-n harmonics have to be provided. This is achieved by connecting the windings in delta. The fifth and seventh harmonic components of the magnetizing current may also be large enough to produce visible distortion and can not be ignored. The magnetizing current harmonics rise to their maximum levels when the system is lightly loaded and the voltage high (e.g. early hours of the day)[19].

3.2.2 Symmetrical overexcitation

Other source of harmonics associated with transformers is due to magnetic saturation that occurs when overvoltage is applied at its input. An optimal designed transformer using a good quality grain-oriented steel might be expected to run with peak magnetic flux density in the steady-state at about 1.6 - 1.7 T. This value is at the knee

of the magnetizing curve of the core material. If the transformer under these conditions is subject to a 30% rise in voltage, the magnetic induction might reach 1.9 - 2.0 T. This can produce considerable saturation and consequently additional harmonics [21].

3.2.3 Inrush current harmonics

If a transformer is switched off, it can be left with a residual flux density in the core of magnitude $+B_R$ or $-B_R$. When the transformer is re-energized, the flux density illustrated in Figure 3.2 can reach peak levels of $B_R + 2B_M$ (almost three times the working value). For the above mentioned transformer this can create peak magnetic inductions of about 3.4 - 4.7 T driving the core to extreme saturation levels and consequently will generate high levels of harmonic currents during the first 50 cycles of the applied voltage [22].

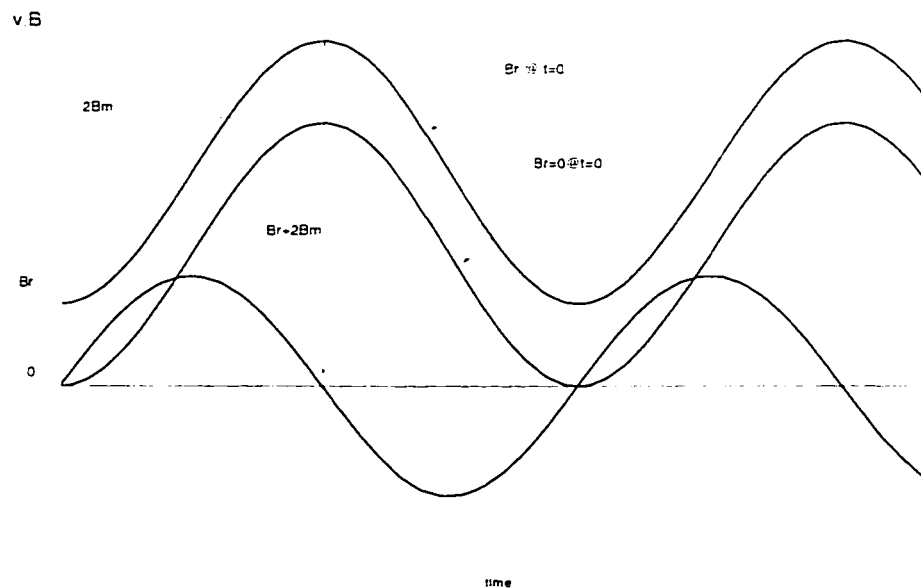


Figure 3.2 Flux density in a transformer at energization with both remnant flux B_R and zero remnant flux density.

3.3 Rotating Machine Harmonics

Due to its rectangular waveshape, the m.m.f. space distribution in one phase of a full-pitched polyphase winding with one slot per pole per phase can be expressed as sum of its frequency components [22]:

$$MMF(x) = \frac{2\sqrt{2}IN}{\pi} \left\{ \sin \frac{2\pi x}{\lambda} + \frac{1}{3} \sin 3\left(\frac{2\pi x}{\lambda}\right) + \frac{1}{5} \sin 5\left(\frac{2\pi x}{\lambda}\right) + \dots \right\} \quad (3.3)$$

where I is the rms current per conductor, N is the number of conductors per slot. $\sqrt{2}IN/2$ is the maximum value of the uniform m.m.f.. λ is the wavelength and x the space coordinate.

For an alternating current of angular frequency $\omega = 2\pi f$. Equation (3.3) becomes

$$MMF(x) = \frac{2\sqrt{2}IN}{\pi} \sin(\omega t) \sum_{n=1}^{\infty} \frac{1}{n} \sin n\left(\frac{2\pi x}{\lambda}\right), \text{ for } n \text{ odd} \quad (3.4)$$

In practice the windings are distributed along the surface with g slots per pole per phase and the m.m.f.s of the g coils are displaced from each other in space. Moreover the displacement angle is different for various harmonics since their pole pitches are different.[19]

It can be shown [19,23] that the m.m.f. distribution for an m -phase machine and for $n = 1, 3, 5, 7, \dots$ can be expressed as:

$$MMF(x) = \frac{3\sqrt{2}IN}{\pi} g\left\{\left(\frac{k_{d1}}{1}\right) \cos\left(\frac{2\pi x}{\lambda} - \omega t\right) + \left(\frac{k_{d5}}{5}\right) \cos\left(5\frac{2\pi x}{\lambda} + \omega t\right) + \left(\frac{k_{d7}}{7}\right) \cos\left(7\frac{2\pi x}{\lambda} - \omega t\right) + \dots\right\} \quad (3.5)$$

where k_{dn} is the distribution factor for the n th harmonic.

Equation (3.5) shows that the fundamental is a traveling wave moving in the positive direction, triple-n harmonics are absent, the fifth harmonic is a wave traveling in the negative direction, the seventh harmonic travels in the positive direction, etc.

As a result of the harmonic content of the m.m.f. distribution, the induction motor develops time harmonics which are speed dependent.

The synchronous machine is generating voltage harmonics (especially the salient pole type) due to the non-sinusoidal distribution of the flux.

3.4 Arc-furnaces harmonics

The combination of arc ignition delays and the highly non-linear arc voltage-current characteristics introduces harmonics of the fundamental frequency. The voltage changes due to sudden alterations of arc length have a stochastic character and produce a spread of frequencies predominantly in the range 0.1 - 30 Hz about each of the harmonics present. The levels of harmonics currents vary markedly with time and also in respect to the fundamental component [19].

3.5 Fluorescent lighting harmonics

Fluorescent tube appliances are highly non-linear and can give rise to considerable odd-ordered harmonic currents. In a three-phase, four-wire load the triplens are basically additive in the neutral and the third is the most dominant. Lighting circuits often involve long distances and have very little load diversity. With individual power factor correction capacitors, the LC circuit can approach a condition of resonance at the third harmonic. It is common practice to avoid individual lamp compensation by providing capacitor banks adjacent to distribution boards connected either in star with floating neutral or in delta. Most recent approaches use electronic ballast topologies which provide higher efficiency and reduced harmonic pollution [24,26].

Harmonic producing loads are being added to distribution systems at an increasing rate. Power system harmonic problems are more frequent because the voltage and the current distortion on the system are increasing. This investigation identified major power system harmonics producers. The static converter makes the subject of the next chapter. Better planning for harmonic producing loads has to be addressed if system harmonic problems are going to be better controlled.

Chapter 4

Solid-state power conversion harmonics and performance factors

Electronic equipment today is essential to the operation of modern industry and offices. A powerful dilemma has arisen in that the western society is more and more dependent upon electronic equipment that is becoming increasingly vulnerable due to disturbances in their ac power source. A selected number of power electronic utility-interface circuits are the subject of this chapter. The basic quality factors are introduced followed by discussions on the most widely used variable speed drives utility interface - the three phase full-bridge diode rectifier. The definitions of quality factors are employed in the following chapter in the development of the virtual instrument for waveform acquisitions and analysis. Some novel stand-alone harmonic correction units are briefly presented with emphasis on aspects associated with harmonic pollution reduction.

4.1 Introduction

Previously, most electric utility loads were motors and incandescent lamps. These loads are rugged and the utility provided adequate power and the necessary protection against harmful disturbances. Presently, the number of loads incorporating electronic circuitry is rapidly increasing and this is much more susceptible to the disturbances that have always existed in an electric utility system. Moreover, many types of electronic loads also cause disturbances in the power system.

4.2 Single phase diode bridge rectifier

To illustrate the basic concepts, consider the single-phase diode bridge rectifier shown in Figure 4.1. This type of converter is used at low power levels and its importance is gaining significance due to the very large and continuously increasing number of appliances employing it such as TV sets and personal computers.

The capacitor filter at the output of the single-phase bridge rectifier in Figure 4.1 is considered to be a large value (e.g. 1000 μ F). The utility supply can be modeled as the voltage source v_s in series with its internal impedance which in practice is predominantly inductive (hence L_s in Fig.4.1).

The line-current i_s at the input to the rectifier deviates significantly from a sinusoidal waveform as shown in Figure 4.2. The distortion in the line-current waveform can be quantified. Using Fourier analysis, the input current i_s , being a periodic function can be expressed in terms of its fundamental frequency component i_{s1} plus other harmonic components. Assuming the input voltage v_s as being pure sinusoidal, the fundamental current i_{s1} will be the only contributor to the average power flow due to the fact that both voltage and current must be at the same frequency for average power flow. Considering the effective values of the input voltage V_s and fundamental line-current I_{s1} the average power P flowing through the rectifier is

$$P = V_s I_{s1} \cos \phi_1 \quad (4.1)$$

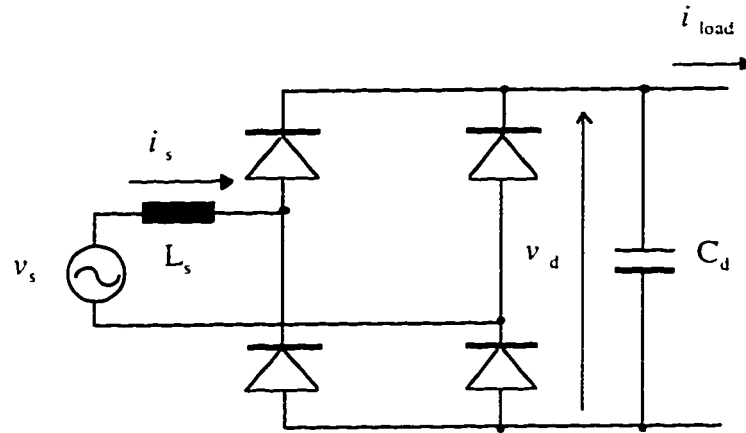


Figure 4.1 Single-phase diode bridge rectifier with capacitor output filter.

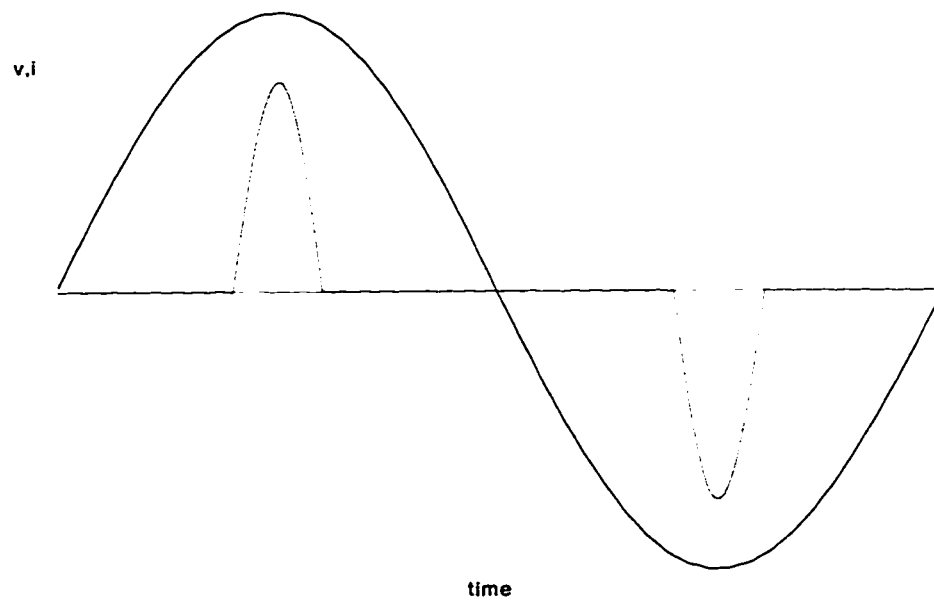


Figure 4.2 Single-phase diode bridge rectifier waveforms (C filter).

where Φ_1 is the angle by which i_{s1} lags v_s as shown in Figure 4.3. The magnitude of the apparent power S is the product of rms voltage V_s and the rms value I_s of the line current i_s

$$S = V_s I_s \quad (4.2)$$

By definition the power factor PF is

$$PF = \frac{P}{S} \quad (4.3)$$

Substituting equations (4.1) and (4.2) into (4.3)

$$PF = \frac{V_s I_{s1} \cos \phi_1}{V_s I_s} = \frac{I_{s1}}{I_s} \cdot \cos \phi_1 \quad (4.4)$$

The power factor has two components:

- the displacement power factor $DPF = \cos \Phi_1$ which is the same as the power factor when both voltage and current are sinusoidal.

- the current distortion factor $CDF = I_{s1} / I_s$ which illustrates the influence of the harmonics in the power factor; for sinusoidal current $CDF = 1$.

Therefore.

$$PF = CDF.DPF \quad (4.5)$$

Equation (4.5) shows that a large distortion in the line current will result in a small value of the current distortion factor (CDF) and hence a small value for PF, even if the displacement power factor (also called fundamental power factor) is closed to unity.

The effective value I_s of the line-current can be calculated by root-mean-squaring the i_s waveform

$$I_s = \left[\frac{1}{T} \int_0^T i_s^2(t) dt \right]^{1/2} \quad (4.6)$$

or considering its rms Fourier components, I_{s1} and I_{sh}

$$I_s = \left[I_{s1}^2 + \sum_{h=2}^{\infty} I_{sh}^2 \right]^{1/2} \quad (4.7)$$

The effective value of the distortion component in the line current can be defined as:

$$I_H = \sqrt{I_s^2 - I_{s1}^2} = \sqrt{\sum_{h=2}^{\infty} I_{sh}^2} \quad (4.8)$$

The distortion in the current waveform can be quantified by defining the total harmonic distortion relative to the fundamental as:

$$\%THD_F = 100X \frac{I_H}{I_{s1}} \quad (4.9)$$

From the equations (4.4), (4.5) and (4.9) the following dependency between CDF and THD_F can be deduced:

$$CDF = \sqrt{\frac{1}{1 + THD_F^2}} = \frac{I_{s1}}{I_S} \quad (4.10)$$

This equation can be re-arranged as:

$$THD_F = \sqrt{\frac{1}{CDF^2} - 1} \quad (4.11)$$

The usefulness of equation (4.10) is illustrated in Chapter 5 where, based on acquired waveform data from power electronics circuits, the THD_F is calculated and consequently the CDF. Similar to equation (4.9), the total harmonic distortion factor can also be calculated relative to the total rms, in which case it is denominated as THD_R .

In many applications it is important to know the peak value $I_{s,peak}$ of the line-current waveform in Figure 4.2 as a ratio of the total rms current I_s , which is defined as crest factor (CF).

$$CF = \frac{I_{s,peak}}{I_s} \quad (4.12)$$

In diode rectifiers the DPF is better than 0.9; however, for given I_d and V_d the power factor is very poor (circa 0.5) at small L_s due to high distortion in the line-current waveform and improves at approximately 0.75 as the L_s value increases. More concrete appreciation of the dc-link filter influence on the input current THD is given in Chapter 7.

A comprehensive treatment of power factor in systems producing nonsinusoidal variables is given in [25], which illustrates the degree of confusion and controversy that still exists about the concept of power factor for nonsinusoidal variables.

4.3 Three-phase full-bridge rectifiers

Three-phase ac voltages are available for most industrial applications making the three-phase rectifiers preferred to the single-phase topologies. In comparison to single-phase, three-phase rectification offers lower ripple content in the waveforms and higher power capability keeping the three-phase power distribution balanced and lowering the currents flowing through cables.

The most widely used rectifier is the three-phase six-pulse diode bridge illustrated in Figure 4.3. When the dc-link filter consists of the capacitor by itself, the input current is very distorted and consequently the power factor of the bridge is low. The output voltage is pulsed (6 pulses per cycle) and the voltage ripple depends on the

size of the capacitor. Very often an inductor is used to improve the current waveform (to lower the harmonic content I_H) and the ripple in the voltage waveform and it is placed on the dc side between the rectifier and the filter capacitor.

It is possible to calculate the minimum value of inductance L_{min} required to make the current i_{dc} continuous for given values of I_{dc} and input voltage at the line frequency. It can be shown [26] that its value is given by the equation:

$$L_{d,min} = \frac{0.013V_{LL}}{\omega I_{dc}} \quad (4.13)$$

where V_{LL} is the effective value of the line-line voltage and $\omega=(2\pi f)$ is the line frequency in radians per second (rad/s).

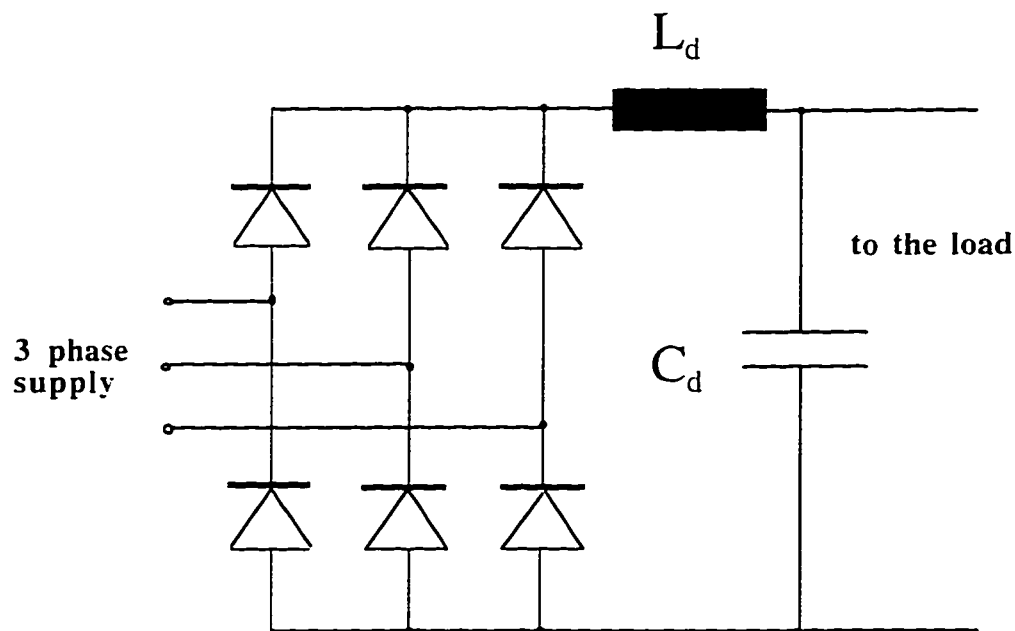


Figure 4.3 Three-phase diode-bridge rectifier with LC dc-link filter.

For continuous conduction, the mean value of the output voltage of the bridge is of constant value

$$V_{dc} = \frac{V_{LL}/\sqrt{2}}{\pi/3} = 1.35V_{LL} \quad (4.14)$$

The effect of L_d on the average voltage V_{dc} is illustrated in Figure 4.4 [14]. The power factor variation as a function of L_d is given in Figure 4.5 [18], which illustrates the attractiveness of the three-phase diode-bridge as input stage for variable speed drives using ac-dc conversion. (PF=0.955 is a good value for most application).

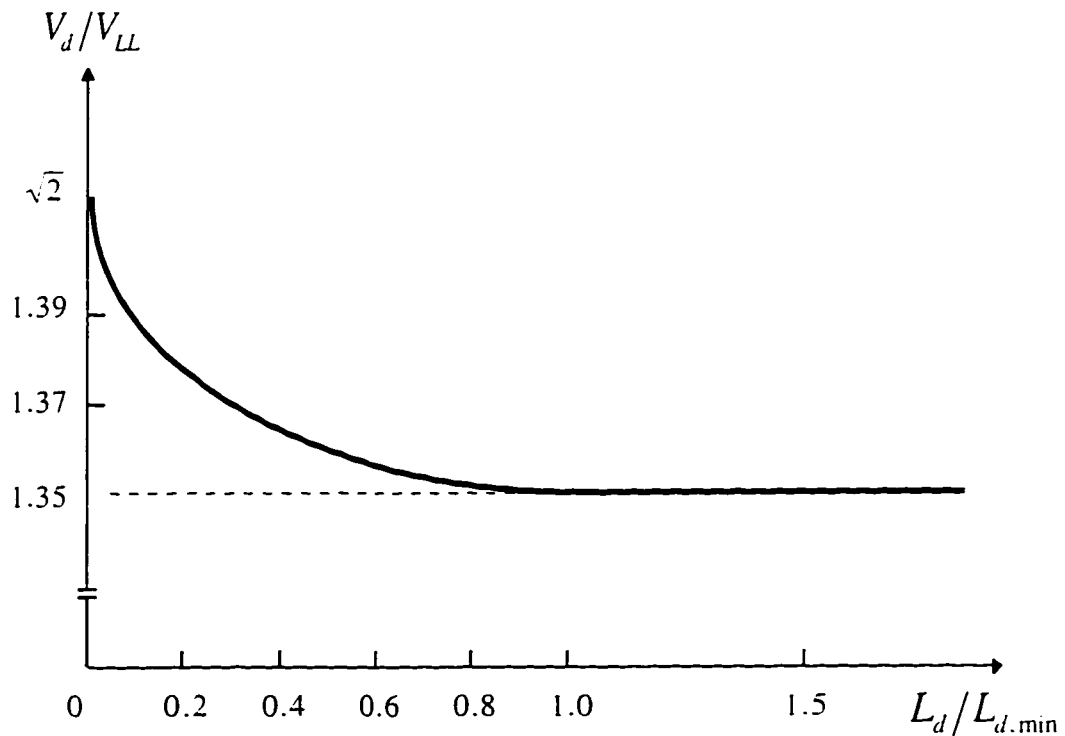


Figure 4.4 The influence of the dc-link inductor size on the dc output voltage [26].

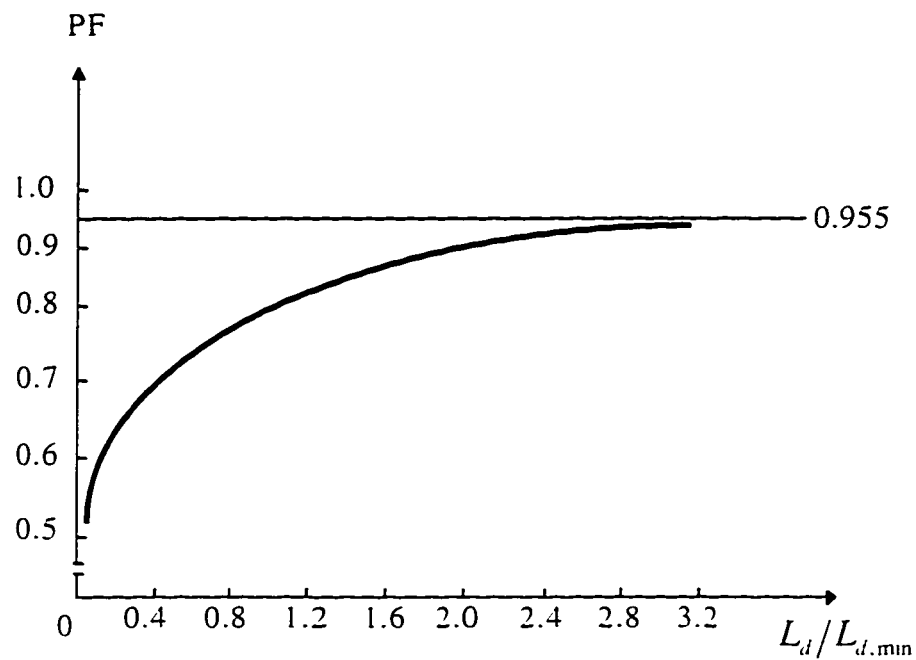


Figure 4.5 Effect of L_d on power factor [26].

The three-phase diode-bridge is simple, not expensive and reliable but its major disadvantage lies in the high THD_1 value. This issue is treated in more detail in section 4.3.

Typical waveforms for the input voltage and current for C dc-link filter and LC dc-link filter are given in Figure 4.6 and Figure 4.7 respectively.

In the previous discussions the ac source inductance L_s was considered of negligible value. In reality a certain non-zero L_s value will always be present leading to commutation overlap. The commutation overlap has a positive contribution in reducing

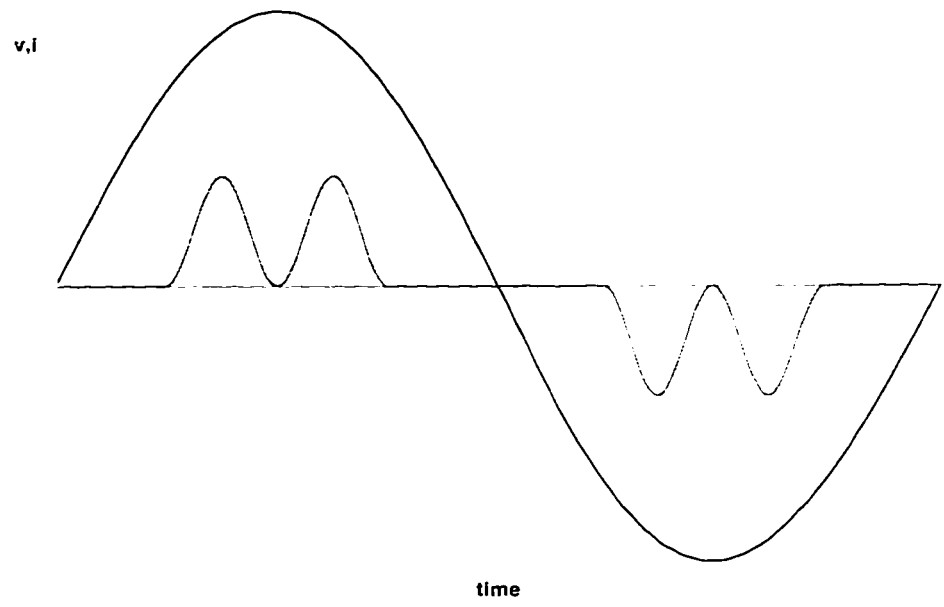


Figure 4.6 Input V_{LL} and I_s for three-phase diode bridge with C filter and R load.

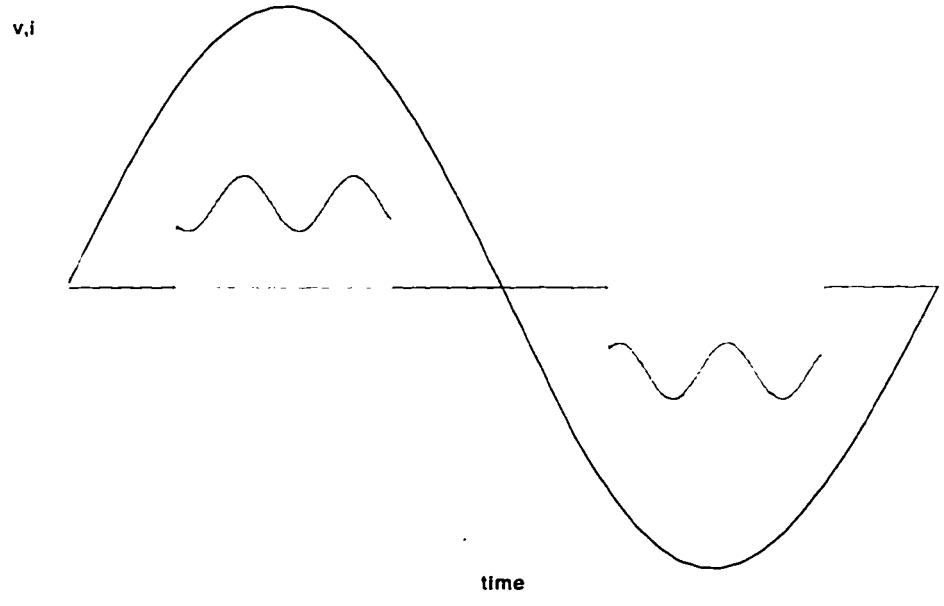


Figure 4.7 Input V_{LL} and I_s for three-phase diode bridge with LC filter and R load.

the THD of the input current. In many cases an input transformer is used to provide the necessary level of input voltage, to filter triple-n harmonics (when in Δ -Y connection) and to provide a electrical isolation between the power system and the converter.

The THD of the input current for a three-phase diode rectifier depends on the dc-link filter topology as well as on the power system parameters. SPICE simulations for “stiff” ac-supply (low ac-side inductance) and an LC dc-link filter with two identical magnetically coupled inductors placed in the positive and negative dc-bars respectively, give a value of $\text{THD}_i=32\%$ (Figure 4.8 (a)). When the same value of inductance is placed in each phase at the input of the bridge and the dc-link filter consists only of the capacitor, the input current distortion is approximately $\text{THD}_i=22\%$ (Figure 4.8 (b)) [12,27,29].

In many modern induction motor variable speed drives, the input stage consists of a three phase full-bridge diode rectifier. In applications where a higher cost is justified, multi-level input is provided by using a Δ - Δ / Δ -Y input transformer and two diode bridges connected in series or parallel that provide a 12 pulse dc-output. For a higher number of pulses, different combinations of Y, Δ and zig-zag connections are used in a multi-wind input transformer [30]. In this manner the THD for the input line current is reduced significantly. The disadvantages associated with multi-pulse transformers are higher price and increased volume of the drive.

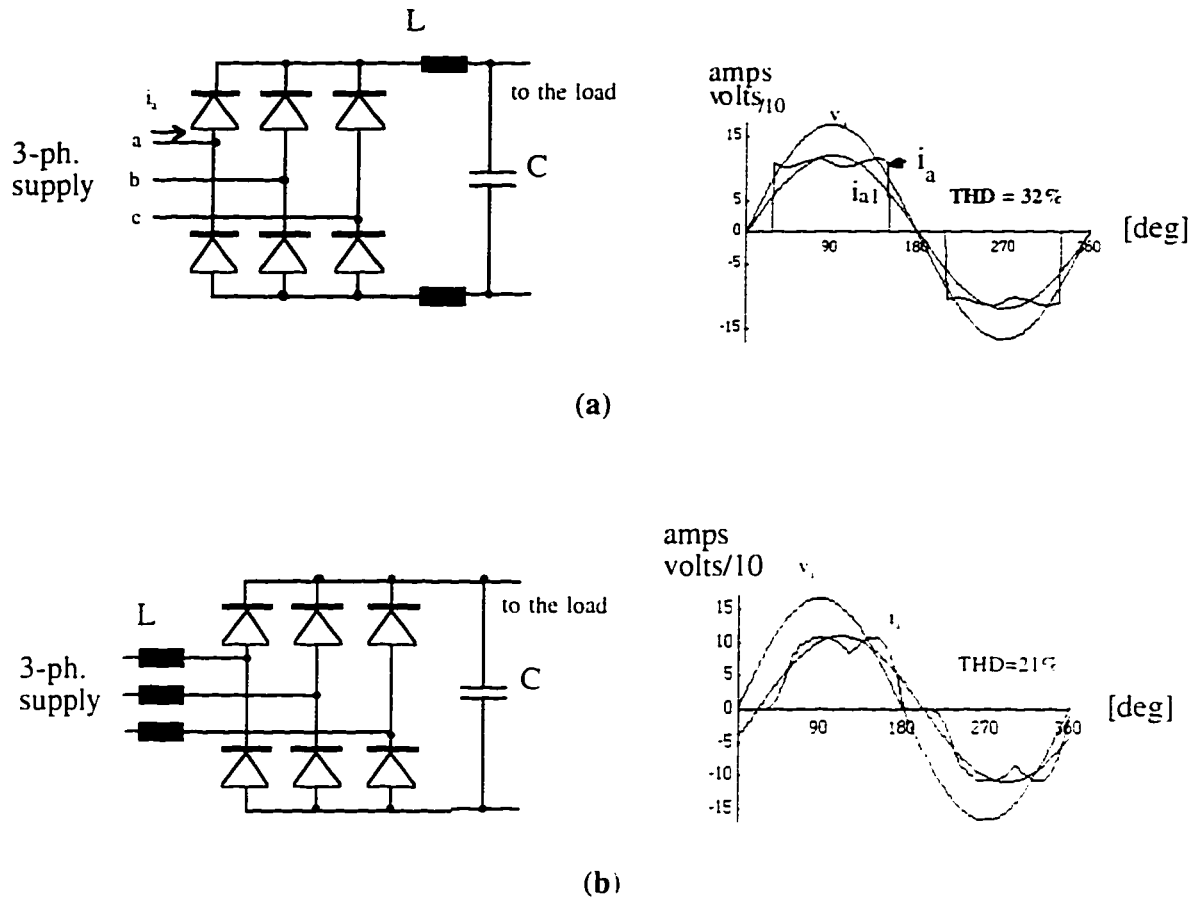


Figure 4.8 Three phase rectifiers and input waveforms: (a) diode bridge with a dc inductor: (b) diode bridge with ac inductors.

The proliferation of power electronic systems has the potential for a significant negative impact on the utilities themselves, as well as their customers. One approach to minimize this impact is to filter the harmonic currents and the electromagnetic interference produced by the diode bridge interface. Another alternative is to design the power electronic equipment such that the harmonic currents and the EMI are either lowered or prevented from being generated in the first place. Quality constrains

regarding load generated harmonics will lead to low harmonics utility interfaces for power electronic circuits in spite of the increase in price.

4.4 Harmonic correction circuits

The problems due to the harmonic currents i_h in the input current i_s are illustrated using the simple block diagram shown in Figure 4.9. Because the internal impedance L_s of the utility source is finite (non-zero), the voltage waveform at the point of common coupling (PCC) to the other loads will become distorted, which can cause interference and malfunctioning.

Furthermore, the harmonic currents i_h cause other undesirable effects such as: heating and overvoltages (due to resonance conditions) in the utility's distribution and transmission equipment, errors in metering and malfunction of utility relays and interference with communication and control signal [22],[25].

4.4.1 Current harmonics and power factor

Diode rectifiers are used to interface single-phase as well as three phase utility voltages. Their current waveforms consist of large harmonic magnitudes and for a finite (non-zero) internal per-phase source impedance L_s , the voltage at PCC (Figure 4.9) will be significantly distorted. This distortion is directly proportional with the value of the internal source inductance L_s .

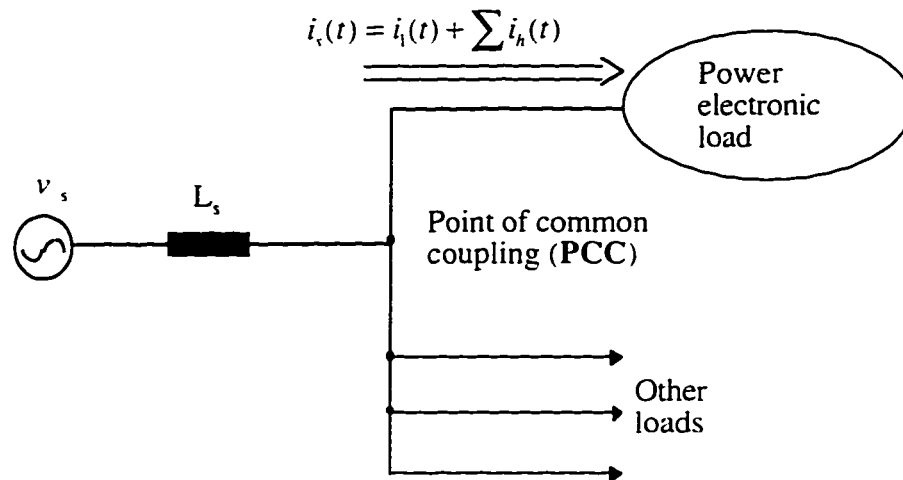


Figure 4.9 Block diagram of utility interface.

The power factor PF at which an equipment operates is the product of the current distortion factor CDF and the displacement power factor DPF. Considering equations 4.4 and 4.5 the power factor is expressed as

$$PF = \frac{P}{S} = \frac{I_{s1}}{I_s} \cdot \cos \phi_1 = CDF \times DPF \quad (4.15)$$

PF indicates how effectively the equipment draws power from the utility: For a given level of power and voltage, a low PF means that the current drawn by the equipment is large, requiring large apparent power ratings of the supplying equipment such as transformers, transmission lines and generators. Thus, it is necessary to design

power electronic circuits with high PF, as closed to the unity as possible. This requires a high DPF and low current harmonics I_h to yield a high CDF.

4.4.2 Harmonic Standards and Recommended Practices

Different national and international agencies have been considering limits on harmonic current injection to maintain good power quality in view of the proliferation of power electronic equipment. Various standards and guidelines have been established that specify limits on the magnitudes of harmonic currents and harmonic voltage distortion at various harmonic frequencies [14, 31-33]. The Comite Europeen de Normalization Electrotechnique (CENELEC), International Electrical Commission (IEC) and VDE - German Standards specify the limits on the voltages (as % of the nominal value) at various harmonic frequencies of the utility frequency when the equipment-generated harmonic currents are injected into a network whose impedances are specified. In contrast, the IEEE-519 Standard specifies requirements on the user as well as on the utility [13,14].

At the point of common coupling (PCC) in Figure 4.9, the voltage distortion depends on the internal impedance of the ac source Z_s and the magnitudes of the injected current harmonics. The internal impedance of the source is highly inductive and therefore is represented by L_s in the block diagram. The effective value of the voltage harmonic h at the line frequency ω at PCC is

$$V_h = (h\omega L_s)I_h \quad (4.16)$$

where I_h is the h harmonic current injected into the ac source.

It is usual practice to specify the internal inductance L_s in terms of short-circuit-current I_{SC} at PCC. Considering the per-phase reference, I_{SC} is the per-phase rms current supplied by the ac source to the fault if all three phases are shorted to the ground at PCC and is expressed as

$$I_{SC} = \frac{V_s}{\omega L_s} \quad (4.17)$$

where V_s is the effective value of the per-phase internal voltage of the ac source assumed to be sinusoidal. An ac system of large capacity at the PCC has a large value for I_{SC} (this was named "stiff" supply in previous discussions). Based on equations (4.16) and (4.17), the harmonic voltage can be expressed as a ratio of the nominal system voltage V_s in percentage:

$$\%V_h = \frac{V_h}{V_s} \times 100 = h \frac{I_h}{I_{SC}} \times 100 \quad (4.18)$$

Considering the line-frequency component of the current I_{S1} drawn by the power electronic load and dividing both I_h and I_{SC} in equation 4.18 by I_{S1} the percent voltage harmonic will be:

$$\%V_h = h \frac{\left(\frac{I_h}{I_{s1}} \right)}{\left(\frac{I_{sc}}{I_{s1}} \right)} \times 100 \quad (4.19)$$

The ratio (I_{sc}/I_{s1}) in equation 4.19 represents the capacity of the utility system with respect to the fundamental-frequency volt-amperes of the load. The equation 4.19 shows that for an acceptable harmonic voltage distortion in percentage, the harmonic current ratio (I_h/I_{s1}) can be higher (although not in linear proportion) for a higher (I_{sc}/I_{s1}) ratio. Moreover, because the internal impedance of the ac system is highly inductive, the harmonic voltage distortion in equation 4.19 is proportional to the harmonic order h . Consequently, the maximum allowable harmonic current ratio (I_h/I_{s1}) decreases (not linearly) with increasing harmonic order h . The total harmonic distortion (THD) increases with (I_{sc}/I_{s1}) [14].

The total harmonic distortion in the voltage can be calculated in a similar manner to equation 4.9:

$$THD_V = \frac{\sqrt{\sum_{h=2}^{\infty} V_h^2}}{V_{s1}} \quad (4.20)$$

Reference [32] is a thorough work in developing harmonic guidelines by establishing an equitable procedure for the control of harmonic distortions shared between the energy producer and its customers.

4.4.3 Improved utility interface

Typical diode rectifiers used for interfacing power electronic equipment with the utility system exceed the limits on individual current harmonics and THD specified in standards due to their large input current harmonic content. In addition to the effect on the power-line quality, the poor waveform of the input affects the power electronic equipment itself in the following ways: reduces the available power to approximately two thirds of the power delivered when the current is sinusoidal. stresses the dc-link capacitors (large pulsed current. Figure 4.7) . increases losses in the diodes (current dependent voltage drop) and derates the input transformer [26.30].

Passive filters can be used in conjunction with the diode-bridge rectifier to improve the waveform of the current drawn from the utility grid. The simplest approach is to add an inductor on the ac side of the rectifier bridge that results in a higher effective value of the ac-side inductance L_s . The improvement of the power factor and the harmonic reduction are illustrated in Figure 4.8 (a) and (b).

Currently, novel utility interfaces are developed which incorporate *active filters* i.e. power electronic converters and networks for current shaping and improvement of the power factor. A boost converter in the dc-link as shown in Figure 4.10 can shape the input current drawn by the diode bridge rectifier to be sinusoidal and in phase with the input voltage. This topology is recommended for several reasons: many applications (e.g. variable speed drives) do not require electrical isolation between the utility input and the output of the power electronic system; the input current in an ideal case is at a unity power factor making the power electronic interface look as a resistor from the utility perspective; for many application it is desirable to have the dc-link voltage stabilized at a slightly higher value than the peak of the maximum ac supply

voltage; the power losses and size of this current shaping circuit is low. The C_d is used to minimize the ripple of the dc-output voltage and to provide for the energy storage requirements of the power electronic system [26]. The disadvantages associated with active filters are increased complexity that reflects into lower reliability and higher price.

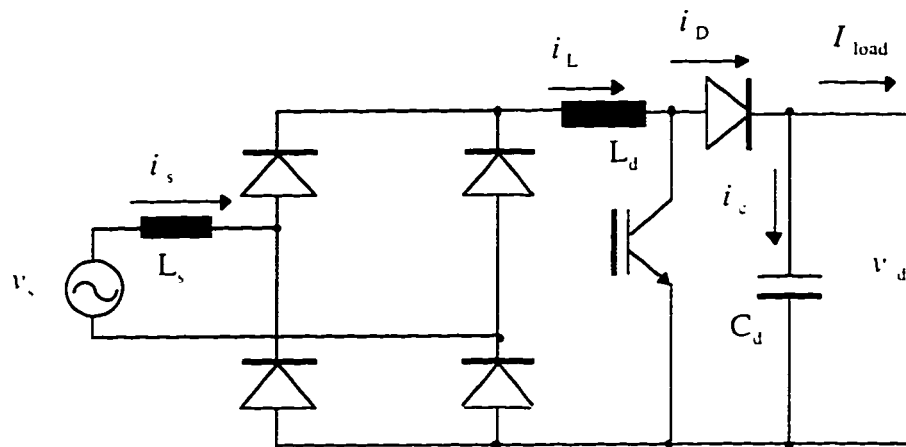


Figure 4.10 DC-link boost converter used as harmonic filter and PF correction unit.

New approaches for passive, active and hybrid filtering techniques in conjunction with 3-phase diode bridge utility interface are proposed in [34-37]. Some of these topologies involve additional transformers rated as high as 0.43 pu at the drive's VA rating. Novel harmonic correction circuits for variable speed drives employing thyristor networks as retrofit units are presented in [12.28.29]. The circuit illustrated in Figure 4.11 lowers the input line-current THD_l from 32% to 5%, without lowering the power factor and without using input filters. The Y-connected switch network employs IGBT or GTO switches and can operate with low switching

frequencies. The additional network is rated at less than 0.15 p.u. and draws 0.06 p.u. power which is passed to the dc-rail.

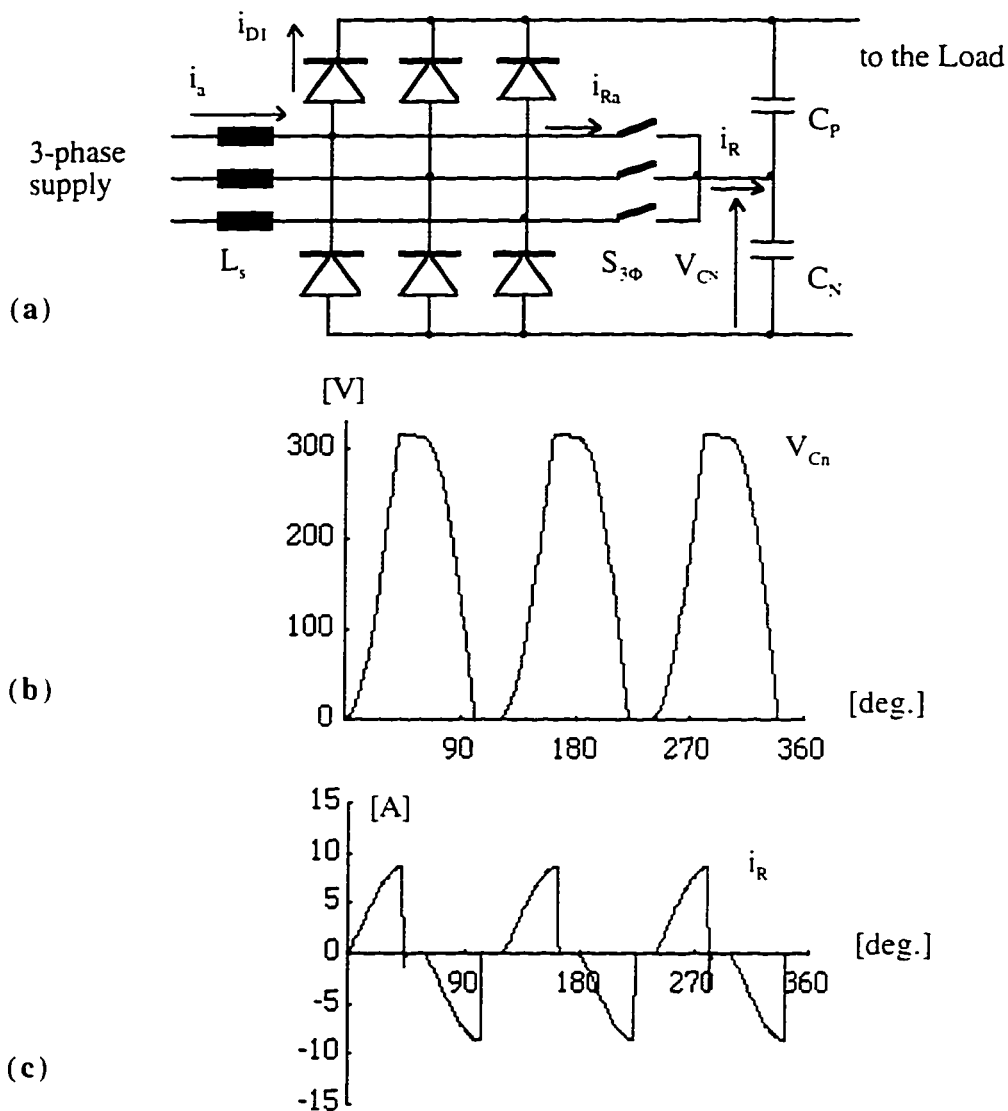


Figure 4.11 Three phase diode bridge utility interface using a 3-phase Y-switch network with resonant capacitors for harmonic correction: (a) schematic, (b) capacitor resonant voltage V_{Cn} , (c) capacitor resonant current i_R [12].

The improved rectifier basic function can be summarized as drawing resonant current pulses from the ac-supply during the zero current regions commonly associated with standard 3-phase diode bridge rectifiers. The current pulses (Figure 4.11 (c)) build up the input current prior to the diode conduction periods, resulting in an improved supply current. Figure 4.12 illustrates SPICE simulated waveforms associated with the improved utility interface rectifier shown in Figure 4.11.

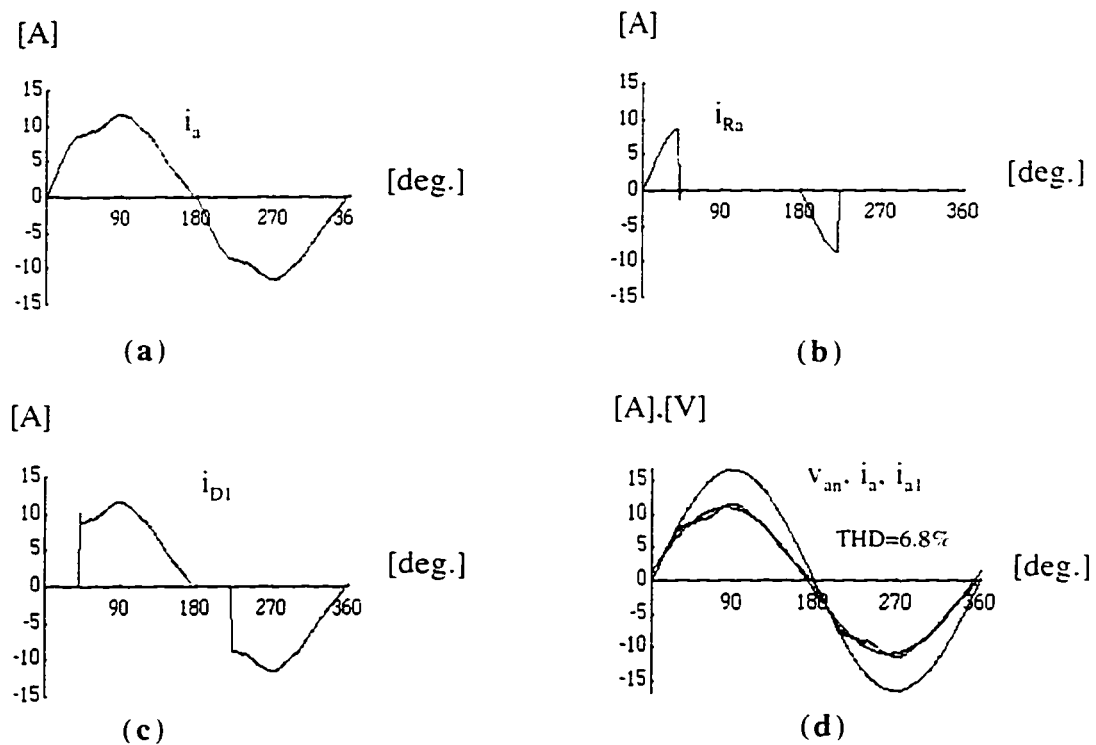


Figure 4.12 SPICE Simulated waveforms for the resonant mode 3-phase Y-switch rectifier: (a) phase-a input current. (b) phase-a resonant current. (c) diode D1 current. (d) phase-a current with the fundamental harmonic and phase-a voltage.

The resonant action also allows a low stress commutation of the rectifier diodes and thyristors. This allows slow switching thyristors and diodes to be used and makes the design and physical layout of the power converter topology non-critical. The harmonic reduction circuitry is suitable as a drive retrofit. Chapter 8 presents passive resonant harmonic correction circuits for 3-phase diode bridge rectifiers which are investigated by means of the data acquisition system described in Chapter 5.

Applications of power electronic equipment increases continuously, especially because of their ability to provide better process control and to conserve energy. It is estimated that by the year 2000 fully 60% of the total electrical power will be processed by solid-state methods [30]. Most variable speed drives and many other applications interface with the electric utility using the diode bridge rectifier. This chapter introduced the power quality factors in conjunction with the diode bridge input stage of power electronic circuits. The quality factors are employed in performance calculations for waveforms analysis obtained by the instrument described in Chapter 5. The harmonic pollution due to power electronic circuits was addressed followed by the description of novel harmonic correction units for three phase diode bridge rectifiers. Data acquisition technology enables accurate measurement of power quality factors of different power electronic circuits. The following chapter present the software environment and the development of a DAQ system for waveform acquisitions and analysis (Chapters 5). The DAQ system is then employed for analysis of single-phase, three-phase and 12-pulse series rectifiers described in this chapter (Chapter 6).

Chapter 5

Data Acquisition Virtual Instrument

The system for data acquisition and analysis, illustrated in Figure 5.1 consists of the following: a Power Macintosh 7100/66 computer running LabVIEW 4.0 interfaced with a Digitizing four channels oscilloscope via an NI-488 card and GPIB cable. The oscilloscope is acquiring waveforms from the circuit under investigation via voltage attenuators and Hall-effect current probes.

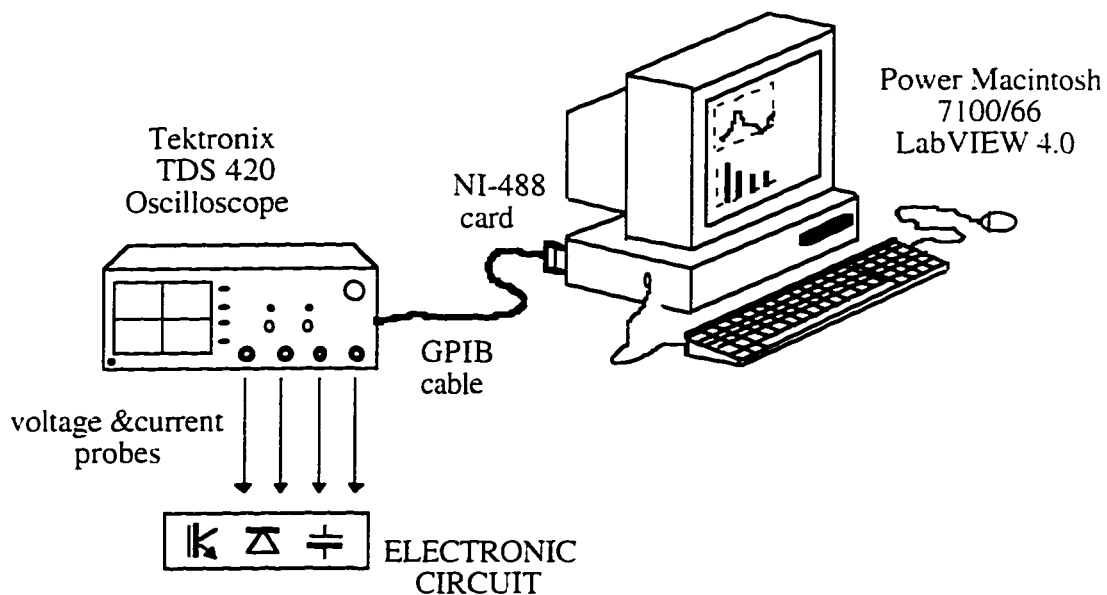


Figure 5.1 Developed data acquisition and analysis system: general arrangement.

This chapter describes specific functions of the hardware employed in the DAQ system, the main features of the LabVIEW environment and the developed Virtual Instrument (VI) for DAQ, analysis and power and performance calculations.

5.1 The digitizing oscilloscope

The signals to be acquired and analyzed are obtained by the Tektronix TDS 420 oscilloscope via voltage attenuators and Hall-effect current probes.

The digitizing oscilloscope acquires four channels, each with a record length of 500 to 15000 points and 8-bit vertical resolution. All four channels are acquired simultaneously at the maximum digitizing rate of 100 Megasamples/second at the full analog bandwidth of 150 MHz. The full programmability feature of the oscilloscope makes possible the serial communication with the computer via GPIB cable.

The acquisition system of the oscilloscope has five modes of operation for converting analog data into digital form: sample, peak detector, high resolution, envelope and average. The first three modes operate in real-time on a single trigger event, provided that the oscilloscope can acquire enough samples for each trigger event. Envelope and average modes operate on multiple acquisition.

Of special interest for the developed data acquisition system described in this chapter is the High Resolution (Hi Res) mode. In this mode, the digitizing oscilloscope averages all samples taken during an acquisition interval to create a record point, as shown in Figure 5.2. An acquisition interval is the time covered by the waveform record divided by the record length. The average results in a higher-resolution, lower-bandwidth waveform. A key advantage of Hi Res mode is its potential in increasing resolution to obtain up to 15 significant bits regardless of the input signal. Resolutions

above 15 bits are not allowed by internal oscilloscope hardware and computation limitations [38].

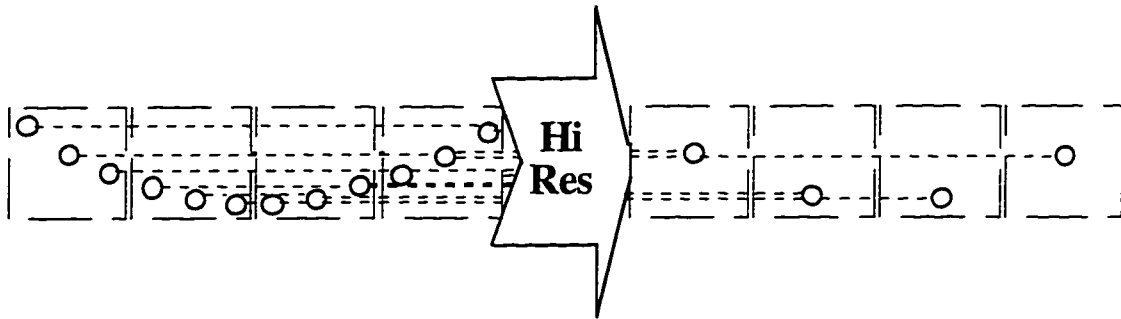


Figure 5.2 Oscilloscope sample averaging in High Resolution mode.

The sampling interval for the Tektronix TDS 420 is $SI=10ns$. For a time base speed of $2ms/Div$, the sample interval Δt is obtained from the above definition as

$$\Delta t = \frac{Time/Div}{NumberPoints/Div} = \frac{2ms/Div}{50Points/Div} = 40\mu s$$

Consequently, the number of points per decimation interval is

$$N_d = \frac{\Delta t}{SI} = \frac{40\mu s}{10ns} = 4000$$

and the resolution enhancement (RE) in bits is given by the expression [38]

$$RE(bits) = 0.5 \times \log_2(N_d) = 0.5 \times \log_2 4000 = 5 \text{ extra bits.}$$

In the above example, which corresponds to the time base employed for acquiring one cycle of a 60 Hz fundamental signal, the oscilloscope provides 13 bits of resolution.

Regarding the acquisition synchronization, the delay between channels is specified by the oscilloscope's manufacturer as less than 200ps between Channel1 and Channel2 and between Channel3 and Channel4 when both channels have equal volts/division and coupling settings, and less than 450ps for any other combination of two channels [38]. For the measurements concerning the power electronic circuits described in Chapters 6, 7 and 8, this synchronization accuracy is sufficient.

5.2 LabVIEW overview

LabVIEW - Laboratory Virtual Instrument Engineering Workbench - is a National Instruments program development application, similar to various commercial C or BASIC development systems. However, LabVIEW is different from those applications in one important respect. Other programming systems use text-based languages to create lines of code, while LabVIEW uses a graphical programming language, G, to create programs in block diagram form. The basic features of LabVIEW, the programming tools, and functions available for writing G code are described in Appendix B. The software is employed to develop the virtual instrument for DAQ, waveform analysis and power and performance factors calculations from power electronic circuits. LabVIEW offers user friendly capabilities by reproducing the appearance of a real instrument on the computer screen. The data acquired can be saved on disk in different formats and further waveform analysis can be performed. The tools

description and the overview of the basic functions available in LabVIEW are presented for a good understanding of the programming techniques employed for the development of the virtual instrument (see Appendix C).

LabVIEW programs are called virtual instruments (VI) because their appearance and operation imitate actual instruments. However, they are analogous to functions from conventional language programs. VIs have both an interactive user interface and a source code equivalent and accept parameters from higher-level VIs.

LabVIEW uses terminology, icons, and ideas familiar to scientists and engineers and relies on graphical symbols rather than textual language to describe programming actions.

The interactive user interface of the VI - the **front panel** - simulates the front panel of a physical instrument. The front panel contains knobs, push buttons, graphs and other controls and indicators. After acquiring the data, the results are viewed on the computer screen. The instructions for the VI are contained by a **block diagram** which is constructed using the language G. The block diagram supplies a pictorial solution to the programming problem and it contains the code for the VI. The VIs use a hierarchical and modular structure. A VI within another VI is called a subVI. The **icon and connector pane** of a VI work like a graphical parameter list so that other VIs can pass data to it as a subVI.

With the three above listed features, LabVIEW promotes and adheres to the concept of modular programming. The application is divided into a series of tasks which can be divided again until a complicated application becomes a series of simple subtasks. A VI is developed to accomplish each subtask and then, by combining these

low-level VIs on another block diagram, the larger task is accomplished. Finally, the top-level VI contains a collection of subVIs that represent application functions (see Appendix C). Because each subVI can be executed by itself, apart from the rest of the application, debugging is a relatively easy task. Furthermore, many low-level subVIs often perform tasks common to several applications so that a set of specialized subVIs can be developed that suits to a multitude of applications.

5.3 DAQ and analysis system

The LabVIEW data acquisition and analysis program developed has two distinctive components: the **front panel** which is a user-friendly interface imitating the appearance of a real instrument (see Figure 5.3) and the background code represented by the **block diagram** (Figure 5.4). Each of these components can be viewed as consisting of two individual parts: the data acquisition part and the data analysis part performing harmonic analysis and power and performance factors calculations.

The hierarchical nature of the program mentioned in section 5.2 is illustrated in Figure 5.5. Each subVI represented by a block in the hierarchy has its own front panel and block diagram.

The data acquisition part of the front panel features a graph or "screen" where the waveforms that have been read are plotted together with the corresponding legend indicating the color assigned to each channel (Figure 5.3). The display looks exactly as it does on the oscilloscope. Probe scaling information is not reflected on the graph. This allows voltages of hundreds of volts to be plotted together with currents of tens of amps, as illustrated by the acquired signals presented in Chapters 6, 7 and 8. Scaling information is available when data is saved to file.

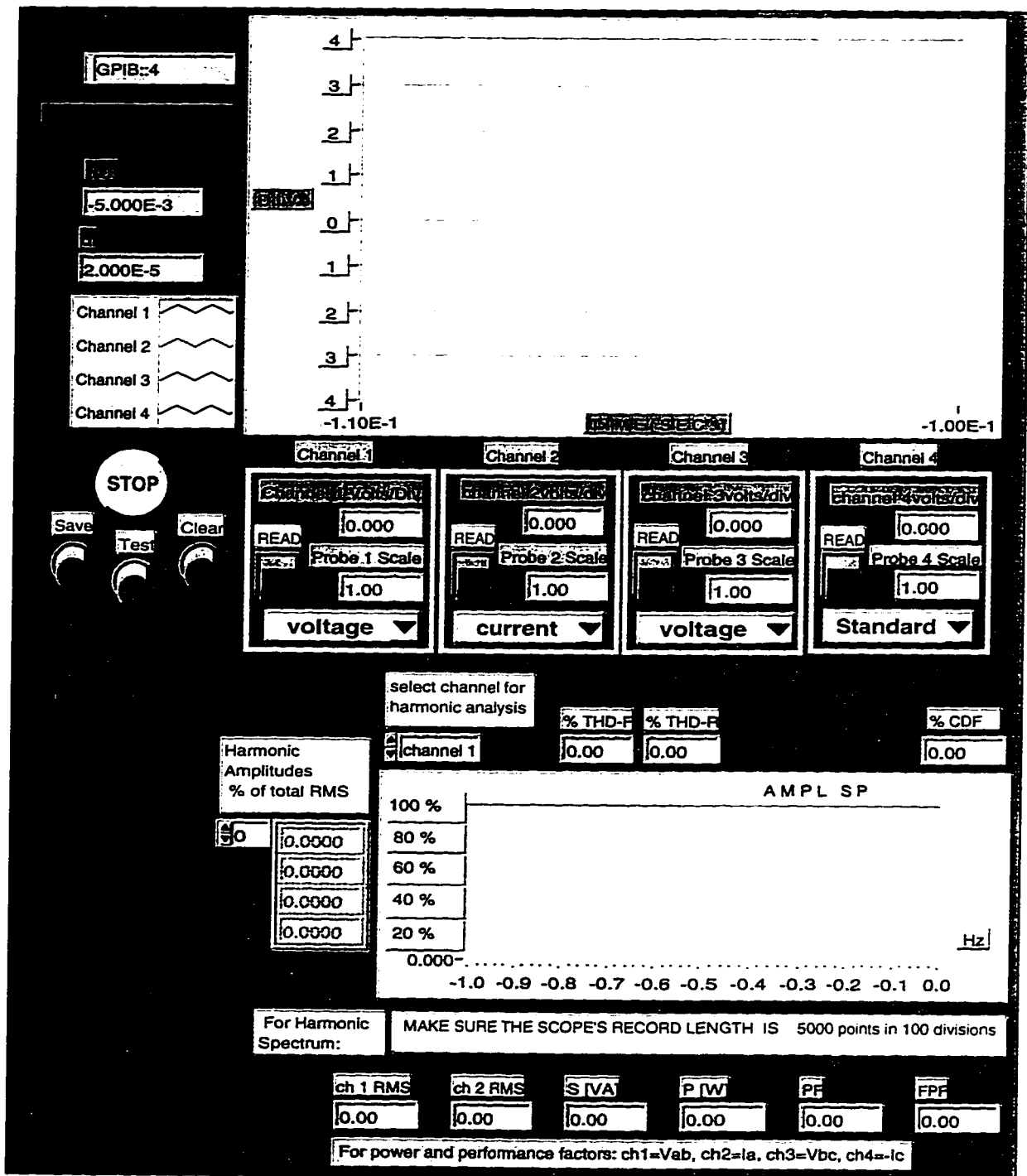


Figure 5.3 Virtual Instrument front panel.

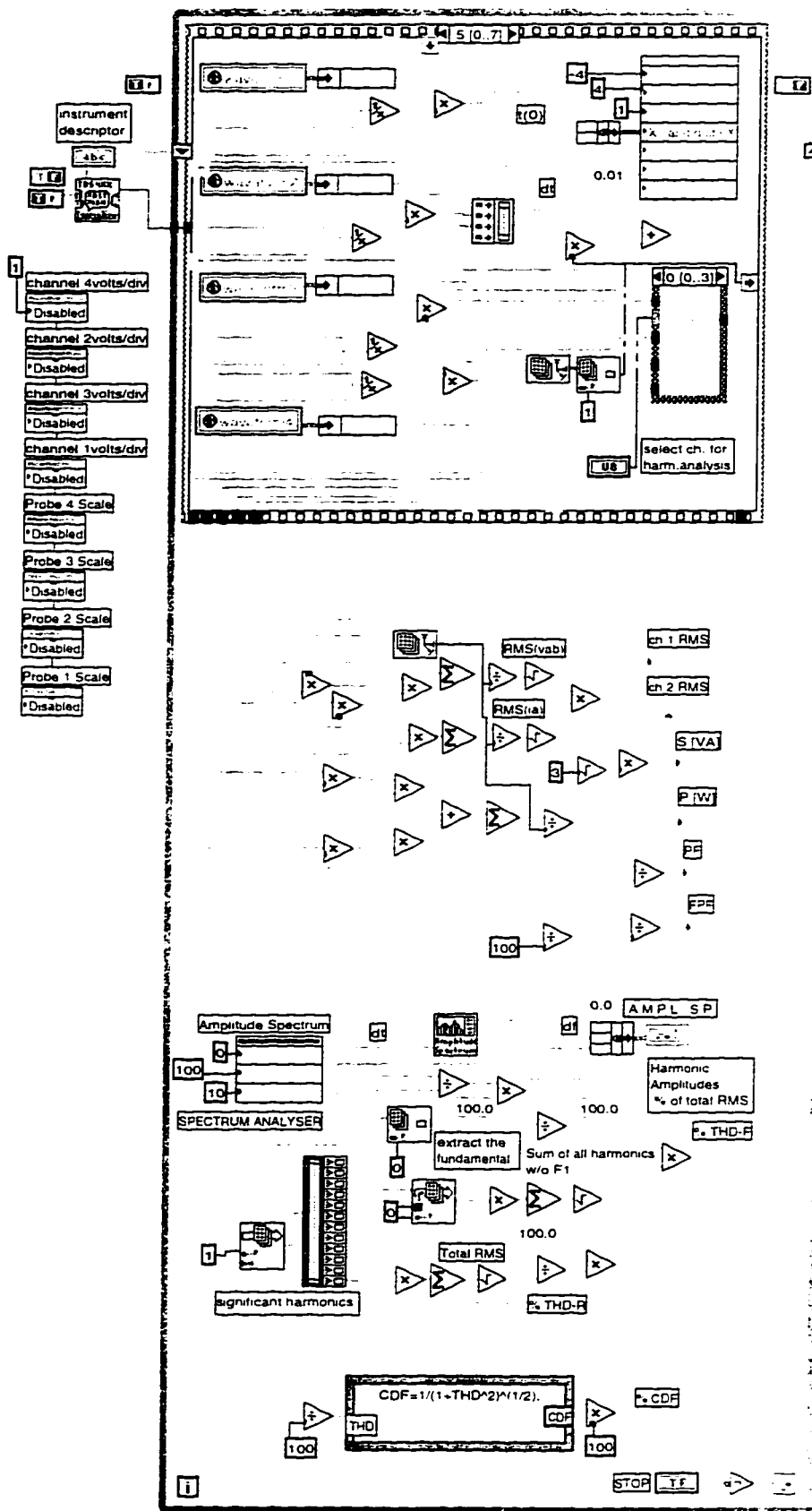


Figure 5.4 Virtual Instrument block diagram.

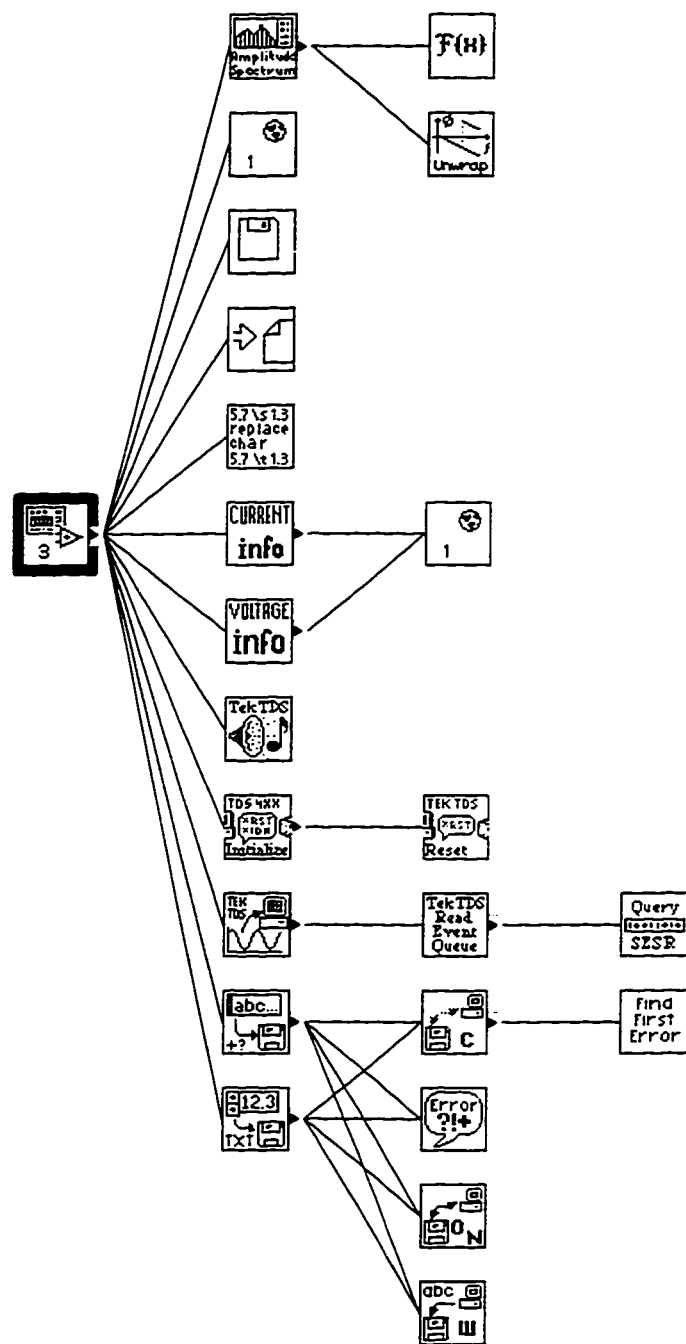


Figure 5.5 Virtual Instrument's hierarchy.

IEEE-519 Standard requires that 12 periods of the fundamental be acquired for obtaining reliable data for harmonic analysis [14]. For this reason, by default, the time axis is spanned over 0.2 s. However these limit can be changed using the labeling tool.

After the digitizing oscilloscope is turned on, a number of controls on the front panel give the user flexibility in acquiring and analyzing data. When data is saved to file, the user is prompted for a file format (either Matlab or Spreadsheet) and a file path name. The spreadsheet format saves the data in tab-delimited columns. The Matlab format saves the data in an array called TDS420. All four channels plus the time array are saved enabling analysis employing different other softwares.

The program prompts the user for scale factors associated with the voltage attenuators and current probes employed in the measurement. If, for example, the acquired waveforms are two voltages and two currents, as in the case of three-phase power measurements, the user is prompted two times to select voltage probe constants and two times for current probe information. The numeric values associated with each probe is employed in program calculations resulting in saved on file voltages and currents expressed in Volts and Amps and power calculations displayed in VA and Watts.

The main program is contained in a While Loop which is controlled by the Stop button on the front panel (see Figures 5.4). The **virtual oscilloscope** waveforms acquisition resides in a Sequence Structure, which performs like frames of film and executes the block diagram sequentially. In conventional programming languages, the program statements execute in the order in which they appear. In data flow programming, a node executes when data is available at all of the node inputs. In this case it is necessary to execute certain nodes in a pre-defined order. LabVIEW places the diagram that the VI executes first inside the border of Frame 0, it places the diagram it

executes second inside the border of Frame 1 and so on. Using this technique, the data acquisition consists of six frames of Sequence Structure that execute the different stages of the process as outlined in the following discussion (Figure 5.6).

The **harmonic analyzer** is a distinctive part of the main virtual instrument developed in this thesis. On the front panel, a numerical ring allows the user to select one of the four acquired signals for harmonic analysis. The analysis subVI plots the harmonic spectrum on the chart and front panel indicators give calculated values for the total harmonic distortion factor relative to the fundamental (THD-F) and relative to the total rms (THD-R). Other front-panel indicators give the calculated value of the current distortion factor (CDF) as well as the power calculations and power factors. The harmonic amplitudes of the signal are listed in the ring indicator beside the chart (see Figure 5.3). This list is resizable with the sizing tool from the tool palette (Appendix B). The index in LabVIEW starts from zero and consequently, to view for example, the 5th harmonic at the top of the harmonic amplitude list, the index has to be set on 4.

The digitizing oscilloscope, set to acquire 5000 data points in 100 divisions in 0.2s, sets the time increment to $\delta t=40\mu s$. This causes the harmonics spectrum to be plotted for a frequency of 12.5 kHz. The circuits investigated in the next chapters display large low frequency harmonics, making the harmonic spectrum histogram not relevant for frequencies larger than 1.2 kHz. For this reason, using the labeling tool, the frequency range of the harmonic spectrum display is set to 1.2 kHz in most cases (see Chapters 6.7 and 8). This covers the first 20 harmonics of a 60 Hz signal. Oscilloscope setup requirements for correct calculations performed by the VI are written as warning labels on the front panel using the labeling tool.

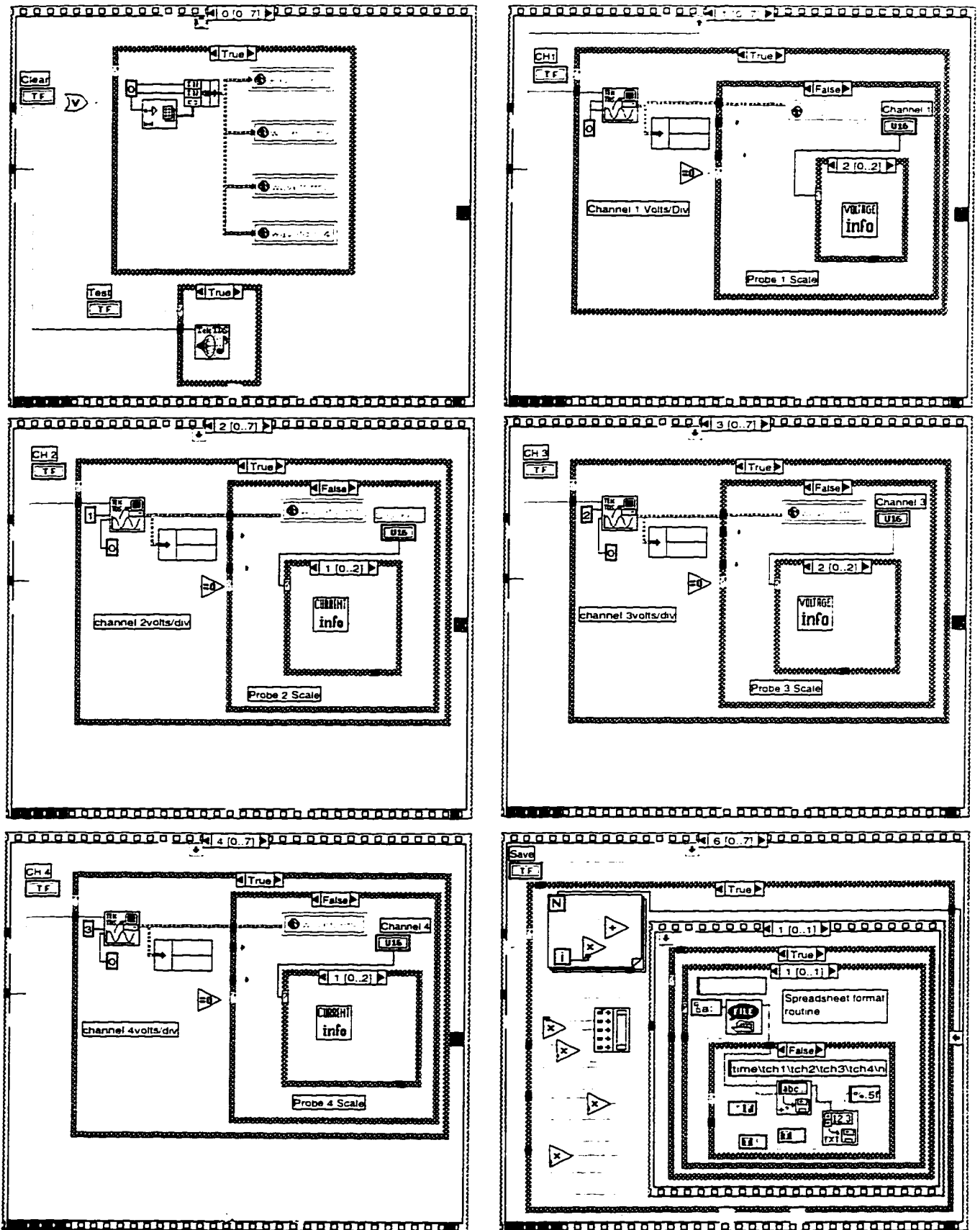


Figure 5.6 Data acquisition sequence structure frames.

The **power and power factors calculations** are performed for a given set-up of the acquired signals. The method of two wattmeters for three-phase power calculations employs two currents and two voltages, as deduced below. Considering the notation in Figure 5.7, the instantaneous power absorbed by the load is

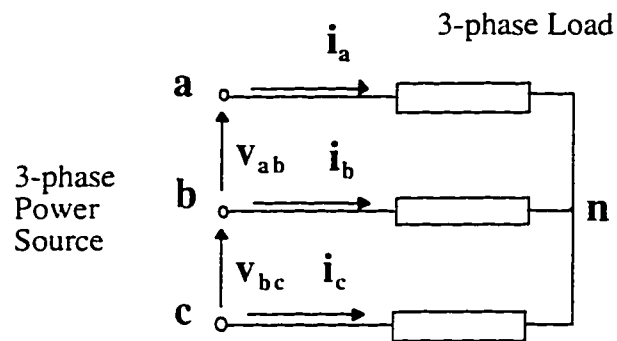


Figure 5.7 Three-phase circuit diagram for power calculation.

$$p = v_{an} \cdot i_a + v_{bn} \cdot i_b + v_{cn} \cdot i_c \quad (5.1)$$

Assuming that $(i_a + i_b + i_c) = 0$, which is the case whenever there is no current flow into or out of the neutral.

$$\begin{aligned} p &= v_{an} \cdot i_a + v_{bn} [-(i_a + i_c)] + v_{cn} \cdot i_c \\ &= (v_{an} - v_{bn}) \cdot i_a + (v_{cn} - v_{bn}) i_c \\ &= v_{ab} \cdot i_a - v_{bc} \cdot i_c \end{aligned} \quad (5.2)$$

The virtual instrument performs power calculations under the following conditions: the oscilloscope channels have to be assigned as ch1: v_{ab} , ch2: i_a , ch3: v_{bc} .

and ch4: -i_c considering the three phases labeled a, b and c, and positive current entering the circuit. The oscilloscope acquired signals are expressed in mV and, prior to calculations, the program multiplies each array by the corresponding probe scale constant which is a local variable in the acquisition subprogram.

As mentioned above, the program performs other calculations from the raw data acquired. These are:

$$\text{rms voltage } V = \sqrt{\frac{1}{n} \sum_{i=1}^n V_i^2}$$

$$\text{rms current } I = \sqrt{\frac{1}{n} \sum_{i=1}^n I_i^2}$$

$$\text{apparent power } S = V \cdot I$$

$$\text{power factor } PF = P/S$$

Power Measurement Accuracy

The digital power measurement is based on the multiplication of the voltage and current signals and can be expressed as

$$P = [v] [i]. \quad (5.3)$$

Therefore,

$$\Delta P = (\Delta v)i + v(\Delta i) \quad (5.4)$$

or, after dividing (5.4) by (5.3),

$$\Delta P/P = \Delta v/v + \Delta i/i \quad (5.5)$$

In order to estimate the accuracy achieved, one has to evaluate the factors that affect the accuracy of the measurement. The accuracy of the Hall-effect current sensors,

according to the manual, is $\pm 1\%$, at a maximum operating permissible operating temperature of 70°C . The bulk of this error is due to drift caused by ambient operating temperature variation ($10\text{E-}4 \times \text{nominal current}/^{\circ}\text{C}$). This variation is small in a laboratory environment and the overall accuracy of the current measurement with Hall-effect probes is conservatively estimated to be $\pm 0.6\%$ [7]. The measurement's precision due to the A/D sampling performed by the digitizing oscilloscope is due to those product harmonics whose frequencies are integer multiples of the sampling frequency (see Chapter 1). The error due to the sampling process is estimated at $\pm 0.25\%$ [1.2.7.8.35]. The voltage attenuators ratio is within $\pm 0.1\%$ for frequencies up to 5kHz. The IGBTs of the PWM inverter investigated in Chapter 7 operate at 1kHz switching frequency and for up to four times the switching frequency (i.e. 4kHz) the voltage probe error remains within $\pm 0.1\%$. Since the contribution to the average power by power harmonic terms above 4kHz is comparatively small, the total error due to the voltage attenuators is estimated at $\pm 0.1\%$. In order to digitize a complete cycle of the signals (i.e. peak-to-peak), a 12-bit vertical resolution of the oscilloscope's A/D converter is sufficient to limit the error due to this effect within $\pm 0.05\%$ [7]. As stated in section 5.3, the Tektronix TDS 420 oscilloscope employs 13-bit vertical resolution when in Hi Res mode for the measurements performed in this work.

The cumulative accuracy of the digital power measurement technique is therefore $(\pm 0.6 \pm 0.25 \pm 0.1 \pm 0.05)\% = \pm 1\%$.

To verify the validity and the accuracy of the measurement system, the quantities obtained from the front panel indicators of the developed Virtual Instrument in the experimental part of the thesis (i.e. Chapters 6-8) were permanently compared with the readings of a commercially available power meter (Fluke-39) which displays an accuracy of $\pm 1\%$. Chapter 7 presents in Tables 7.1 and 7.2 compared results with measurements obtained from a PWM inverter drive system employing both the VI and the Fluke-39 power meter.

This chapter described digital measurement techniques, the digitizing oscilloscope as part of the DAQ system, the LabVIEW environment, the developed program for data acquisition and analysis, and system measurement accuracy estimations. The features provided on the front panel of the virtual instrument (the user interface) are explained in correlation with their role in the block-diagram (the actual code) in Appendix C. The performance of the developed DAQ system is illustrated in the next three chapters. Waveform acquisitions, harmonic analysis, power and performance factors calculations are obtained from a selected number of power electronic circuits including rectifiers, induction motor variable speed drives and research level circuits for harmonic control.

Chapter 6

Experimental Results- Rectifier Circuits

The performance of the LabView data acquisition system is demonstrated in this chapter with reference to the harmonic spectrums and the total harmonic distortion (THD) of the electrical waveforms associated with diode bridge rectifiers. The single-phase and the three-phase diode bridge rectifiers are examined with two output filter topologies: capacitive filter and inductive-capacitive filter. The load in each case is a resistor. These extensively used utility interface rectifiers are treated in Chapter 4. Another front-end topology examined in this chapter is the 12-pulse series rectifier.

The experimental measurement system consists of the following: Tektronix TDS 420 four channel oscilloscope. Power Macintosh 7100/66 computer running LabVIEW 4.0 software. GPIB card NI-488. GPIB cable. high-voltage probe insulators with scaling factors of 1/500 and 1/50, clamp-on Hall-effect current probe insulators with scaling factors of 100 mV/A and 10 mV/A.

6.1 Single phase diode bridge rectifier

Many modern office and household appliances use the single phase diode bridge rectifier to interface to the utility. These are low power level circuits fed from the wall receptacle: 120 V_{ac} at 60 Hz frequency. The negative influence of these non-linear loads on the power quality is increasing especially with the proliferation of computers and office equipment. Variable speed drives for heat pumps and air conditioning, compact fluorescent lights (electronic ballasts), and electric vehicle battery chargers use diode bridge rectifiers in the front end. All of these new nonlinear loads have the potential to

cause residential and commercial loads to become a significant source of harmonics on a distribution system.

6.1.1 Single-phase diode bridge rectifier with C output filter

The single phase diode bridge rectifier with capacitive output filter was introduced in Chapter 4 (Figure 4.1). The experimental circuit used for data acquisition is described by the following values: input voltage $V_{ph} = 115$ V at 60 Hz, input power: $P_{in} = 0.1$ kW, dc-link filter: $C = 940$ μ F, resistive load : $R = 200$ Ω .

The data acquisition rate of 25.0 kS/s is determined by the Tektronix oscilloscope setup. The scaling factors are obtained by multiplying the V/div constant with the probe scale associated to the corresponding channel, which are given by the front panel controls and indicators of the virtual instrument (Figure 6.1).

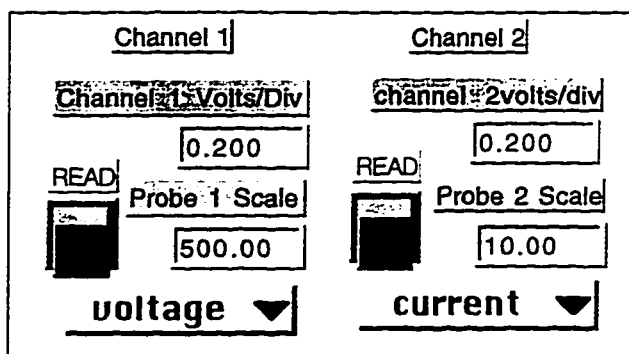
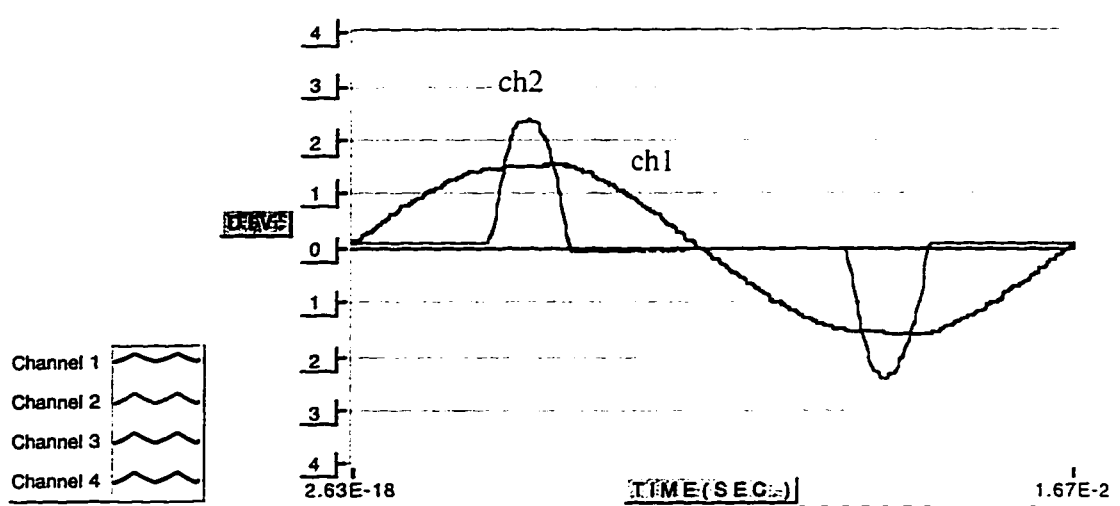
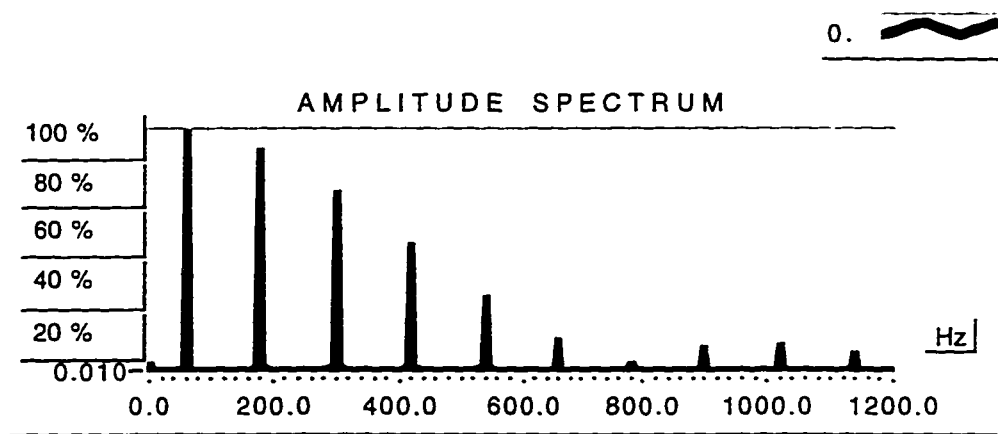


Figure 6.1 Voltage and current scale constants associated with data acquisition from single phase diode rectifier (virtual instrument front panel controls and indicators).

The rectifier input voltage waveforms shown in Figure 6.2 were obtained with the data acquisition system and settings described above. Figure 6.2 (b) shows the input current harmonic spectrum and THD_i , as well as the fundamental current and harmonics expressed as percentage of the total RMS input current.



(a)



% THD-F	% THD-R
132.82	79.89

(b)

I_1	I_3	I_5	I_7	I_9	I_{11}	I_{13}
60.1494	54.5896	44.2414	31.2463	18.1342	6.9575	1.1137

(c)

Figure 6.2 Single phase diode bridge rectifier with C dc-link filter and R load:
 (a) Acquired input voltage and current waveforms (channel 1: phase voltage. channel 2: line current); (b) Input current harmonics spectrum and THD_I ; (c) Fundamental input current and harmonics in per-cent (%) of the total RMS current.

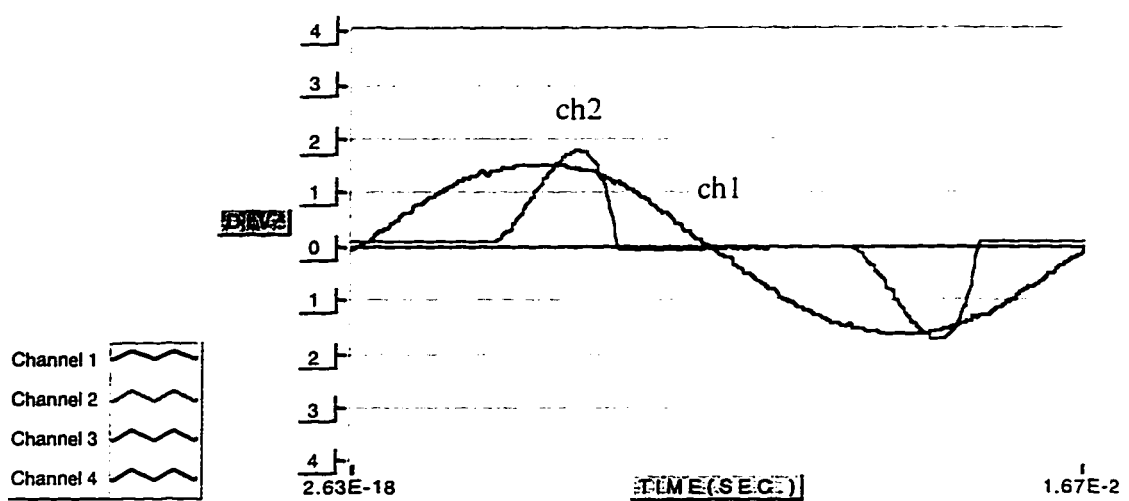
The harmonic amplitudes are available on the front panel of the virtual instrument in a ring indicator. Using the operating tool, the user can browse through the harmonics of the analyzed signal. The maximum harmonic frequency is set by the sampling rate of the data acquisition. For 25 kS/s sampling rate, the harmonic spectrum frequency range is 12.5 kHz. The virtual instrument allows the user to set a smaller frequency range so that only the relevant harmonics are viewed. For 60 Hz fundamental frequency, the harmonics spectrum is illustrated for $f_{\max}=1200$ Hz (Figure 6.2 (b)).

The large low-order harmonics of the input current of the single phase diode bridge rectifier with C filter (Figure 6.2 (c)) makes this topology a major harmonic polluter. The harmonic currents can result in concerns for neutral conductor overheating, transformer overheating, and interference with communication systems. The cumulative effects of the different sources depends on the equipment characteristics and the overall system design.

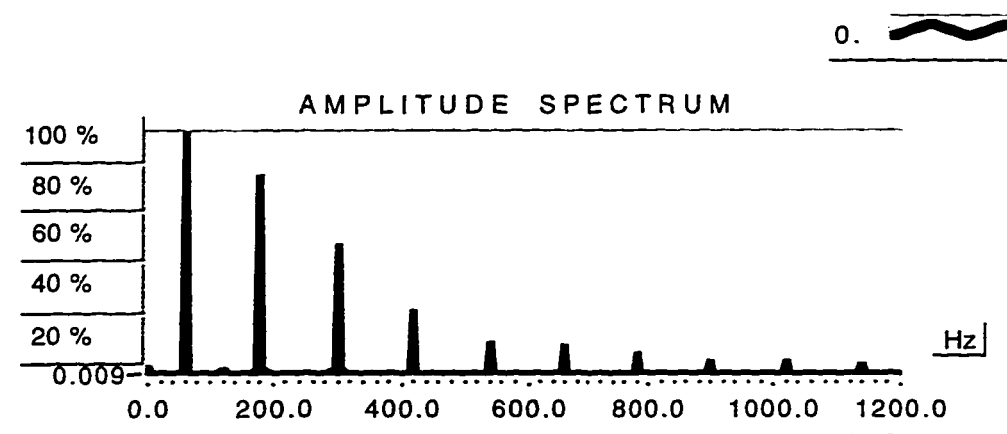
6.1.2 Single-phase diode bridge rectifier with LC filter

Considering the same circuit as in section 6.1.1, by adding an inductor ($L= 2.5$ mH) in the positive rail of the single phase diode bridge rectifier output, the current waveform is flattened (Figure 6.3 (a)) and its harmonic content reduced (Figure 6.3 (b)) in comparison to the capacitive filter topology. The inductive-capacitive filter improves the power performance of the diode bridge rectifier: the larger the inductor the lower the harmonics.

For a better comparison of the two filter topologies with respect to the input current harmonic content, the data acquisition system waveform scales maintained the same values for the input current and voltage in Figures 6.2 and 6.3.



(a)



% THD-F	% THD-R
102.69	71.64

(b)

I_1	I_3	I_5	I_7	I_9	I_{11}	I_{13}
69.7651	57.0641	36.8508	17.8885	8.4204	7.5244	5.5096

(c)

Figure 6.3 Single phase diode bridge rectifier with LC dc-link filter and R load:(a) Acquired input voltage and current waveforms (channel 1: phase voltage, channel 2: line current): (b) Input current harmonics spectrum and THD_i : (c) Fundamental input current and harmonics in per-cent (%) of the total RMS current.

When single phase electronic loads are supplied with a 3-phase, 4-wire circuit, there is a concern for large current magnitudes in the neutral conductor. For relatively balanced circuits, the neutral current magnitude is very small resulting in practice in undersizing the neutral conductor. The triple-n harmonics (3rd, 9th, 15th ..) of the input current of electronic loads supplied by single-phase diode rectifiers show up as zero sequence components in the neutral. Instead of canceling in the neutral as in the case of positive and negative sequence components, the zero components add directly in the neutral. As illustrated in Fig. 6.2 (c) and 6.3 (c), the third harmonic is the largest component in single phase power supplies. In the experimental case the LC filter lowers the third harmonic current with 10% of the fundamental current in rapport to the C filter.

The overloaded neutral conductor can be addressed by some the following solutions: increased neutral conductor cross-section, zig-zag transformer connection on the load side, third harmonic parallel filter on the load side.

On the high voltage side of the 480:120 distribution transformer, the neutral current concern is not significant. The triple-n harmonics are canceled in the delta connected primary windings.

6.2 Three phase diode bridge rectifier

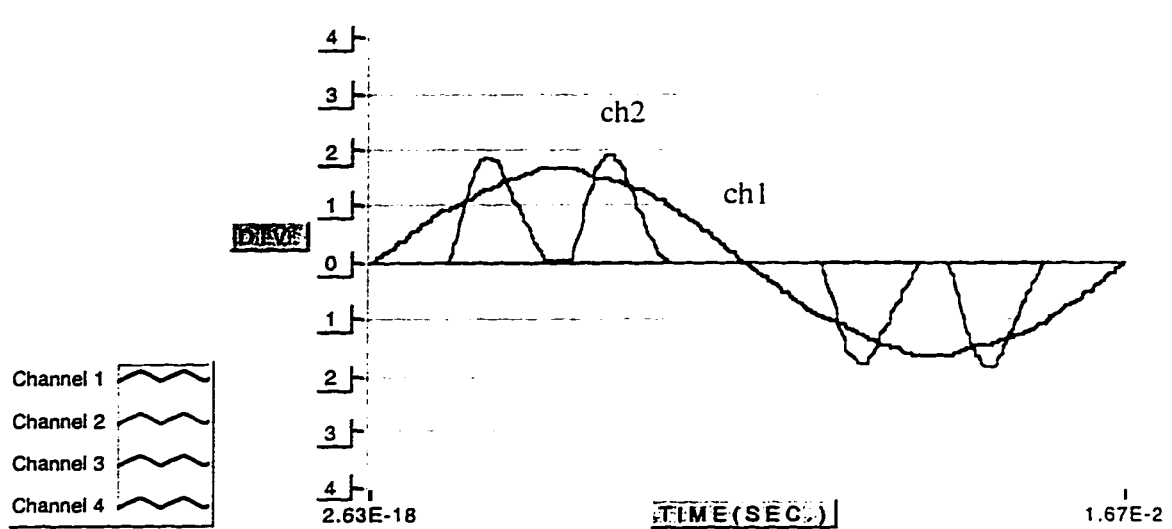
The three phase diode bridge rectifier is widely used as a utility interface in variable speed drives for induction motors. Similar to the single phase diode rectifier, the waveforms of the input line current (i_s) and the phase-voltage (v_{an}) are acquired for two dc-link filter topologies: capacitive and inductive-capacitive filter.

The experimental circuit consists of a three phase diode bridge rectifier, dc-link filter and resistive load.

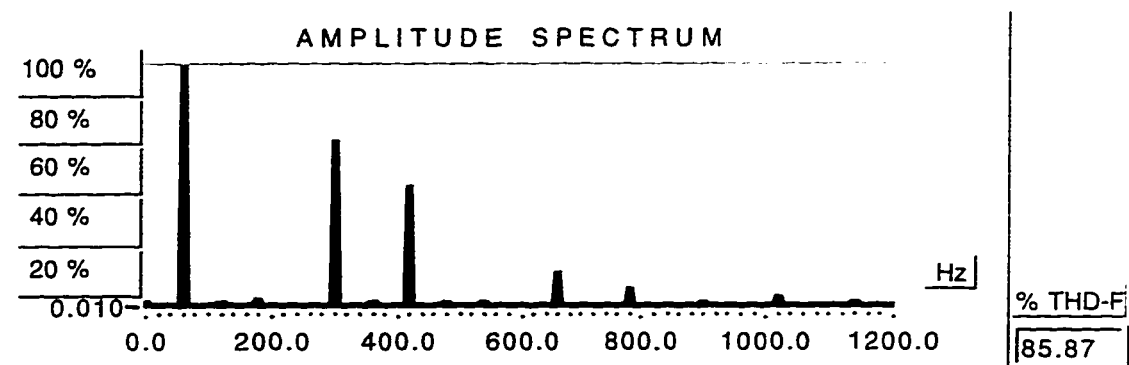
6.2.1 Three-phase diode bridge rectifier with C filter

The three phase diode bridge rectifier with capacitor dc-link filter is a cost effective alternative for the input stage of voltage source inverters. The experimental results were obtained under the following conditions: input power $P=4.4$ kW ($S= 5.7$ kVA, $Q= -0.5$ kvar), power factors: $PF= 0.77$, $FPF=1$, input voltage and current: $V_{ab}= 198$ V, $I_a= 16.7$ A , dc-link filter: $C = 940$ μ F, resistive load: $R= 16.67$ Ω . The resultant waveforms of the input line current (i_a) and the phase voltage (v_{an}) (Figure 6.4 (a)) indicate some advantages and disadvantages associated with this topology, such as a unity fundamental power factor and a high harmonic distortion respectively. Scaling factors associated with the data acquisition (100V/div and 20A/div) are obtained from the front panel controls indicators (see section 6.1.1). Input current spectrum and current harmonic values relative to the total RMS are given in Figure 6.4 (b) and (c). New regulations regarding power quality make the C filter undesirable for many industrial applications [13]. The power electronic group of the University of Alberta is investigating retrofit harmonic correction units for diode bridge rectifiers that aim at harmonic reduction and improved power factor [12,28,29]. Chapter 8 describes some of the topologies under investigation, using the DAQ system.

The input current waveform illustrated in Figure 6.4 (a) can be the input current waveform to a low-power variable speed drive. Chapter 7 presents a PWM inverter fed from a three-phase diode bridge with C filter. On-line UPS systems with phase input rectifiers can have similar characteristics [18]. In the harmonics spectrum of the rectifier input current, triple-n harmonics have an insignificant value and the main contributors to the current distortion are the 5th and 7th harmonics. The “pulsed” line-



(a)



(b)

I_1	I_3	I_5	I_7	I_9	I_{11}	I_{13}
70.6387	2.0245	52.8307	42.4928	1.9706	17.0211	9.2332

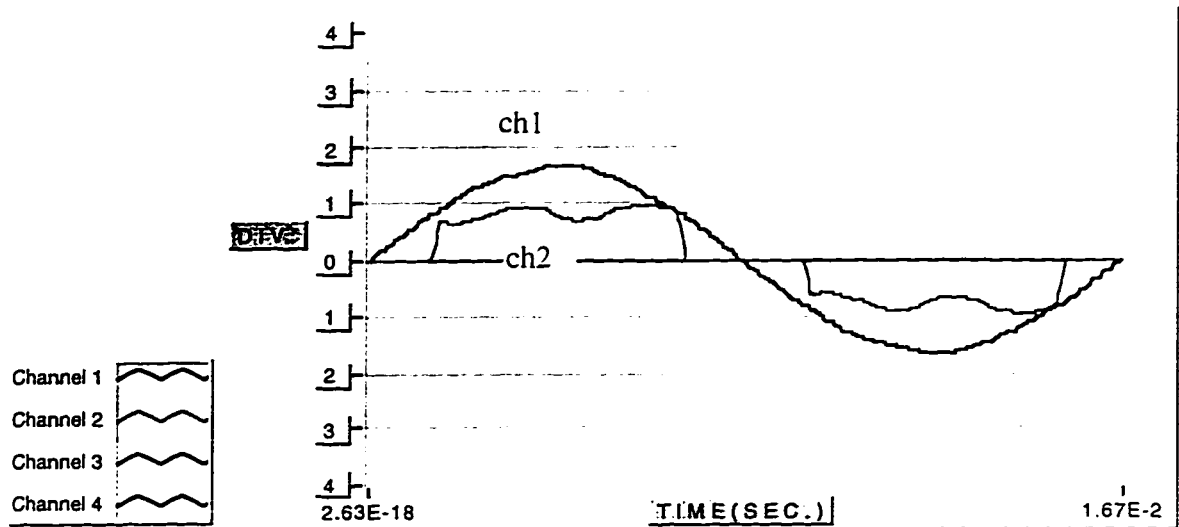
(c)

Figure 6.4 Three-phase diode bridge rectifier with C dc-link filter and R load:(a) Acquired phase-voltage and current waveforms (ch1: phase-voltage @ 100V/div. ch2: line current @ 20 A/div); (b) Input current harmonics spectrum and THD_I ; (c) Fundamental input current and harmonics in per-cent (%) of the total RMS current.

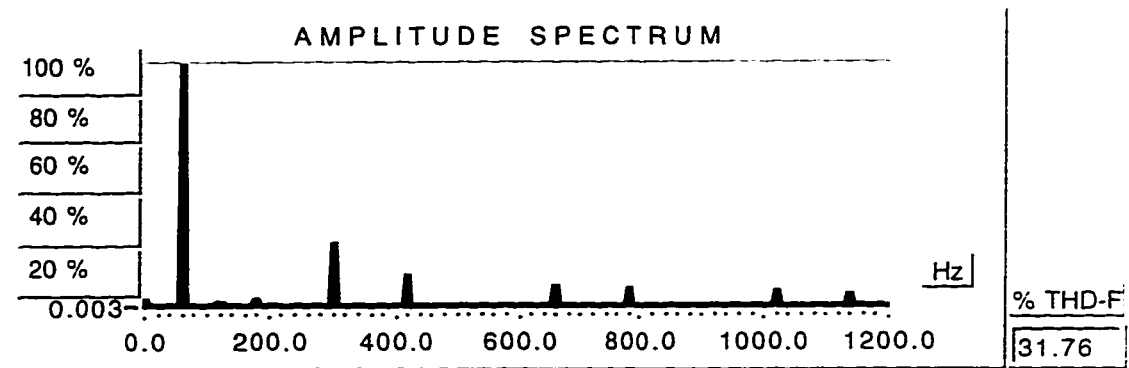
current is due to the capacitor filter in the dc-link. The diodes are turned on and off in response to the anode-cathode voltages applied and consequently the phase-delay between the fundamental current and voltage remain nearly constant at a very low value (approximately zero). In the above experiment the fundamental power factor, also known as displacement power factor DPF, is $FPF=1$. The total power factor is $PF=0.77$ and its low value is due to the high harmonic content in the current, reflected in the large THD value. The current distortion factor (CDF) as function of THD is described by Equation (4.10) in Chapter 4. Traditional utility schemes for metering reactive power respond to fundamental frequency phase displacement and for this type of load will indicate a power factor close to unity. The true power factor is much lower and has effects on the power system similar to a poor displacement power factor.

6.2.2 Three-phase diode bridge rectifier with LC filter

By adding an inductor $L=2.5$ mH in the positive rail of the three phase diode rectifier, an LC low-pass filter is created. The experimental setup maintained the power level indicated in section 6.2.1. The improvement in the input side of the bridge is reflected by the lowered peak value and longer time for the current pulse drawn from mains (Figure 6.5 (a)) and by the higher power factor $PF=0.96$. The 5th and 7th harmonic are lowered (Figure 6.5 (b), (c) vs. Figure 6.4 (b), (c)) and the THD_1 decreases from 85 % to 31.76%. Most variable speed drives with a three-phase diode bridge rectifier input stage, have inductors in the dc-link for harmonic control. Disadvantages associated with the addition of a dc-link inductor are higher cost, increased mass and larger volume.



(a)



(b)

I_1	I_3	I_5	I_7	I_9	I_{11}	I_{13}
94.9964	2.3837	24.2370	12.8214	0.2537	8.1910	6.5646

(c)

Figure 6.5 Three-phase diode bridge rectifier with LC dc-link filter and R load:(a) Acquired phase-voltage and current waveforms (ch1: phase-voltage @100V/div. ch2: line current @ 20 A/div); (b) Input current harmonics spectrum and THD_I ; (c) Fundamental input current and harmonics in per-cent (%) of the total RMS current.

6.3 12-Pulse diode rectifier

The harmonic content of the supply line-current decreases as the pulse number increases in the rectifier circuits. The three phase diode bridge rectifier displays 6 pulses for every cycle of line voltage and is called 6-pulse rectifier. A series connection of two 6-pulse bridges results in a 12-pulse rectifier if the ripples of the two bridges are phase-shifted relative to each other. With two transformers connected Δ/Δ and Δ/Y (Figure 6.6) a 30° phase-shift between the secondary line-voltages is obtained, resulting in a 12-pulse total output voltage.

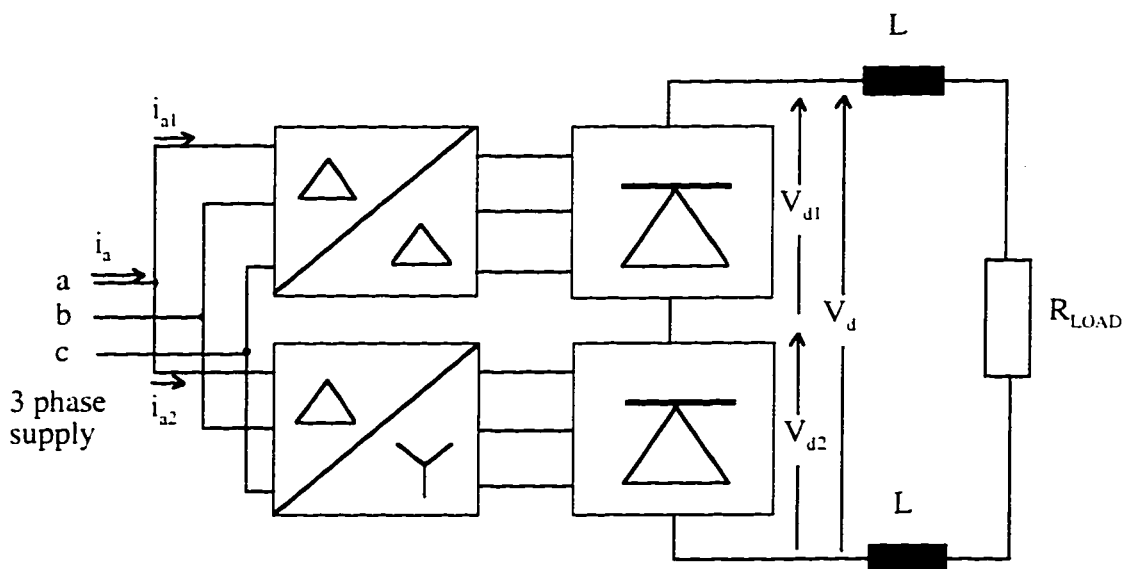


Figure 6.6 Block diagram of a 12-pulse rectifier with L dc-link filter.

The experimental 12-pulse rectifier setup for data acquisition and analysis is described by the following values: input power $P = 6.3$ kW, ($S = 6.5$ kVA, $Q = 1.3$ kvar), power factors: $PF = 0.97$, $FPF = 0.98$, input line voltage: $V_{ab} = 195$ V ($THD_v = 1.32\%$), input current: $I_a = 19.4$ A ($THD_i = 11.54\%$), dc-link filter: $2xL = 2.5$ mH and resistive load $R = 41.6$ Ω . The plotting constants were obtained from the virtual instrument's probe indicators as: 200V/div and 10 A/div respectively. Figure 6.7 (a) illustrates the acquired waveform of the total input current (i_a) of the 12-pulse rectifier and the input phase voltage (v_{an}). The shape of the input current is affected by the distorted transformer magnetizing currents resulting in slopes of the theoretical "horizontal" portions. The commutation overlap introduces a delay in the raising time of the current steps resulting in trapezoidal shapes. The harmonic spectrum of the total line current is illustrated in Figure 6.7 (b). The 5th and 7th harmonics are noticeably absent, the first significant harmonics being the 11th and 13th. The 5th and 7th harmonics are present in each Δ primary (Figures 6.8 (a) and 6.9 (a)) but are canceled in the total input current.

The total dc-output voltage (V_d) is plotted in Figure 6.10 with a line-line input voltage for magnitude reference. High dc-link voltage with low voltage ripple is desirable for large rectifier installations because it allows high power transfer and reduces the size of the filter.

Power line harmonics and power factor are of secondary importance for small power supplies where simplicity and cost are the first requirement, but it becomes a leading factor when choosing the rectifier configuration for large power applications. Because of the lower harmonic distortion (11.54% vs. 26.52%), the 12-pulse rectifier causes less interference with other electrical systems than the 6-pulse rectifier.

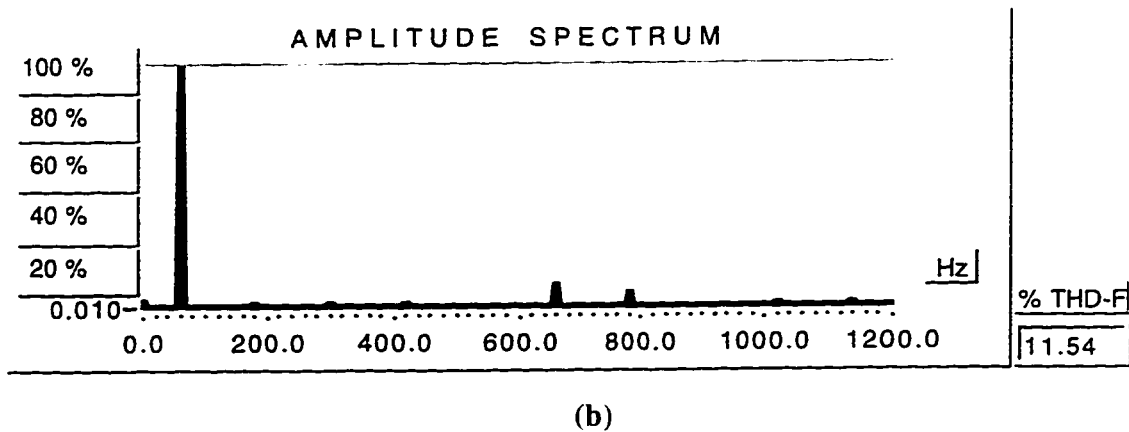
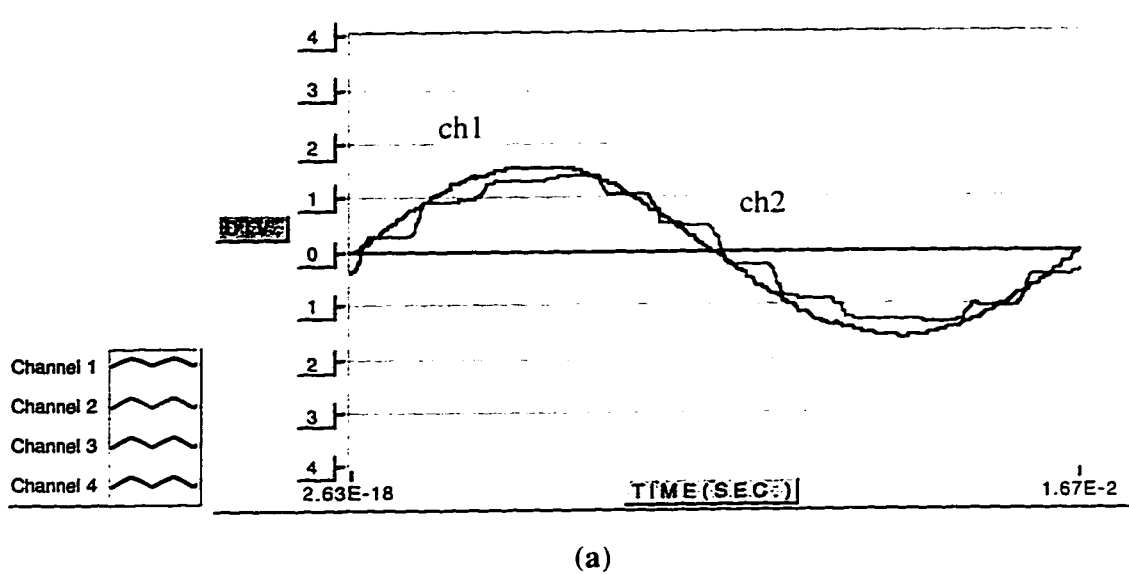
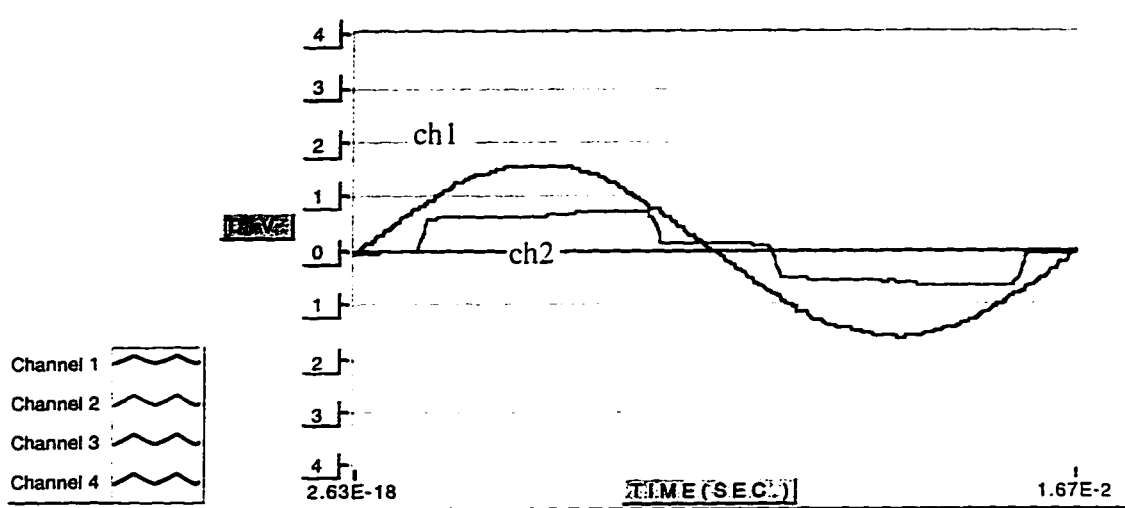
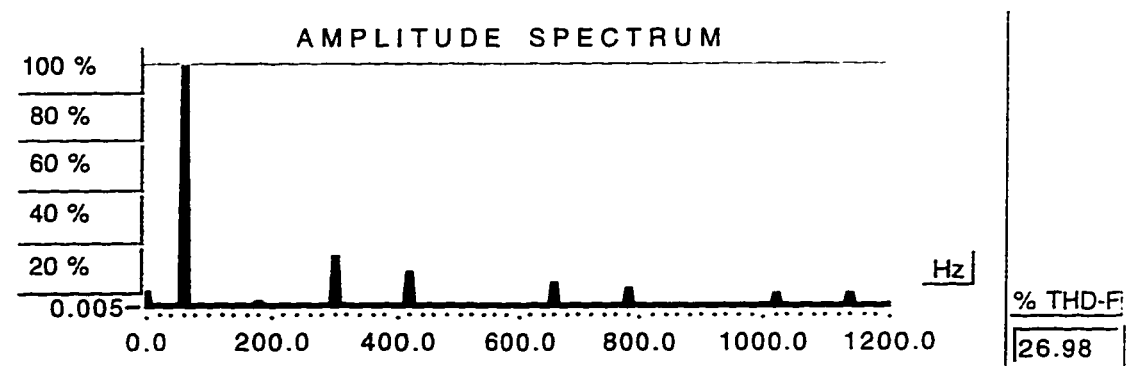


Figure 6.7 12-pulse diode bridge rectifier with L dc-link filter and R load:(a) Acquired input phase-voltage and total line-current (i_s) waveforms (ch1: phase-voltage @ 100V/div, ch2: line current @ 10 A/div); (b) Total input current harmonics spectrum and THD₁.

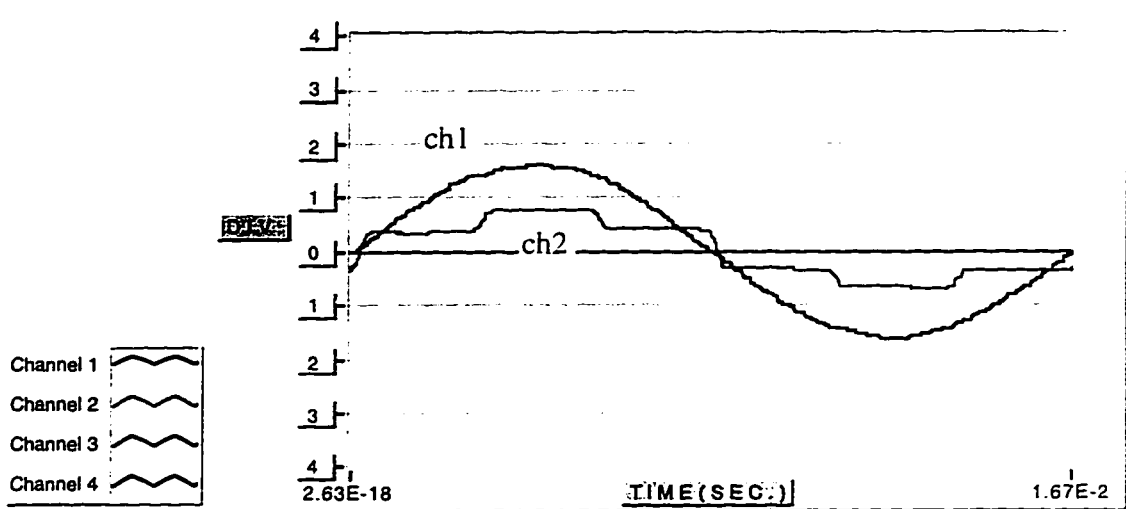


(a)

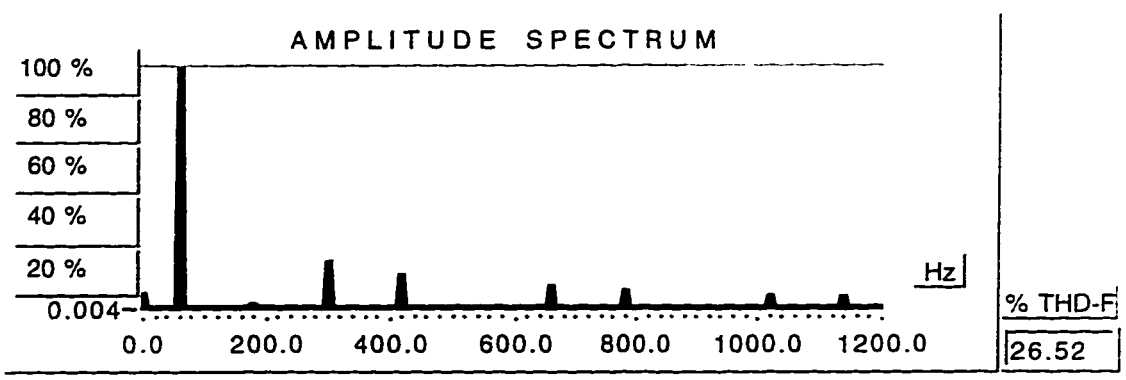


(b)

Figure 6.8 Δ/Δ transformer of the 12-pulse rectifier: (a) Acquired input phase-voltage and line current waveforms (ch1: phase-voltage @100V/div, ch2: line current @ 10 A/div); (b) input current (i_{a1}) harmonics spectrum and THD_1 .



(a)



(b)

Figure 6.9 Δ/Y transformer of the 12-pulse rectifier: (a) Acquired input phase-voltage and line current (i_{L1}) waveforms (ch1: phase-voltage @100V/div. ch2: line current @ 10 A/div); (b) Total input current harmonics spectrum and THD_I.

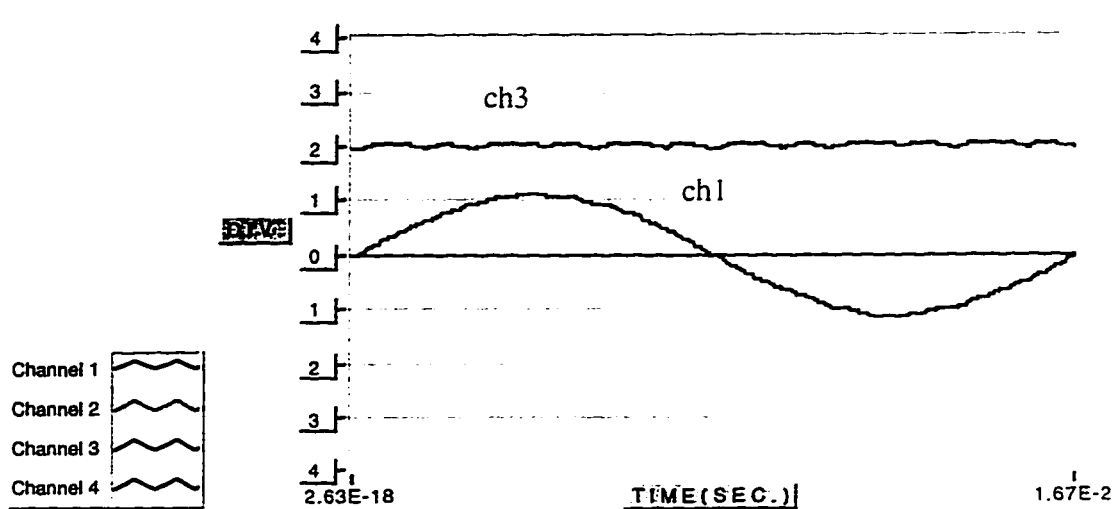


Figure 6.10 12-pulse rectifier output voltage (V_d) and input line-line voltage (V_{ab}) acquired at 250V/div.

Many high-power level applications require a larger number of pulses per fundamental cycle. Extrapolating the methodology described for 12-pulse rectification, a 18-pulse rectifier is obtained by connecting in series three 3-phase rectifiers. Similar results regarding harmonic control are obtained by parallel connections of three phase diode bridges. In the power electronics industry, rectifier topologies operating in a three-phase system with a larger than 6 number of pulses are generically called multi-pulse rectifiers. The multi-pulse rectifiers offer a simple and effective technique for reducing power electronic converter harmonics. The expanding use of power electronic converters for variable speed drives is stimulating the development of multi-pulse methods in power ratings down to 100 HP and less.

This chapter presented a set of experiments using different rectifier topologies with different dc-link filters. The waveforms illustrated as well as their harmonic spectrums and performance factors were obtained from the front panel of the Virtual

Instrument described in Chapter 5 and Appendix C. Several features of the DAQ system were presented. The discussion outlined the harmonic pollution specific to single-phase, three-phase and 12-pulse series diode rectifier topologies, and insight of the harmonic effects on the power system was given.

Chapter 7

Data Acquisition from Variable Speed Drives

Modern, energy efficient methods for speed control of induction motors involve variable speed drives (VSD). This chapter describes the investigation of two VSDs with the LabVIEW-based data acquisition system (see introduction of Chapter 6 for system description). The first drive topology employs a three phase semi-controlled rectifier as front-end and a square wave inverter for controlling the motor. The second drive has a three phase diode bridge rectifier as front-end and PWM inverter output for motor control. On PWM VSDs, thousands of pulses per second are applied to the motor. The plots and spectrums presented emphasize the DAQ system's ability to perform accurate acquisitions and measurements under these conditions. Figure 7.1 illustrates the basic concept of induction motor drives using variable frequency voltage source inverters.

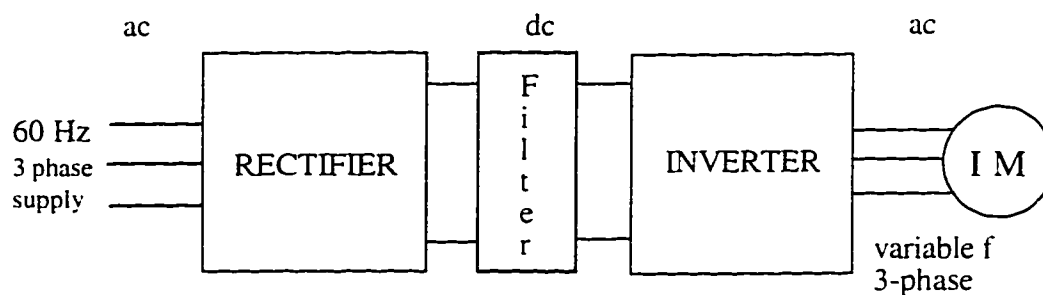


Figure 7.1 Block-diagram of variable frequency drive for induction motor applications

Historically, the rectifier-fed dc-motor was widely used in variable speed drives. Presently, variable frequency control allows good running and transient

performance to be obtained from a squirrel-cage induction motor when the dynamic of speed control need not be very fast and precise. The squirrel-cage induction motor has a number of advantages over the dc motor: it is cheap, rugged, reliable and because of the absence of a commutator and brushes, it requires practically no maintenance. It can also be employed in contaminated environments, and can be designed for higher speeds, voltage, and power ratings. The speed of an induction motor can be controlled by varying the frequency f , which controls the synchronous speed, keeping the airgap flux constant by varying the applied voltage in a linear proportion to f . This technique is often referred to as constant volts/herz ($V/Hz=const.$).

The experimental system used for data acquisition and waveform analysis is presented in principal in Figure 7.2. The squirrel-cage induction machine fed from the variable speed drive is mechanically coupled with the dc machine. The armature winding of the separately excited dc machine is connected to an adjustable resistive load. By varying the load resistance and the field excitation of the dc machine, one can adjust the input power level of the drive. The nameplate data of the machine set and drives characteristics are given in Appendix E.

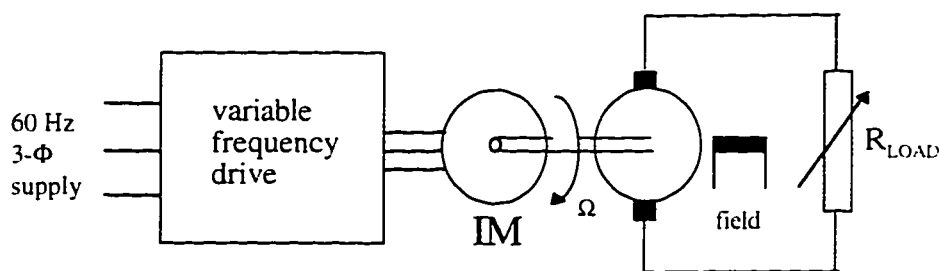


Figure 7.2 VSD experimental setup for data acquisition and analysis.

7.1 Square Wave Inverter Drive

The dc voltage applied to the input of a square wave inverter needs to be controllable. For this reason, the input stage of the drive employed for data acquisition and analysis consists of a three phase semi-controlled rectifier (Figure 7.3). For a comprehensive analysis, two different sets of measurements are performed: one set of measurements investigates the front-end of the drive (i.e. utility interface), and the other investigates the motor-end (i.e. inverter output). Both utility interface and inverter are analyzed for three speed settings of the induction motor as follows: full speed, 2/3 and 1/3 of the full speed. These settings correspond to inverter output frequencies of 60 Hz, 40 Hz and 20 Hz respectively.

7.1.1 VSD front end: Semi-controlled Rectifier

As compared to the three phase fully-controlled rectifier, this topology is an economical method to obtain a variable dc voltage. The semi-controlled rectifier, also called semi-converter, consists of three diodes and three thyristors and provides a dc voltage output whose ripple depends on the firing angle of the SCRs and the size of the dc-link filter.

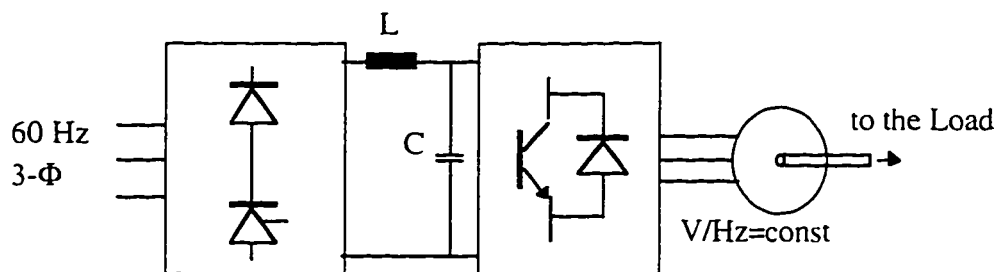


Figure 7.3 Square wave inverter drive with semi-converter input stage.

For 60 Hz inverter output frequency (i.e. full speed for the induction motor), the virtual instrument set of power and performance factors calculations gives the results from Figure 7.4. The effective values of the input line-line voltage and input line current given by (ch 1) and (ch 2) are employed in apparent power calculation (S).

ch 1 RMS	ch 2 RMS	S [VA]	P [W]	PF	FPF
199.83	13.72	4749.72	4542.42	0.96	1.00

Figure 7.4 Square wave inverter drive input power and performance factors for 60Hz output frequency.

The power factors at this speed setting have large values as one can expect by observing the acquired waveforms of the input current (i_a) versus the input phase voltage (v_{an}) in Figure 7.5. The semi-converter output voltage resembles the output of a diode bridge rectifier.

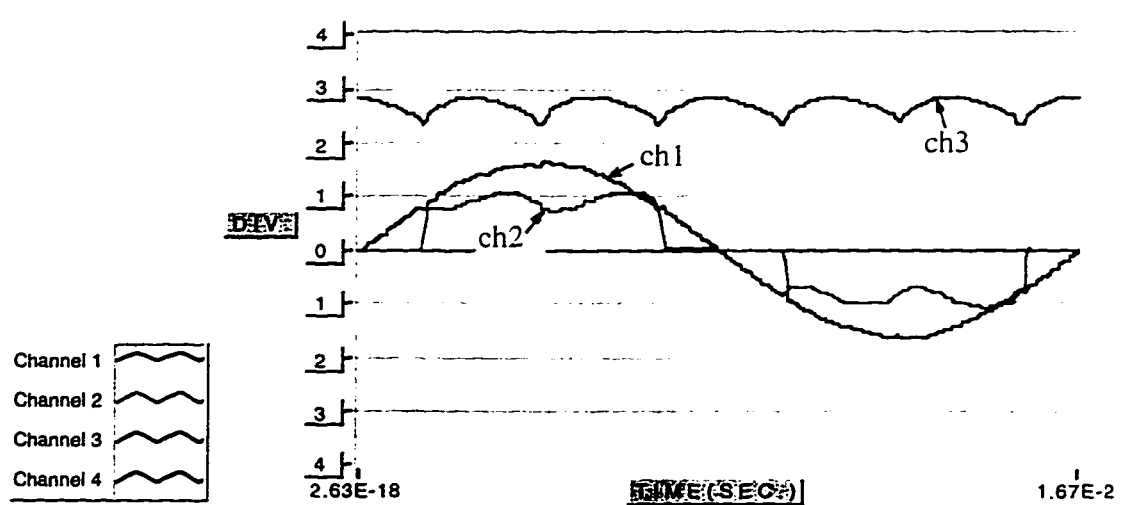


Figure 7.5 Square wave inverter drive input stage waveforms at 60 Hz output frequency: input phase voltage (ch1: 100 V/div), input line current (ch2: 20 A/div) and dc-link voltage (ch3: 100 V/div).

Figure 7.5 also illustrates the commutation overlap due to the source inductance causing notching in the dc-link voltage. The harmonic content and THD of the input current are illustrated in Figure 7.6.

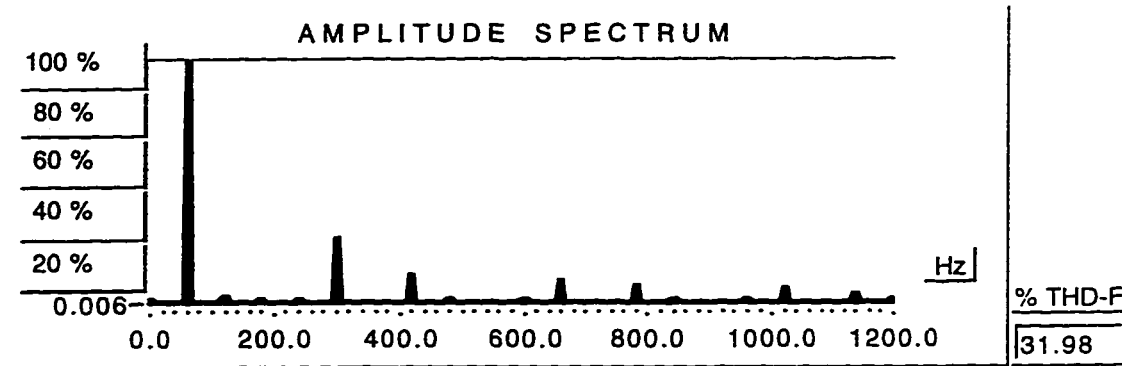


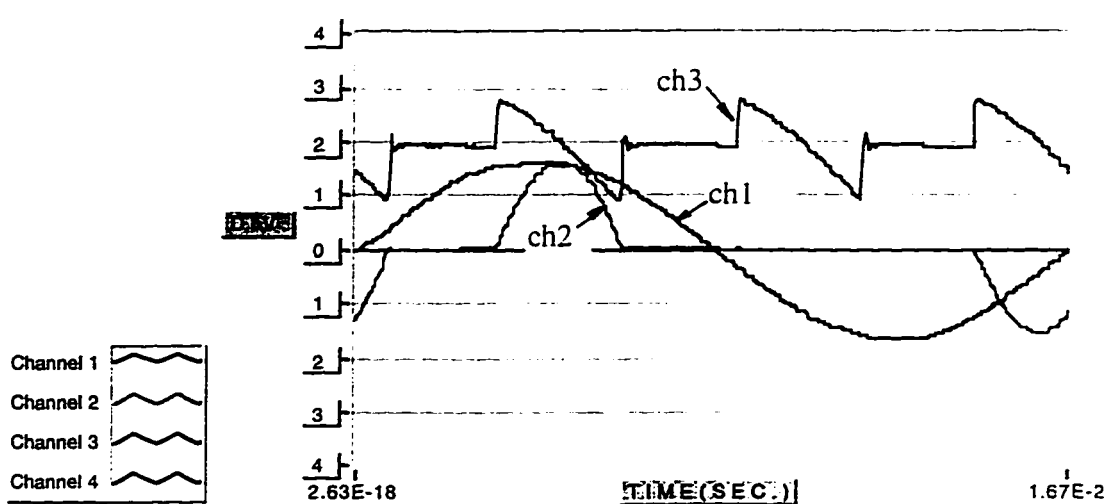
Figure 7.6 Harmonic spectrum of semi-converter input current for 60 Hz drive output.

Neglecting the voltage drop across the rectifier active components, in continuous conduction the dc-link voltage is expressed as a function of input line-line voltage and thyristors control angle as shown by the equation (7.1). The firing angle is consequently given by equation (7.2).

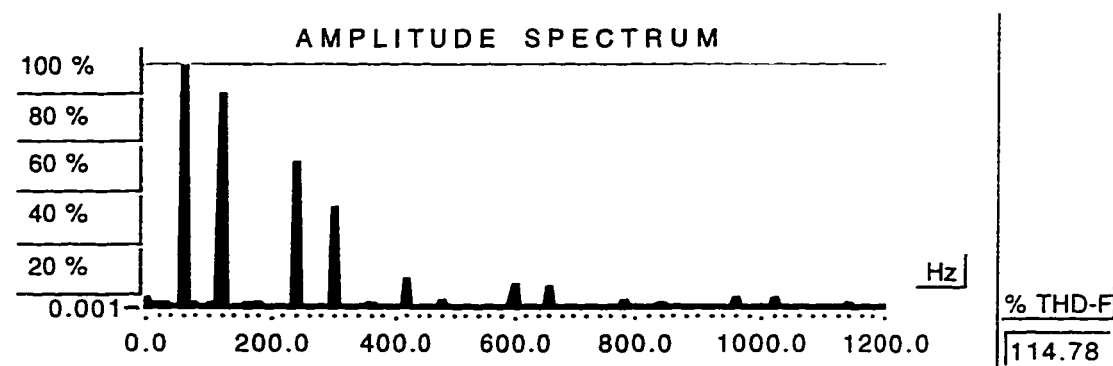
$$V_{dc} = \frac{3}{\pi\sqrt{2}} V_{LL} (1 + \cos \alpha) \quad (7.1)$$

$$\alpha = \cos^{-1} \left(\frac{\pi\sqrt{2}V_{dc}}{3V_{LL}} - 1 \right) \quad (7.2)$$

To obtain 2/3 of the full speed setting of the induction motor, the firing angle of the SCRs is increased. The dc-link voltage decreases and the dc-link current reaches the boundary of discontinuous conduction. The input current of the semi-converter is distorted, and the power factor decreases. For 40 Hz inverter output, the acquired drive input waveforms, line current harmonics and power calculations are given in Fig. 7.7.



(a)



(b)

ch 1 RMS	ch 2 RMS	S [VA]	P [W]	PF	FPF
201.44	13.87	4840.05	2257.22	0.47	0.71

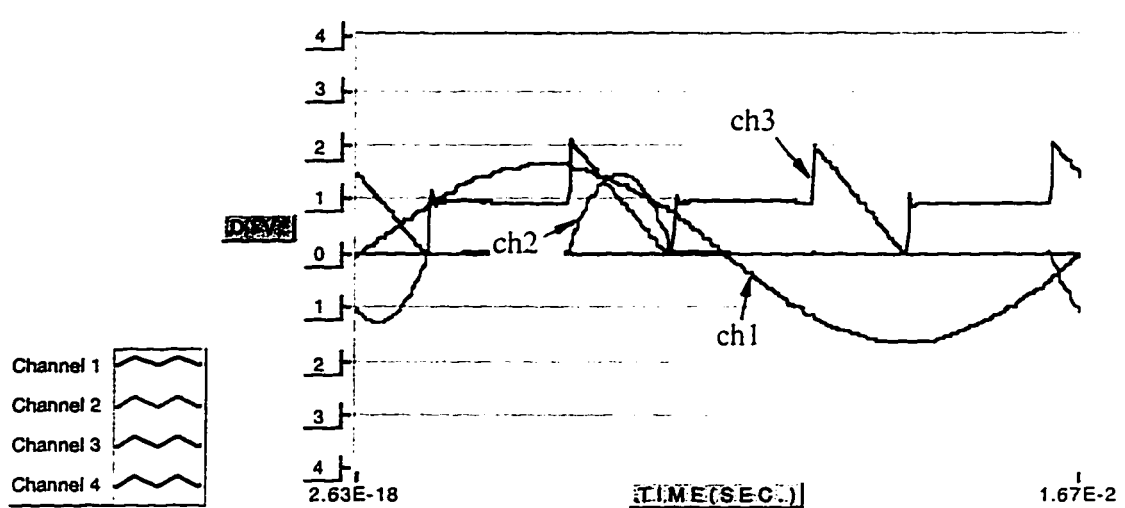
(c)

Figure 7.7 Square wave inverter drive input at 40 Hz output frequency: (a) input phase-voltage (ch1:100V/div), input line current (ch2: 20 A/div), semi-converter output voltage (ch3: 100V/div); (b) input line current harmonic spectrum and THD_I ; (c) input line-line effective value (ch1RMS), input current (ch2RMS), input power and power factors.

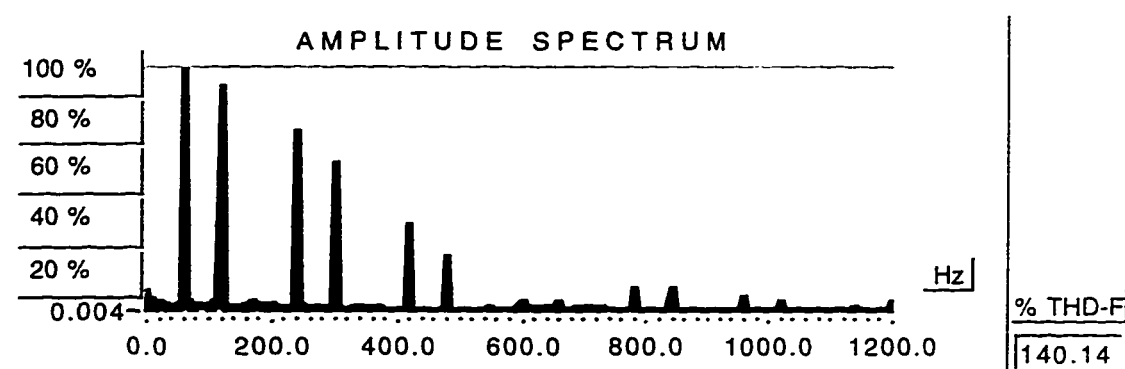
With the decrease in the drive output frequency, the input power factor decreases and large harmonic currents are generated in the utility grid. This is a main disadvantage of the square wave inverter drive input stage. Another drawback are the high magnitudes of the low-frequency harmonics in the semi-converter output voltage. The purpose of the L-C filter is to maintain a ripple-free dc voltage at the input of the inverter, and thus, prevent the harmonics in the bridge output from interfering with the inverter and the harmonics in the inverter input current from interfering with the rectifier. Because of the low-frequency harmonics in the rectifier output voltage, the filter capacitor is large (7200 μF) affecting negatively the transient response of the drive.

All above mentioned characteristics of the input stage of the square wave inverter are further emphasized by the drive input waveforms acquired at 1/3 of the full speed of the induction motor. The inverter output frequency is 20 Hz and the dc-link voltage 1/3 of the initial value. For a consistent comparison Figure 7.8 illustrates the same set of drive input waveforms as Figure 7.7, the input current harmonic spectrum, power calculations and power factors. At this setting the line current is further distorted and the input power factors are very poor.

The drawbacks for the scheme of Figure 7.3 are eliminated if the semi-converter is replaced by a diode bridge rectifier followed by a chopper. The fundamental power factor remains to unity under all conditions of operation and fast response is obtained. However, the losses are increased due to the use of an additional power stage.



(a)



(b)

ch 1 RMS	ch 2 RMS	S [VA]	P [W]	PF	FPF
201.43	10.06	3508.59	763.67	0.22	0.37

(c)

Figure 7.8 Square wave inverter drive input at 20 Hz output frequency: (a) input phase-voltage (ch1: 100V/div), input line current (ch2: 20 A/div), semi-converter output voltage (ch3: 100V/div); (b) input line current harmonic spectrum and THD_1 ; (c) input line-line effective value (ch1RMS), input current (ch2RMS), input power and power factors.

7.1.2 VSD output stage: Square Wave Inverter

The square wave inverter employed for data acquisition consists of six bipolar junction transistors (BJT) arranged in a three phase bridge topology. Each transistor has a fast recovery diode in antiparallel to allow reverse flow of current.

The inverter output waveforms associated with the three motor speed settings mentioned in the previous section are acquired for 50 ms. This time-span corresponds to three fundamental cycles for 60 Hz, two cycles for 40 Hz and one cycle for 20 Hz inverter output frequency (Figure 7.9). Each plot illustrates the inverter output line-line voltage, phase voltage and motor phase current. During a cycle, the line-line voltage has three levels: $+V_{dc}$, 0 and $-V_{dc}$ and the phase voltage is generated in six steps. Hence, a square wave inverter is also known as a six-step inverter. The levels of the phase voltage steps are $\pm 1/3 V_{dc}$ and $\pm 2/3 V_{dc}$ respectively. The line-line voltage is described by the following Fourier series:

$$V_{ly} = \frac{2\sqrt{3}}{\pi} V_{dc} \left[\sin(\omega t + \pi/6) + \frac{1}{5} \sin(\omega t - \pi/6) + \frac{1}{7} \sin(\omega t + \pi/6) + \dots \right] \quad (7.3)$$

Similarly, the Fourier series of the inverter output phase voltage is given by:

$$V_{xn} = \frac{2}{\pi} V_{dc} \left(\sin \omega t + \frac{1}{5} \sin 5\omega t + \frac{1}{7} \sin 7\omega t + \dots \right) \quad (7.4)$$

The harmonic content of the line-line and phase voltages is the same. The different waveforms are due to a different phase relationship between the harmonics and the

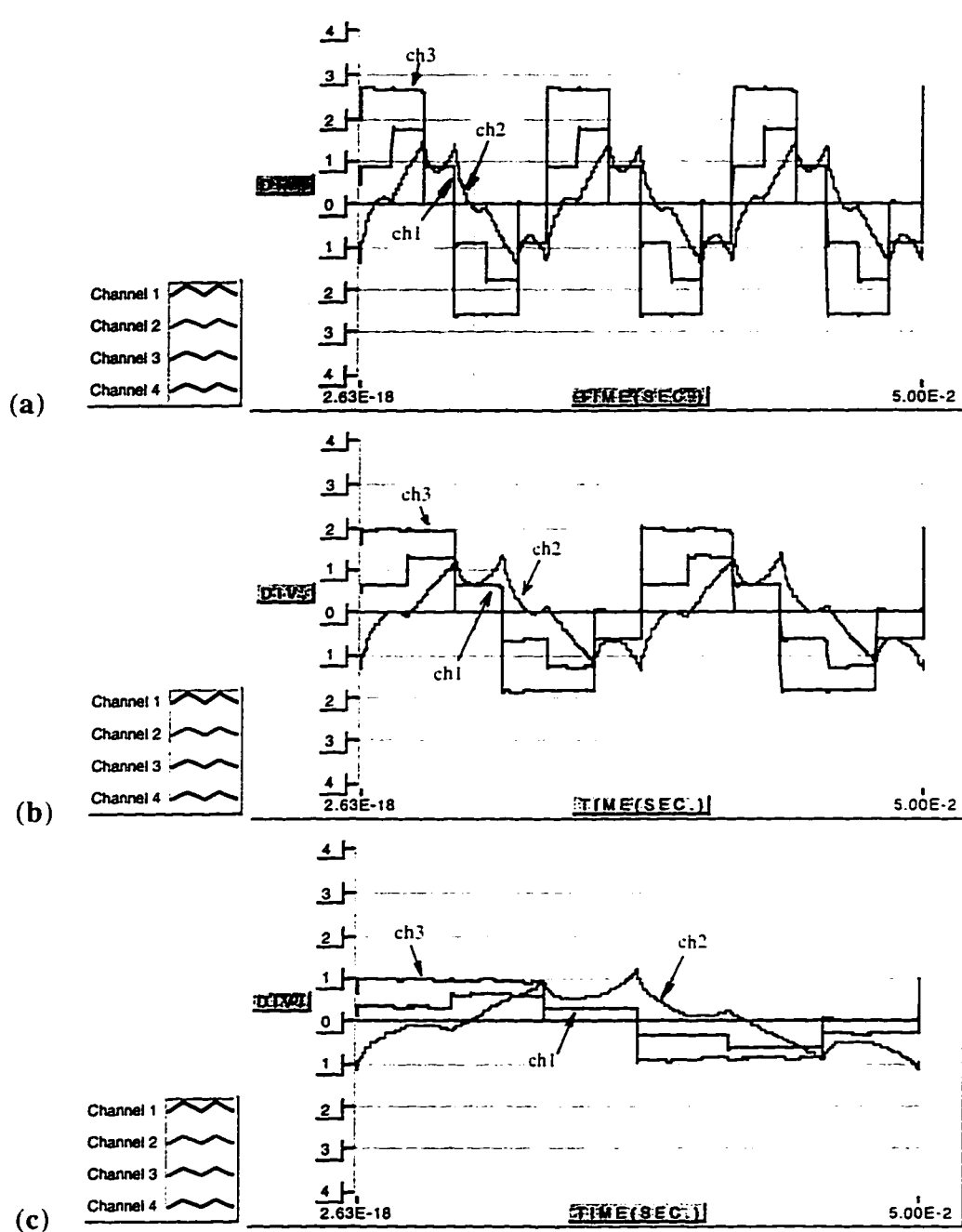


Figure 7.9 Square wave inverter output waveforms: phase voltage (ch1: 100V/div), phase current (ch2: 20 A/div), line-line voltage (ch3: 100V/div) at output frequencies of (a) 60 Hz. (b) 40 Hz. (c) 20 Hz.

fundamental. Only odd harmonics of the order $k=6n \pm 1$ are present, where n is integer. The motor driven by the square wave inverter investigated has a wye-connected stator. The phase current waveforms illustrated in Figure 7.9 has an identical form for a delta-connected stator.

The harmonic spectrums of the inverter output phase voltage and phase current for 60, 40 and 20 Hz output frequency remain practically unchanged in terms of harmonics order and their weight relative to the fundamental (Figure 7.10 (a) and (b)).

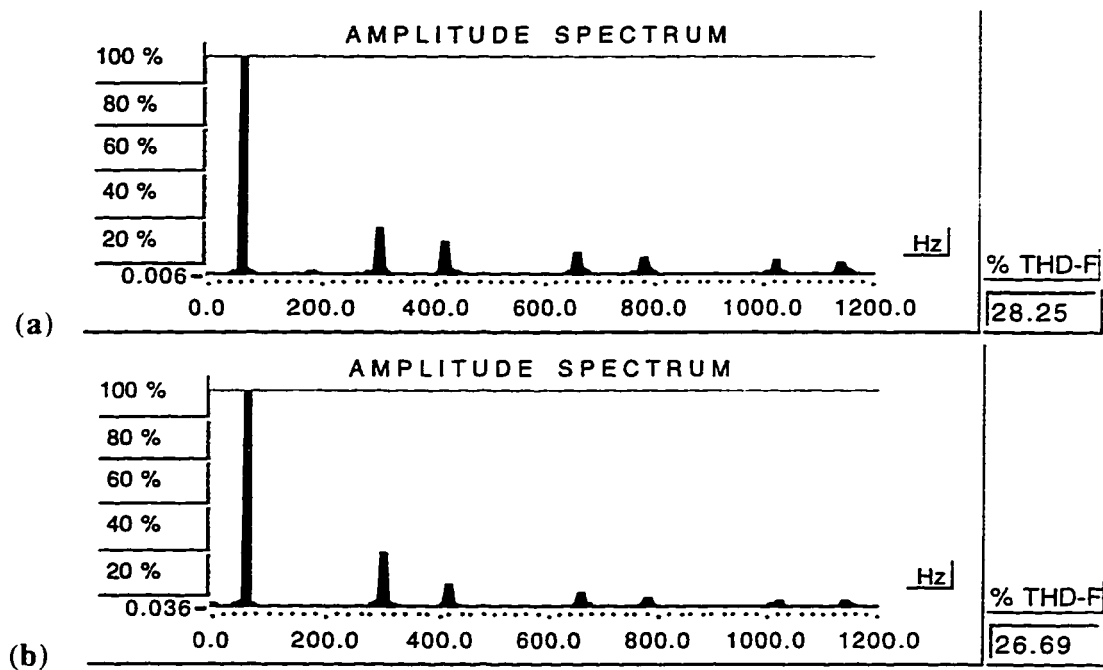


Figure 7.10 Harmonic spectrum of the square wave inverter output waveforms at $f_{OUT}=60$ Hz : (a) phase voltage spectrum and THD_V : (b) phase current spectrum and THD_I .

The dominant harmonics are the 5th and 7th, followed by 11th and 13th. The presence of the low-frequency harmonics in the inverter output contributes to increased

motor losses (copper losses) at all speeds causing motor derating. For this reason the motor employed is a class B design induction machine, suitable for voltage source inverter drives.

When the filtering is ideal, the inverter output voltage waveform remains unchanged except its magnitude. Theoretically, the equations (7.3) and (7.4) are applicable to any value of the inverter output voltage. In reality, at low frequencies the filter is less effective due to the low-frequency harmonics in the inverter input current and large harmonic content in the output voltage of the semi-controlled rectifier. Consequently, the harmonic content of the inverter output voltage increases with the decrease in the motor speed.

Regarding the mechanical characteristics of the induction machine, the interaction between the fundamental flux and the 5th and 7th harmonic rotor currents produces a pulsating torque 6 times the fundamental frequency. Similarly, 11th and 13th harmonic rotor currents produce a pulsating torque 12 times the fundamental frequency but its magnitude is comparatively much smaller. At low fundamental frequency for which the motor speed is low, the pulsating torque cause large fluctuations in speed, producing a stepped motion. A high motor reactance (class B) helps reducing the motor derating and torque pulsations.

7.2 PWM Inverter Drive

The disadvantages of the square wave inverter drive described in the previous paragraph are eliminated in the pulse-width modulated (PWM) inverter drive shown in Figure 7.11. Analogous to the 6-step inverter drive, the performance of the virtual instrument is shown first on the front end of the drive for three speed settings of the induction motor. For consistency reasons, the investigation takes into consideration the

same speed settings of the motor corresponding to the inverter output frequencies of 60, 40 and 20 Hz. Following the input stage analysis, acquired data on the inverter output is presented for all three motor speed settings.

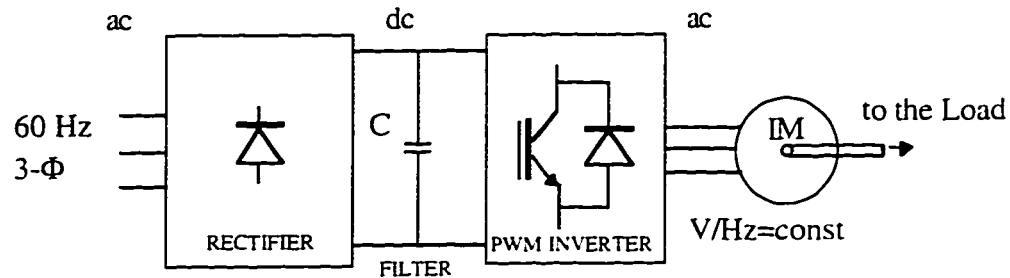


Figure 7.11 PWM inverter drive.

7.2.1 Drive front-end: Diode Rectifier

The PWM inverter has provision for the control of the output voltage and it is fed from a fixed dc voltage. The utility interface of the drive consists of a three phase diode bridge rectifier with a capacitor dc-link filter. Because of the low harmonic content in the output voltage of the diode bridge and in the input current of a PWM inverter, the filter capacitor is smaller and consequently the drive response is faster than in the case of the square wave inverter.

The acquired input waveforms of the PWM drive for 60, 40 and 20 Hz are illustrated in Figure 7.12. The harmonic content of the input current and THD_1 for each output setting are presented for comparison in Figure 7.13. As the output frequency is decreased, the harmonic distortion of the input current increases. However, the supply harmonic pollution is not larger due to a smaller effective value of the input current. The input power level and power factors calculated by the virtual instrument for each speed setting are given in Figure 7.14.

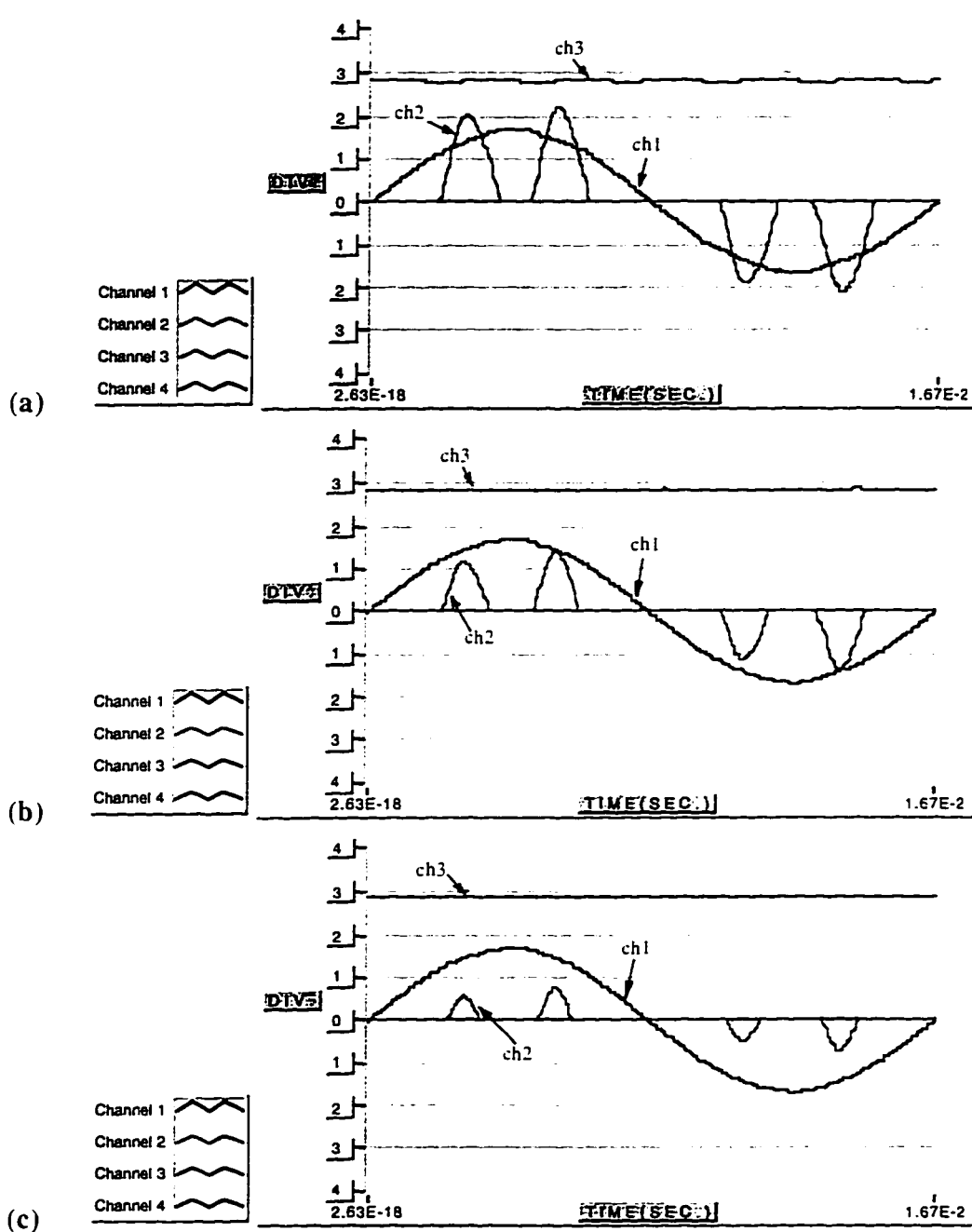
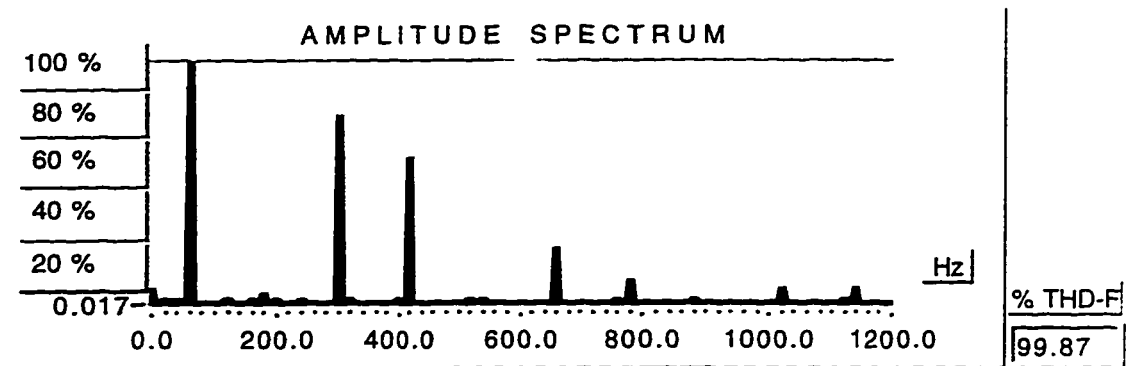
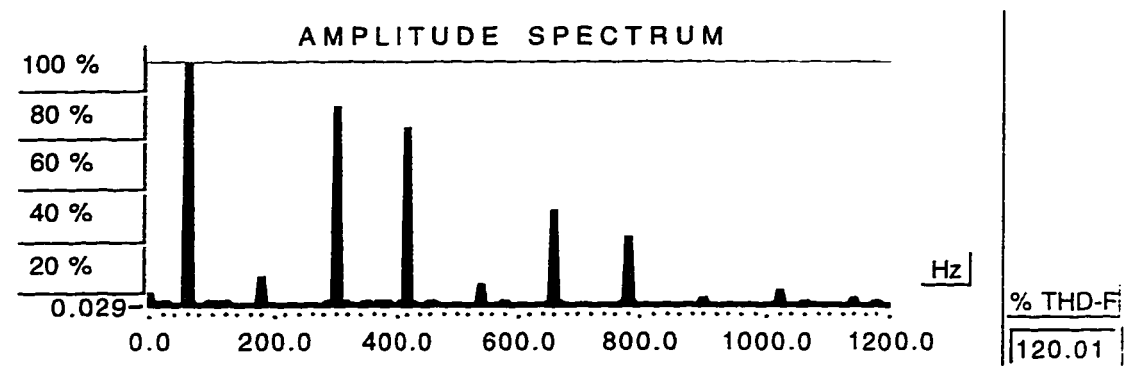


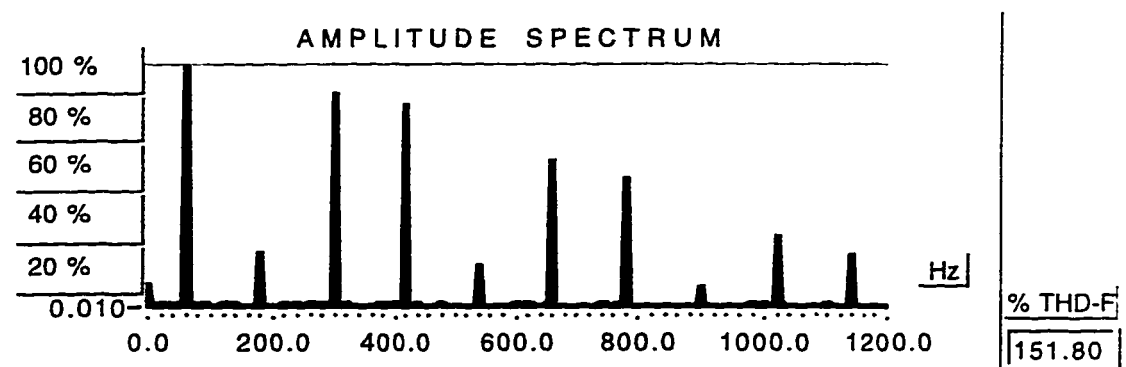
Figure 7.12 PWM drive input current (ch2: 20 A/div), phase voltage (ch1: 100 V/div) and dc-link voltage (ch3: 100 V/div) for drive output frequency of: (a) 60 Hz. (b) 40 Hz. (c) 20 Hz.



(a)



(b)



(c)

Figure 7.13 Input current harmonic spectrum and THD_i of the PWM drive for drive output frequency of: (a) 60 Hz. (b) 40 Hz. (c) 20 Hz.

The input power level of the PWM drive at low output frequency is limited by motor temperature considerations.

	ch 1 RMS	ch 2 RMS	S [VA]	P [W]	PF	FPF
(a)	200.99	18.54	6454.46	4473.01	0.69	0.97
(b)	203.05	10.16	3573.40	2214.49	0.62	0.97
(c)	204.52	4.50	1593.16	820.79	0.52	1.00

Figure 7.14 Virtual instrument data acquisition based calculations: PWM drive input line-line voltage, input current, input apparent power, input active power, total power factor and fundamental power factor for drive output frequencies of: (a) 60 Hz, (b) 40 Hz, (c) 20 Hz.

7.2.2 PWM inverter

Considering the output of the drive i.e. the PWM inverter output, the waveforms acquired for the above mentioned motor speed settings are illustrated in Figure 7.15. Because of a low harmonic content in the inverter output voltage (Figure 7.15 (a)), the drive has smooth low-speed operation, free from torque pulsations and cogging, with a lower derating of the motor and higher efficiency than in the square wave inverter case. A disadvantage of the increase in the frequency of operation are the increased inverter switching losses. This requires IGBTs rated for higher voltage and current levels as well as higher rated snubbers and commutation circuits. Figure 7.15 (c) shows the effective value of the motor phase input current as calculated by the virtual instrument.

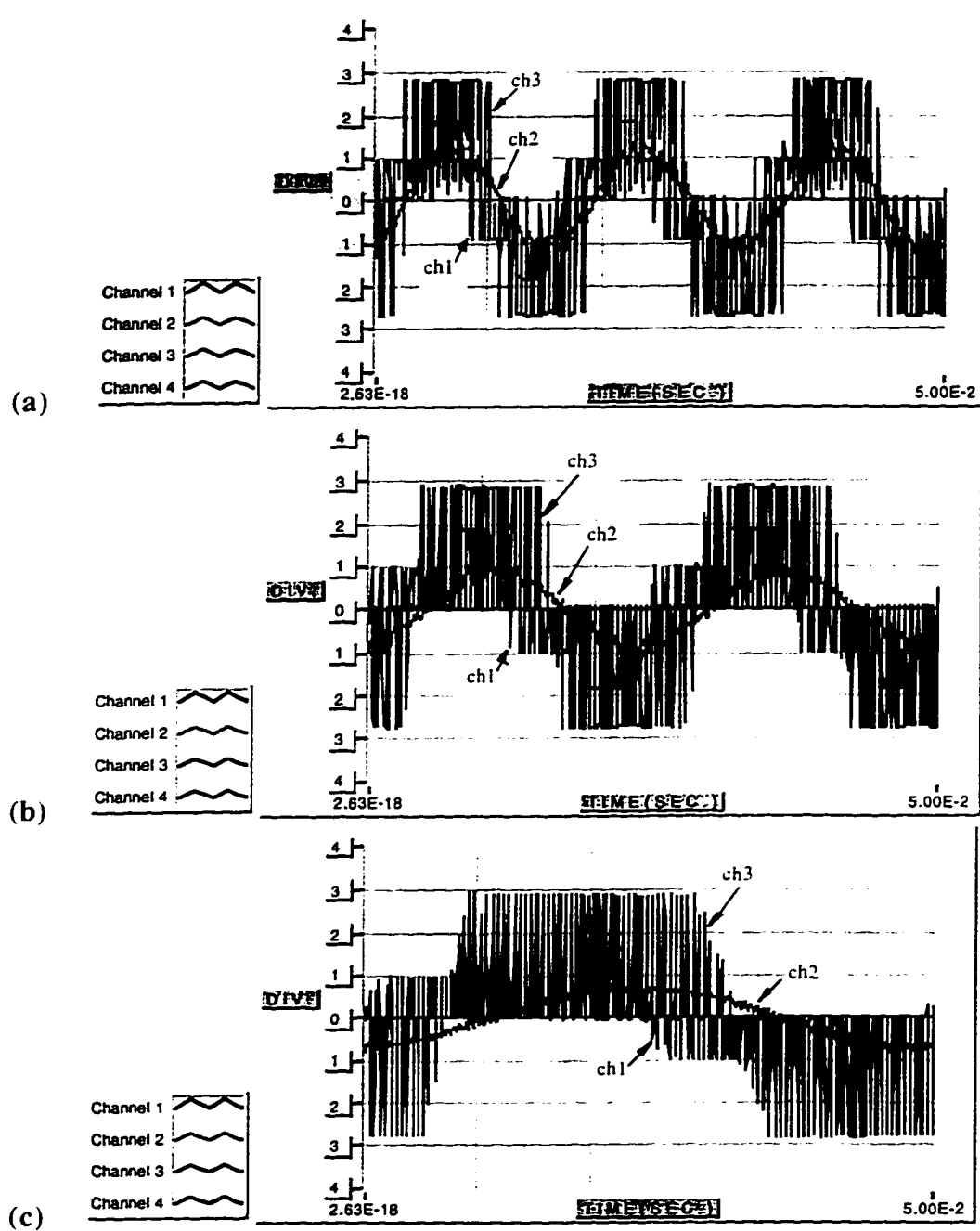
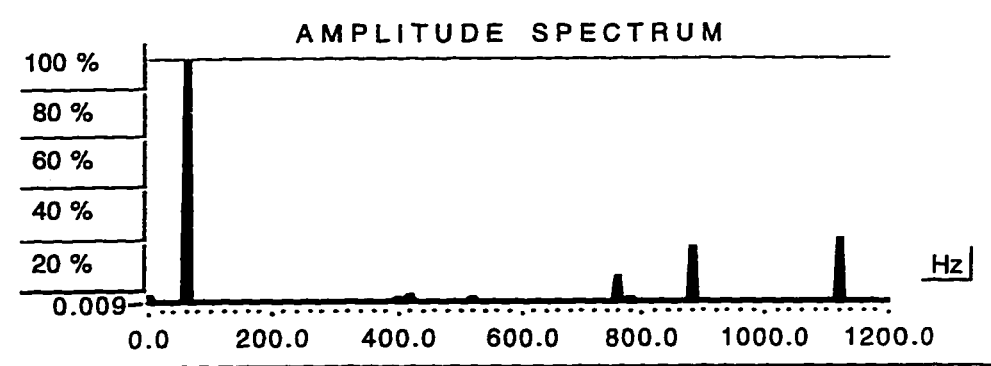
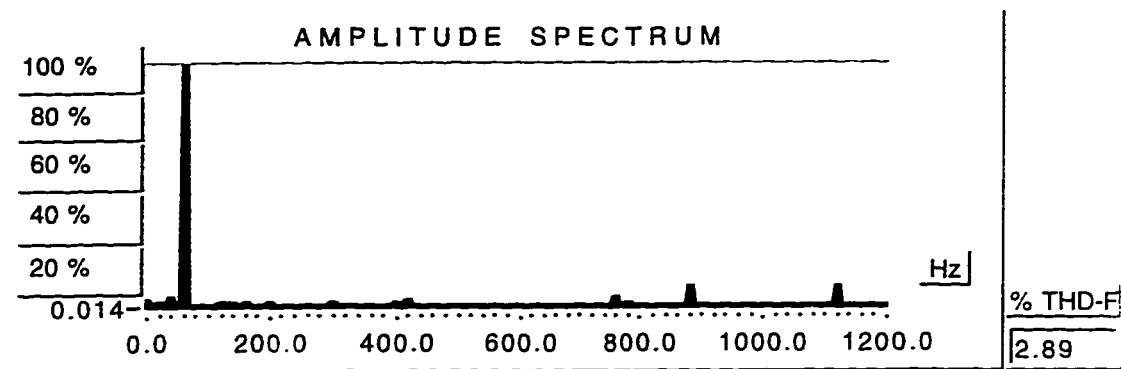


Figure 7.15 PWM drive output current (ch2: 20 A/div), output phase voltage (ch1: 100 V/div) and line-line voltage (ch3: 100 V/div) for drive output frequency of: (a) 60 Hz. (b) 40 Hz. (c) 20 Hz.



(a)



(b)

ch 1 RMS	ch 2 RMS	S [VA]	P [W]	PF	FPF
203.05	10.16	3573.40	2214.49	0.62	0.97

(c)

Figure 7.16 60 Hz PWM inverter drive output: (a) phase voltage harmonics spectrum, (b) motor phase current spectrum and THD_I , (c) inverter output data: line-line voltage, phase current, apparent power, total power factor and fundamental power factor.

The high frequency current harmonics are sidebands of the switching frequency and its multiples (Figure 7.16 (b)). The characteristic noise associated with motor winding vibrations at this frequencies are in the disturbing range of the audible

spectrum. The voltage and current spectrums at 2/3 and 1/3 of the motor full-speed setting are similar to Figure 7.16 (a) and (b), with the exception of the fundamental frequency of 40 and 20 Hz respectively. The harmonics remain sidebands of the switching frequency and its multiples. Table 7.1 lists the virtual instrument calculated values given in Figure 7.16 (c) for 60 Hz output frequency, for all three investigated speed settings. The corresponding set of measurements obtained from a Fluke 39 meter are given Table 7.2. The accuracy of the developed VI is within 1% with respect to the Fluke 39 readings. This precision level was estimated in Chapter 5. The relatively large motor current at 20 Hz operation frequency is explained by the current control capabilities of the PWM inverter.

Table 7.1 PWM inverter output data - VI readings.

Motor speed [rpm]	I _{ph.} [A]	V _{ph.} [V]	P _{in} [kW]	S _{in} [kVA]	PF	FPF
1170	16.97	207.66	4.231	6.102	0.695	0.798
780	12.54	179.58	2.063	3.900	0.538	0.709
390	10.04	126.26	0.692	2.195	0.329	0.650

Table 7.2 PWM inverter output data - Fluke39 meter readings

Motor speed [rpm]	I _{ph.} [A]	V _{ph.} [V]	P _{in} [kW]	S _{in} [kVA]	PF	FPF
1170	16.85	206.33	4.198	6.052	0.69	0.79
780	12.44	178.12	2.055	3.869	0.53	0.70
390	9.95	125.28	0.687	2.178	0.32	0.64

From Tables 7.1 and 7.2, the error of the current reading of the VI relative to the Fluke39 reading for 2/3 of the full-speed of the induction motor is given by the expression:

$$\Delta I = \frac{I_{VI} - I_{Fluke}}{I_{VI}} \times 100\% = \frac{12.54 - 12.44}{12.54} \times 100\% = 0.79\% < 1\%$$

All other errors can be obtain in a similar mode.

Other effects of the high PWM inverter output frequency and its multiples are associated with stator laminations currents and prematurely worn-out of rotor shaft bearings. The high switching frequency causes large values of dV/dt . The stator wire insulation acts as capacitor dielectric in the stator slots allowing high frequency currents to pass trough and, transversally to the shaft direction, through stator laminations to neighbor slots. This effect is more prominent at the tip of the slot since winding inductance of the deeper turns together with the wire insulation capacitance are damping the dV/dt . High frequency current will flow in the rotor shaft as well and, due to the potential difference between the shaft and the motor case (which is grounded), the oil film in the motor bearings becomes the dielectric of a capacitor. Through friction developed in the bearings during normal run, the oil film is heated and consequently its dielectric rigidity weakened. The break-down of the oil film causes increased friction and leads eventually the rotor locking. The disadvantages associated with high frequency effects are addressed by filtering techniques.

This chapter presented waveforms acquired and data calculated by the virtual instrument in connection with two topologies of voltage source inverter drives: the square wave inverter drive and the PWM inverter drive. Spectrum analysis of the input

and output waveforms of each drive were discussed in connection with harmonic influence in the front-end and in the motor end. The discussion also exemplified good quality waveform plots, harmonic spectra, performance factors and power calculations obtained with the DAQ system from high frequency PWM voltages associated with the VSD at different speed settings. Compared readings from a Fluke39 multi-meter were given and the predicted accuracy of the VI was proven.

Chapter 8

Passive circuits for harmonic correction

Many voltage source inverter drive systems use diode bridge rectifiers for the ac/dc conversion. The three phase diode bridge rectifier is employed in PWM inverters as described in Chapter 7. Multi-pulse rectification techniques use phase-shift transformers and multiple bridges to reduce the input current harmonic content specific to the three phase diode bridge. Both 6-pulse and 12-pulse rectifiers are examined in Chapter 6 by means of data acquired and analyzed with the DAQ system described in Chapter 5. This chapter presents new passive network-circuit topologies associated with diode bridge rectifiers for input current harmonic reduction.

8.1 Harmonic correction for 3-phase diode bridge rectifiers

The input current of a three-phase diode bridge rectifier with LC dc-link filter displays a total harmonic distortion of 32% (Chapter 6, Figure 6.5 (b)). When only a capacitor filter is employed, as in the case of the input stage of the PWM inverter drive, the harmonic distortion has a much larger value. For the drive investigated in Chapter 7, $\text{THD}_{60\text{Hz}} = 100\%$ at full-speed and $\text{THD}_{20\text{Hz}} = 152\%$ at 1/3 of the full speed of the driven motor. Innovations in IGBT switch technology are allowing active front-end rectifiers to be more cost effective and more reliable at industrial power levels. Chapter 4, section 4.4.3 illustrates an active switch network recommended for harmonic reduction. [12,28,29] describe an array of circuit topologies employing active resonance circuits that can lower the THD associated with diode rectifiers under the 5% level.

The operation of a 6-pulse diode rectifier can be improved by placing inductors in series with rectifier input terminals and Δ connected capacitors across the input.

Figure 8.1 illustrates the circuit connections of the additional network. The circuit used in the experimental setup for waveform acquisitions and data analysis employs resonant line inductors $L_R = 8.5$ mH and resonant capacitors $C_R = 33$ μ F.

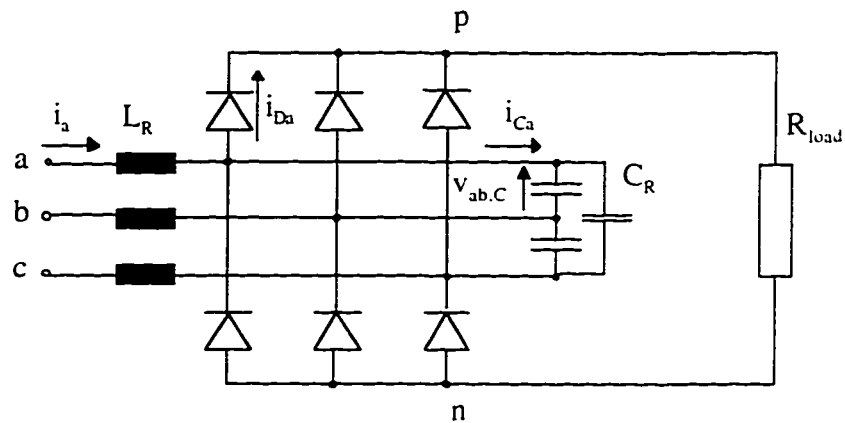


Figure 8.1 Resonant harmonic correction circuit for 3-phase diode bridge.

The operation of this circuit is similar to a diode bridge rectifier with large line inductors L_R with the difference that the capacitors C_R draw a resonant pulse in advance of the normal diode conduction periods. The waveforms of the current (i_a) and the phase-voltage (v_{an}) shown in Figure 8.2 (a) are acquired under the following conditions: input power $P=4.79$ kW ($S= 4.82$ kVA), line-line voltage $V_{an}= 196$ V, input current $I_a= 14.1$ A, input power factors $PF= 1$, $FPF= 1$, output voltage $V_{dc}= 277.4$ V, load resistance $R_{load}= 16.67$ Ω . The harmonic spectrum of the input current reproduced in Figure 8.2 (b) illustrates that the only significant harmonics are the 5th and the 7th and their small contribution is reflected by the low harmonic current (THD= 6.6%).

The current drawn by the LC resonant circuit builds up the current in each phase prior to the normal conduction periods associated with the diode bridge rectifier. To

appreciate the resonant pulse action. Figure 8.3 (a) illustrates the acquired waveform of the resonant current in phase-a: i_{Ca} (see circuit schematic: Figure 8.1). The difference

$$i_{Da} = i_a - i_{Ca}$$

is plotted in Figure 8.3 (b).

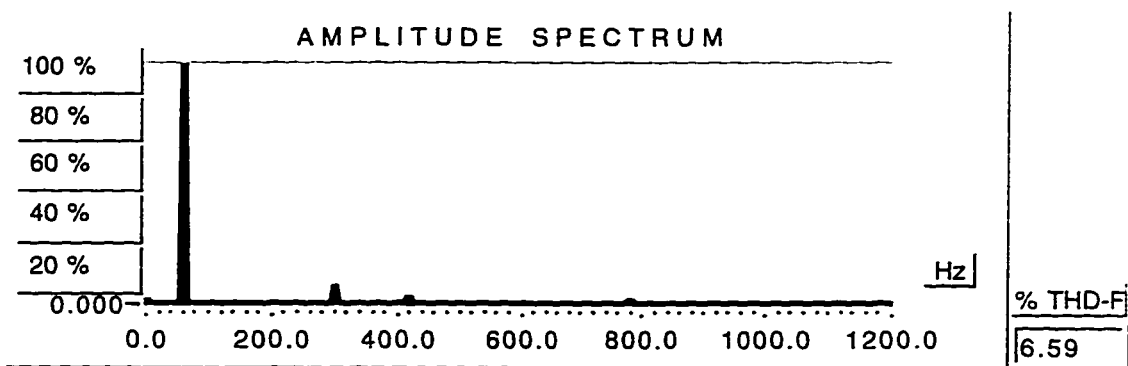
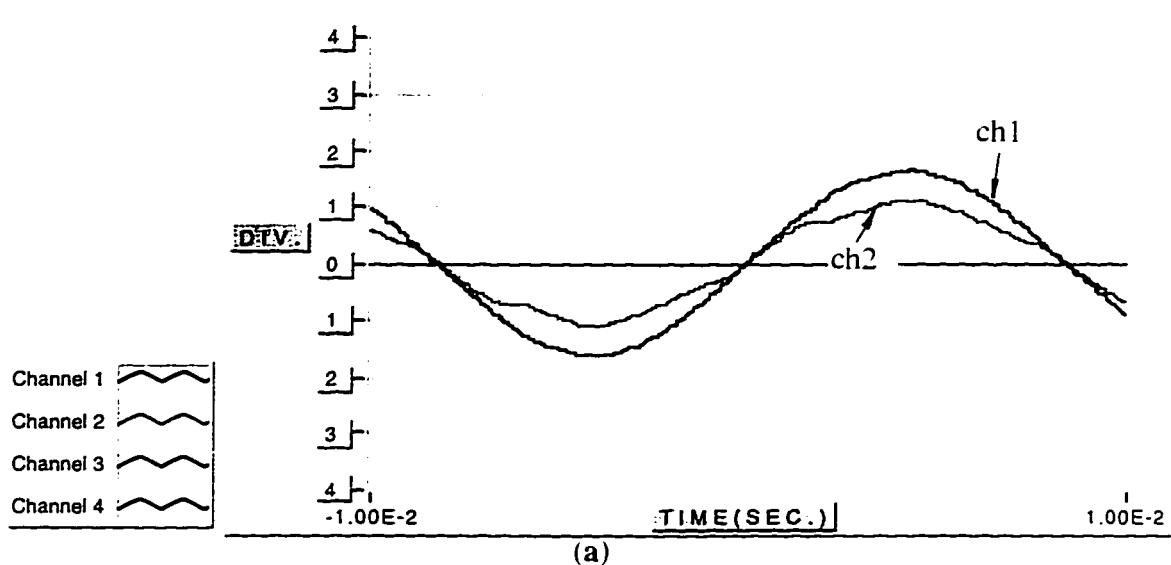


Figure 8.2 Diode bridge with harmonic correction unit: (a) input phase current (ch2: 20 A/div) and phase-voltage (ch1: 100v/div), (b) harmonic spectrum and THD of bridge input current.

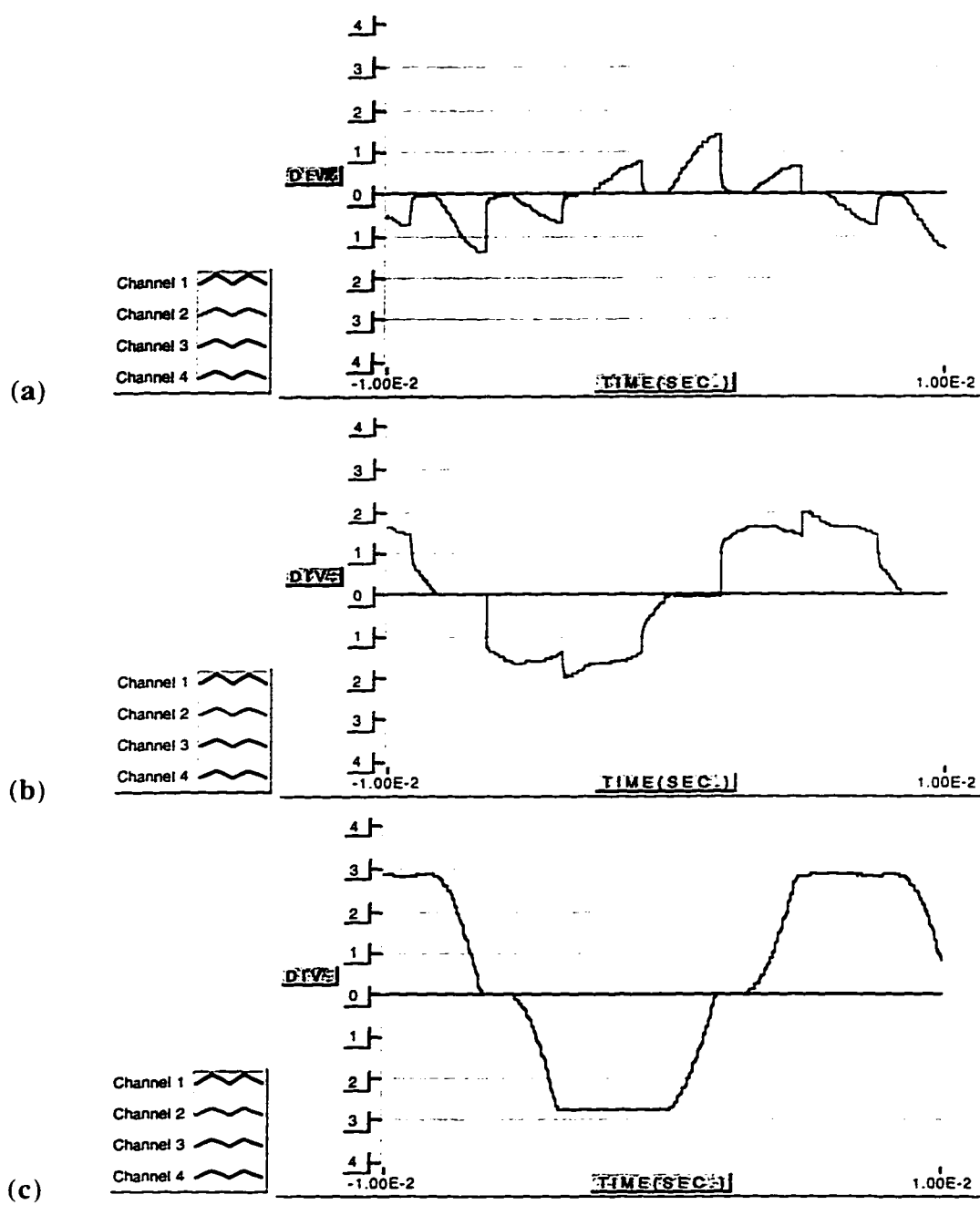


Figure 8.3 Harmonic correction unit waveforms: (a) resonating current i_{c_a} (10 A/div), (b) diode current i_{D_a} (10 A/div), (c) voltage across resonant capacitor C_{at} (100V/div).

The resonant action of the passive network is explained with reference to the zero time instant in Figure 8.3. The capacitor C_{ab} being charged at the $-(V_{dc})$ potential, discharges at 0V as the large i_{ca} resonating pulse is drawn from phase-a. During this time period no current is flowing through the diode ($i_{Da} = 0$). When the capacitor voltage reaches 0V, the diode starts conducting. The next i_{ca} pulse represents half the resonating current which splits in C_{ab} and C_{ac} charging C_{ab} at $v_{ab,C} = +V_{dc}$ (see Figure 8.3 (c)). The dip in the $v_{ab,C}$ during the next time period, when the voltage across the capacitor C_{ab} remains quasi-constant at V_{dc} level, is due to the negative pulse in i_{ca} which is part of the resonating current discharging capacitor C_{bc} . The large negative current pulse is due to the discharging of C_{ab} from $+V_{dc}$ to zero. The shape of the current in phase-a during the non-resonance periods has a soft slope caused by the large line inductor.

Resonant techniques employing SCR networks are currently investigated by the power electronics group of the University of Alberta. The active switching networks (see Chapter 4) improve the controllability of harmonic correction circuits. The low power ratings and electrical stresses associated with switch-mode converters make the harmonic correction units economical and reliable.

8.2 Harmonic correction for 12-pulse rectifiers

The 12-pulse rectifier is widely used to cancel the most dominant harmonics of the input current of three-phase diode bridge rectifiers. Two series connected bridges fed from phase shifting transformers are presented in Chapter 6 using the data acquired and analyzed with the LabVIEW data acquisition system. 12-pulse rectification can also be obtained by connecting the two diode bridges in parallel. The parallel connected rectifiers need inter-phase reactors between the bridges to prevent circulating currents.

The experimental circuit used for data acquisition employs in principal the 12-pulse rectifier described in Chapter 6. To further reduce the THD of the total input current, banks of Δ connected capacitors are placed in the input of each diode bridge. The resonating currents are obtained by including series inductors in the input of each rectifier. Under these conditions the circuit has no dc-link filter. The diagram of the experimental circuit is illustrated in Figure 8.4.

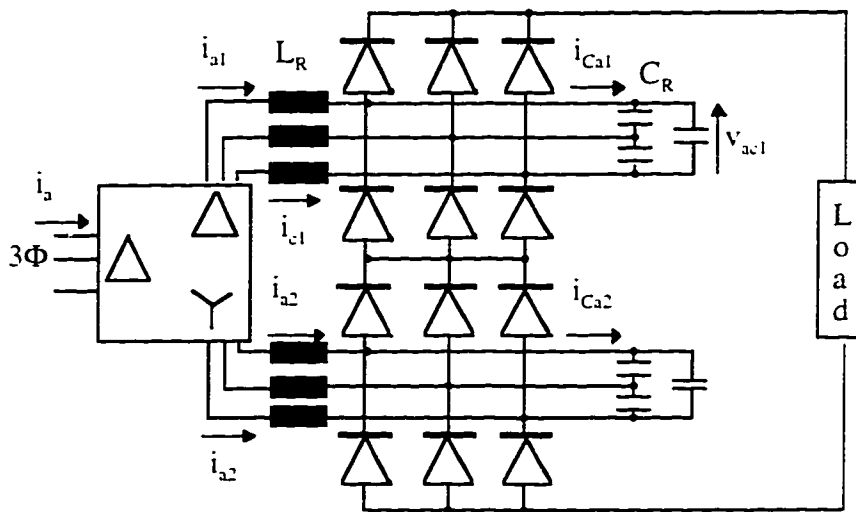
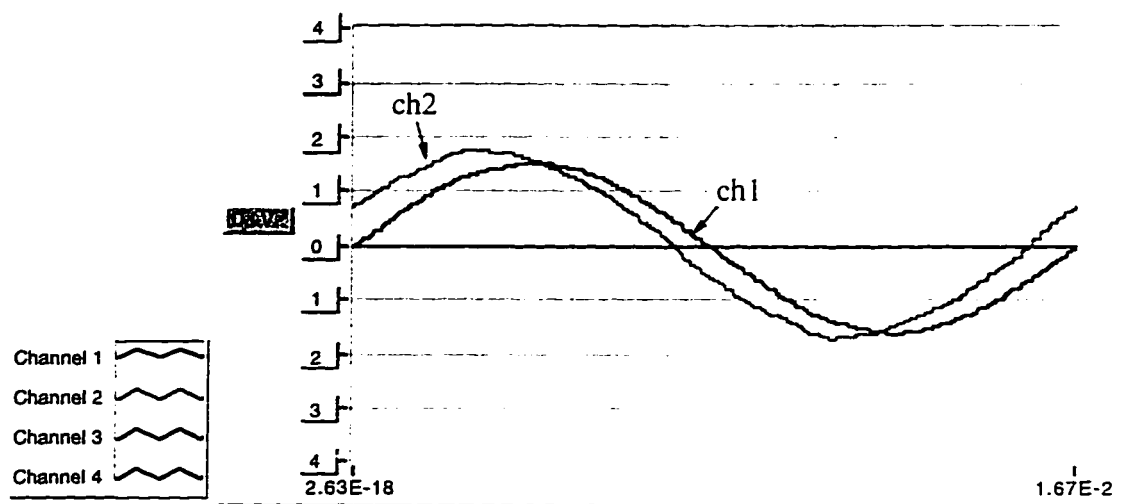
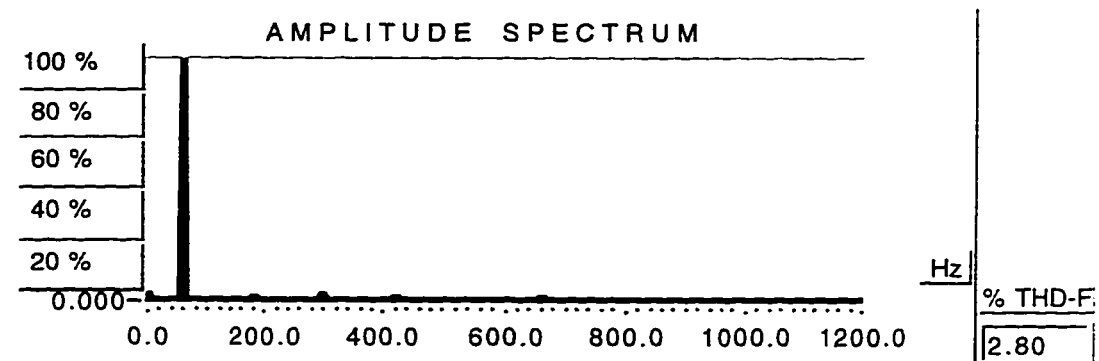


Figure 8.4 12-pulse rectifier with resonant-mode harmonic correction circuits.

The passive components used in the resonant circuits are $L_R = 5$ mH and $C_R = 40$ μ F. The experimental data was acquired under the following conditions: input power $P = 7.5$ kW ($S = 7.9$ kVA), power factors $PF = 0.95$, $FPF = 0.96$, input line-line voltage $V_{ab} = 196$ V, input current $I_3 = 23.4$ A.



(a)



(b)

Figure 8.5 Input waveforms and harmonic spectrum for the 12-pulse rectifier with harmonic correction unit: (a) input phase voltage v_{an} (ch1: 100 V/div), input current i_a (ch2: 20 A/div), (b) input current spectrum and THD₁.

Each set of inductors and capacitors operate similar to the harmonic control unit described in the previous section. The total input current i_a of the 12-pulse rectifier illustrated in Figure 8.5 (a) displays a leading angle relative to the phase voltage. This is

due to the large value of the available capacitors. A smaller value for C_R (e.g. $30 \mu\text{F}$) and the same series inductor would shift the current in the lagging region relative to the phase voltage. The resonant LC circuits are lowering the THD to 2.8% making the topology very attractive.

The resonant current i_{ca1} drawn from phase-a of the Δ secondary during a fundamental cycle is illustrated in Figure 8.6. The plot shows how the pulses of i_{ca1} contribute in shaping the current of phase-a and phase-c.

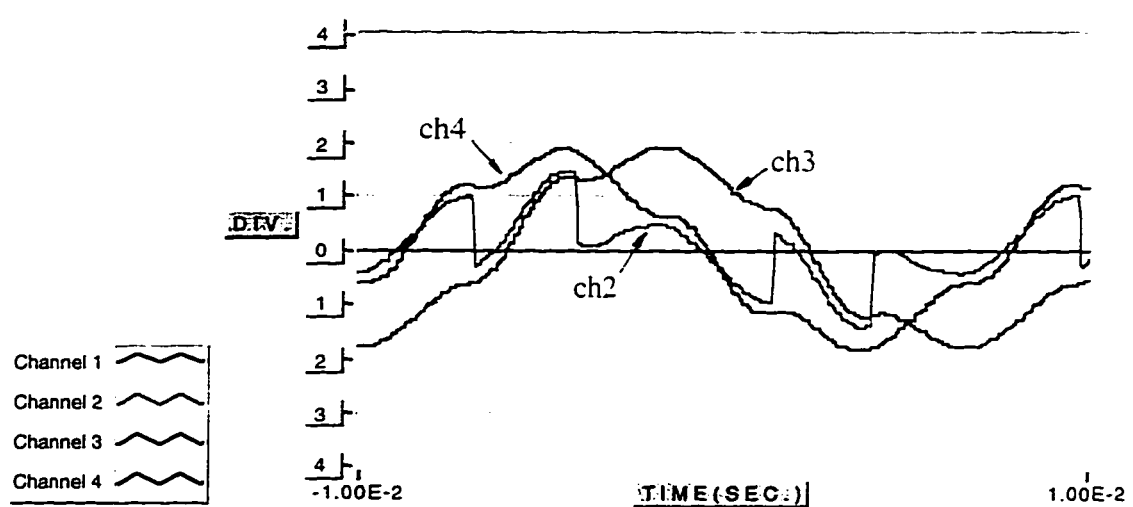


Figure 8.6 Resonant action of the Δ connected capacitors of the Δ - Δ -fed rectifier: resonant current i_{ca1} (ch2: 10 A/div), input line-current i_{a1} (ch3: 10 A/div), input line-current $-i_{c1}$ (ch4: 10 A/div).

A similar resonance action occurs in the network associated with the second diode bridge. The resonant current i_{ca2} is plotted in Figure 8.7 together with the line-currents i_{a1} and $(-i_{c1})$ which are shaped by the resonant pulses prior to the turn-on instant of the corresponding diodes. Without the resonant network, the input currents of each diode bridge of the 12-pulse rectifier displays a harmonic distortion of 26.5%. In

contrast, the harmonic analysis performed by the virtual instrument on the acquired data plotted in Figures 8.6 and 8.7. gives THD values of 12.1 % for the Δ - Δ transformer and 12.7 % for the Δ -Y transformer.

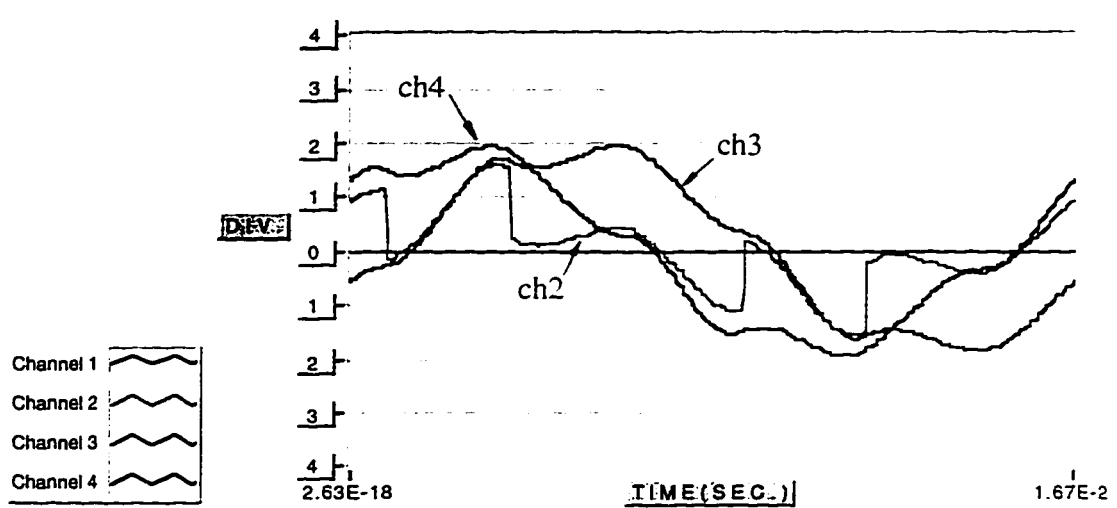


Figure 8.7 Resonant action of the Δ connected capacitors of the Δ -Y-fed rectifier: resonant current $i_{C_{a1}}$ (ch2: 10 A/div). input line-current i_{L1} (ch3: 10 A/div). input line-current $-i_{L1}$ (ch4: 10 A/div).

Since the input harmonics drawn by the 6-pulse rectifiers are concentrated in the 5th and 7th harmonics, the input current distortion obtained for the 12-pulse rectifier with resonant harmonic cancellation is well under 5 % limit recommended in standards (see Figure 8.5 (b)). The capacitors used in the harmonic correction units can be alternatively connected in Δ or Y. The delta connection lowers the capacitor size but increases their RMS current rating. The resonant operation is functionally the same in both instances. The disadvantages associated with leading power factor under light load

conditions can be addressed with thyristor networks to control the position of the resonant pulse drawn in advance of the normal diode conduction periods [28].

This chapter described the successful investigation of research level circuits by means of the LabVIEW-based DAQ and analysis system. The quest for developing novel topologies of power electronic circuits which provide low harmonic content of the input current of the diode bridge rectifiers is currently a main research priority of the power electronics group of the University of Alberta. Some of the circuits employing active networks and currently under investigation with the DAQ system were presented in section 4.4.3.

Chapter 9

Conclusions

9.1 Author's contribution and general conclusions

This thesis presents the development of a LabVIEW based data acquisition system for waveform acquisitions and analysis for power electronics circuits. The system consists of a Power Macintosh 7100/66 computer with a NI-488 card linked via GPIB cable to a Tektronix TDS 420 oscilloscope which can acquire four channels of data from the circuit under investigation.

The virtual instrument simulates the front panels of a four channel oscilloscope and an harmonic analyzer and gives calculated values for effective values of two acquired channels, active and apparent power, power factors and harmonic amplitudes.

In the first part of this work the power system disturbances are briefly examined together with their causes. The harmonics associated with power transformers, electrical machines, arc furnaces and fluorescent lights as established harmonics polluters were identified.

The main concern regarding harmonics comes from the current proliferation of power electronic circuits. The largest nonlinear loads are the power converters used in the metal reduction industry and high voltage direct current transmissions. The following category includes medium size converters employed in the manufacturing industry for motor control or railway applications. Energy conservation measures such as those for improved motor efficiency or load matching are lowering the power level at which variable speed drives are employed. High productivity office equipment, personal computers and an increasing number of house-hold appliances use single-

phase switch-mode power supplies as utility interface. The prospected increase in the amount of power processed by power electronic devices makes the solid-state harmonics problem become one of the most important problems in the power system. Consequently an entire chapter is dedicated to diode bridge rectifiers as harmonic producers.

To facilitate the understanding of the LabVIEW program, the graphical programming environment is briefly described. Details regarding the tools available to create the front panel of a virtual instrument, the source code behind it - called the block diagram, and the pane connector are given in the Appendix B.

The developed virtual instrument has two distinctive parts: the virtual oscilloscope, and the harmonic analyzer together with the indicators corresponding to power calculations and power factors. Each part was presented, beginning with its front panel which is the user interface. The front panel objects are described with reference to their role as indicators or controllers in the block diagram. A detailed description of the block diagram is given in Appendix C with reference to each program's part enabling a good understanding of the different programming techniques employed. Each front panel object has a corresponding image in the block diagram. The block diagram of the instrument driver associated with the Tektronix oscilloscope consists of six frames of a sequence structure which control the program's flow. Each program sequence is described in detail with reference to the front panel controls and indicators.

The harmonics generated by solid-state devices in general and diode bridge rectifiers in particular are the target of the current research efforts of the power electronics group of the University of Alberta. The virtual instrument is employed for waveform acquisitions and data analysis from a selected number of power electronics circuits. After experimental data regarding diode bridges is presented, the thesis

describes from a power quality perspective the behavior of two induction motor variable speed drives: the square wave inverter drive and the PWM inverter drive. Acquired waveforms from both the utility interface and the inverter output are presented, along with waveform harmonic spectra, power and power factors calculations. The analysis regarding each drive refers also to the harmonic effects on the utility side and the internal effects in the motor.

The thesis concludes by presenting the investigation of research level circuit topologies for harmonic correction associated with 6-pulse and 12-pulse series rectifiers. The resonant action of the retrofit circuits is illustrated by plots of acquired waveforms. Harmonic analysis of the rectifier input current performed by the virtual instrument is presented, and calculated total harmonic distortion values are given.

Throughout the experimental part of the thesis (Chapters 6, 7 and 8), all measurements obtained from the virtual instrument were compared with the readings from a FLUKE 39 Power Meter. The differences between the values obtained from the LabVIEW based virtual instrument and those obtained from the power meter were within 1% for active power P , reactive power S , power factor PF , fundamental power factor FPF as well as the harmonic amplitudes and THD calculations.

9.2 Suggestions for further work

In equal measure for the beginner and for the advanced LabVIEW programmer, the LabVIEW users-group from <info-labview@pica.army.mil> proves to be an invaluable resource of help and information. More than 2000 people from all over the world are ready to give advice and suggestions whenever a question is posted. Many problems encountered during the programming stage were confirmed by other LabVIEW users. Computer crashes associated with memory management failures of the

Macintosh computer running LabVIEW was the most frequent and annoying problem. Bugs in some LabVIEW library functions, and reported on the user group are still discovered. Some of these bugs were fixed in the recent released new version: LabVIEW 4.1. Unfortunately, this version with enhanced data acquisition capabilities is currently available only for IBM compatible PCs.

The developed system can be expanded to communicate with two Tektronix TDS 420 oscilloscopes to obtain efficiency calculations from three-phase power electronic circuits.

A logical future step would be the development of a data acquisition program employing analog/digital (A/D) board instead of the oscilloscope. A much higher acquisition rate (300 - 500 kHz) for measurement accuracy and an E-series card for time synchronization will facilitate precise calculations employing waveforms from different channels. At this acquisition rate, the THD.VI available in the Advanced Measurements library of LabVIEW 4.1 will allow phase-angle calculations associated with the signal harmonics. The THD calculations are very computing intensive and computer resourced have to be allocated for proper functionality of the main VI.

Due to the increasing market-share of the PC computers, PC compatible A/D boards and other instrumentation hardware are produced at improved performance. Consequently, the idea of switching to PC based LabVIEW programming is strongly encouraged.

Bibliography

- [1] Corney, A.C., Pullman, R.T. - "Digital Sampling Laboratory Wattmeter". IEEE Transactions on Instrumentation and Measurement, vol.IM-36, No. 1, March 1987.
- [2] Clarke, F.J.J., Stockton, J.R. - "Principles and theory of wattmeters operating on the basis of regularly spaced sample pairs". Journal of Physics Engineering: Scientific Instruments, vol. 15, 1982.
- [3] Chen.C.H.: "Digital waveform processing and recognition". CRC Press. Inc., Boca Raton, Florida, 1982.
- [4] Butler, D., Haway, G.: "The Fast Fourier Transform and its implementation"- Signal Processing- Proceedings of the NATO Advanced Study Institute on Signal Processing. Academic Press Ltd., London, 1973.
- [5] Oppenheim, A.V., Schafer, R.W.: "Digital signal processing"- Prentice Hall, Inc., Englewood Cliffs, NJ, 1975.
- [6] Elliot, F.D.: "Handbook of digital signal processing- Engineering applications". Academic Press, Inc., 1987.
- [7] Mukherjee, S., Hoft, R.G., McCormick, J.A., - "Digital Measurement of Efficiency of Inverter-Induction Machines", IEEE Transactions on Industry Applications, vol.26, No 5, Sept./Oct., 1990.
- [8] Stenbakken, G.N. - "A wideband sampling wattmeter", IEEE Transactions on Power Apparatus and Systems, vol. PAS-103, No. 10, October 1984.
- [9] * * * : "The Dranetz field handbook for power quality analysis". Dranetz Technologies, Inc., Edison, New Jersey, 1991.

- [10] Griscon, S., B.: "Lamp flicker on power systems" - Central Station Engineers of the Westinghouse Electric Corporation, Electrical Transmission and Distribution Reference Book, East Pittsburg, Pennsylvania.1964.
- [11] * * * : "Power quality for electrical contractors", Application guide. Vol.1- Electrical Power Research Institute (EPRI), 1994.
- [12] Salmon, J.C., Bocancea, E., Nowicki, E.: " Harmonic Correction Circuits for VSI Drives using 3-phase Thyristor Networks", Conf.Rec. 1996. IASTED-High Technology in the Power Industry.
- [13] * * * : "Guide for applying harmonic limits on power systems"- Document prepared by P519A Task Force of the Harmonics Working Group (IEEE PES T&D Committee) and SCC22-Power Quality, May 1996.
- [14] * * * : IEEE Std. 519-1992. "IEEE Recommended Practices and Requirements for Harmonic Control in Electric Power Systems". 1993.
- [15] * * * : Emerald book. "IEEE Recommended Practice for Powering and Grounding Sensitive Electronic Equipment P-1100". Institute for Electrical and Electronic Engineers, New York, 1992.
- [16] Monteith, A.C., Harder, E.L., Clayton. J.M.: "Line design based upon direct strokes" - Central Station Engineers of the Westinghouse Electric Corporation. Electrical Transmission and Distribution Reference Book. East Pittsburg. Pennsylvania.1964.
- [17] Witzke, R. L.: "Power system voltages and currents during abnormal conditions" - Central Station Engineers of the Westinghouse Electric Corporation, Electrical Transmission and Distribution Reference Book. East Pittsburg. Pennsylvania.1964.

- [18] Victor, D., Standridge, J., Aseerwatham, N., Hemesath, B.: "Project report for technical support services for SMES technology evaluation. UPS evaluation". Science Application International Corporation, CA, Sept. 1996.
- [19] Arillaga, J., Bradley, D.A., Bodger, P.S., : "Power System Harmonics". New York: Wiley, 1985.
- [20] Johnson, A.A.: "Application of capacitors to power systems"- Central Station Engineers of the Westinghouse Electric Corporation, Electrical Transmission and Distribution Reference Book, East Pitsburg, Pennsylvania, 1964.
- [21] Say, M.G.: "Alternating current machines". Pitman Publishing Ltd., London. 1984.
- [22] Dordea, T.: "Masini electrice", Editura Didactica si Pedagogica. Bucharest. 1977.
- [23] Bala, C.: "Masini electrice" . Editura Didactica si Pedagogica. Bucharest. 1982.
- [24] Preda, M., Cristea, P., Spinei, F.: "Bazele Electrotehnicii", vol. 1 and 2. Editura Didactica si Pedagogica. Bucharest. 1980.
- [25] Emanuel, A.E.: "Powers in nonsinusoidal situations. A review of definitions and physical meaning". IEEE Transactions on Power Delivery, Vol.5, No.3, July 1990.
- [26] Mohan, N., Undeland, T.M., Robbins, W.P.: "Power electronics - converters, applications and design", John Willey & Sons. 1995.
- [27] Wasserab, T.: "Schaltungslehre der Stromrichtertechnik". Springer-Verlag, Berlin. 1962.
- [28] Salmon, J.C., Nowicki, E.: "Harmonic Correction of Voltage Source Inverter Drives", Conf.Rec. . CCECE-1995.

- [29] Salmon, J.C., Bocancea, E., Bhargava, R., Nowicki, E.: "SCR harmonic correction topologies for VSI drives", Conf.Rec., CCECE-1996.
- [30] Paice, D.A.: "Power electronic converter harmonics". IEEE Press, New York. 1996.
- [31] * * * : IEC Norm 555-3 prepared by International Electrical Commission, 1993.
- [32] Xu, W., Masour, Y., Siggers, C., Hughes, M.B.: "Developing Utility Harmonic Regulations based on IEEE Std. 519 - B.C. Hydro's Approach". IEEE Transactions on Power Delivery, Vol. 10. No. 3, July 1995.
- [33] Xu, W. - "A Practical Harmonic Guideline for Adjustable Speed Drive Applications", IEEE Trans. on Power Delivery, Vol. 7, Jan. 1992.
- [34] Mukul, R., Naik, R., Mohan, N.: "A comparative evaluation of harmonic reduction techniques in three-phase utility interface of power electronic loads". Conf. Rec. 1993, IEEE- IAS. Ann. Mtg., pp. 971-978.
- [35] Naik, R., Mukul, R., Mohan, N., Nilssen, R., Henze, C.P.: "A magnetic device for current injection in a three-phase, sinusoidal-current utility interface". Conf. Rec. 1993, IEEE-IAS, Ann. Mtg., pp. 926-930.
- [36] Kim, S., Enjeti, P., Packebush, P., Pitel, I.: "A new approach to improve power factor and reduce harmonics in a three phase diode rectifier type utility interface". Conf. Rec. 1993, IEEE-IAS. Ann. Mtg., pp. 993-1000.
- [37] Enjeti, P., Shireen, P., Packebush, P., Pitel, I.: "Analysis and design of a new active power filter to cancel neutral current harmonics in three phase four wire electric distribution systems", Conf. Rec. 1993, IEEE-IAS. Ann. Mtg., pp. 939-946.
- [38] * * * Tektronix TDS420 & TDS460 Digitizing Oscilloscopes - User Manual. Tektronix Inc. Beaverton. March 1993.

[39] * * * LabVIEW Tutorial Manual - National Instruments Corporation, 1996.

[40] * * * LabVIEW User Manual - - National Instruments Corporation, 1996.

[41] Johnson. G.W.: "LabVIEW graphical programming. Practical applications in instrumentation and control" , McGraw-Hill, Inc., New York,1994.

Appendix A

Example of Harmonic Current Limits

The Guide for Applying Harmonics Limits on Power System [9] lists values for the harmonic current I_h as evaluated at the PCC (i.e. where the utility can supply other loads). The limits are dependent on the customer load in relation to the system short circuit capacity at the PCC. All current limits are expressed as a percentage of the customer's average maximum demand load current (I_L).

For a nominal voltage of $V_n < 69$ kV and $I_{sc}/I_L < 20$, the harmonic currents are limited as follows:

$$I_h / I_L = 4.0 \text{ for } h < 11$$

$$= 2.0 \text{ for } 11 \leq h < 17$$

$$= 1.5 \text{ for } 17 \leq h < 23$$

$$= 0.6 \text{ for } 23 \leq h < 35$$

$$= 0.3 \text{ for } 35 \leq h, \text{ and the Total Demand Distortion is limited at TDD} = 5.0 \%$$

All these values increase with the increase of the system capacity and decrease with the increase of the nominal voltage. The harmonic order "h" refers to odd numbers. The even harmonics are limited to 25% of the listed values. These limits are recommended to be applied when harmonic filter resonance magnifies one of the even harmonics causing unacceptable voltage distortion levels.

The I_{sc} is the short circuit at the point of common coupling under normal system conditions. I_L is the fundamental frequency component of the maximum demand load current at PCC and it can be calculated as average of the maximum monthly demand currents for the previous 12 month or it can be estimated based on predicted load profiles.

The Total Demand Distortion (TDD) is defined as:

$$TDD = \frac{\sqrt{\sum_{h=2}^{\infty} I_h^2}}{I_L} \times 100\%$$

For loads consisting of power converters with pulse number (q) higher than six, the limits recommended are increased by a factor equal to $\sqrt{\frac{q}{6}}$ under the above mentioned considerations regarding even harmonics.

Appendix B

LabVIEW environment and tools

A description of the basic capabilities, tools and functions as well as the main features of the LabVIEW environment is necessary for enabling a better understanding of the programming environment of the DAQ system developed. This discussion provides also important information for operating the developed virtual instrument.

LabVIEW uses terminology, icons, and ideas familiar to scientists and engineers and relies on graphical symbols rather than textual language to describe programming actions. It also has extensive libraries of functions and subroutines for most programming tasks and it contains application-specific libraries for GPIB (general purpose interface bus) and serial instrument control, data analysis, data presentation and data storage. LabVIEW includes conventional program development tools allowing the user to set breakpoints, animate program execution to see how data passes through the program, and single-step through the program to make debugging and program development easier.

B1. LabVIEW's main features

The interactive user interface of a VI is called the **front panel** because it simulates the panel of a physical instrument. The front panel can contain knobs, push buttons, graphs and other controls and indicators. The instructions for the VI are contained by a **block diagram** which is constructed by the programmer using the language G. The block diagram supplies a suggestive pictorial solution to a programming problem and it contains the code for the VI. The VIs use a hierarchical and modular structure. They can be used as top-level programs or as subprograms

within other programs or subprograms. A VI within another VI is called a subVI. The **icon and connector pane** of a VI work like a graphical parameter list so that other VIs can pass data to it as a subVI.

The Front Panel

The front panel contains a toolbar of command buttons and status indicators (Figure B.1) that are used for running and debugging VIs. It also contains font options and alignment and distribution options for editing VIs.

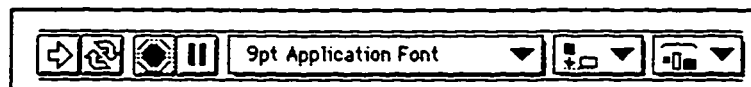




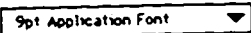




Figure B.1 Front panel toolbar

The buttons are operated by mouse-click and are listed below:

- | | |
|---|---|
|  | <ul style="list-style-type: none"> • Run button - runs the VI: it changes appearance to indicate that the VI is running. |
|  | <ul style="list-style-type: none"> • Continuous Run button - runs the VI over and over: it is useful for debugging. |
|  | <ul style="list-style-type: none"> • Stop button - aborts VI execution. |
|  | <ul style="list-style-type: none"> • Pause/ Continue button - pauses VI execution/continues VI execution. |
|  | <ul style="list-style-type: none"> • Font Ring - sets font options including font type, size, style and color. |
|  | <ul style="list-style-type: none"> • Alignment Ring - sets alignment options including vertical, top edge, left and so on, for two or more objects on the front panel. |
|  | <ul style="list-style-type: none"> • Distribution Ring - sets distribution options including gaps, compression and so on for two or more objects on the front panel. |

The front panel of a VI is the user interface that reproduces the appearance of the real instrument's front panel and in many cases can be the only part being accessed by the user. An example of a front panel of a VI, used as a subVI in the program presented in this work, is illustrated in Figure B.2. This subprogram called CopyToFile.VI prompts the user to select Spreadsheet or Matlab format when data is saved to file. By pressing the OK button, the selection is taken into consideration by the main program.

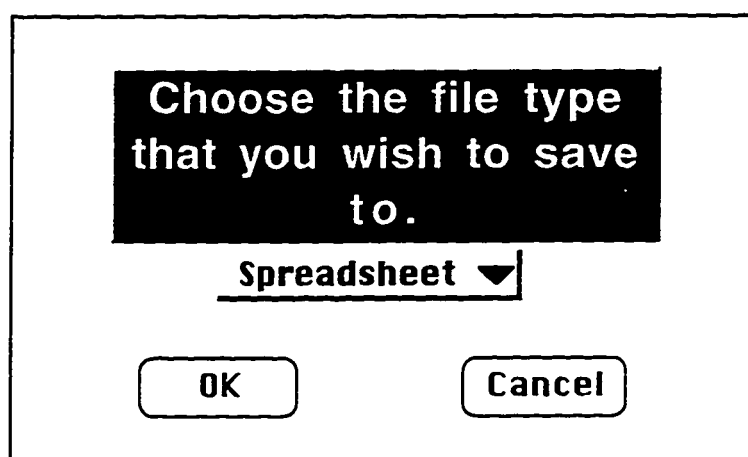


Figure B.2 Example of front panel: ChooseFileType.VI.

The Block Diagram

Each front panel has an accompanying block diagram which is the VI equivalent of a program. The block diagram, constructed using the graphical programming language G, can be considered as the source code. The components of the block diagram represents program nodes such as For Loops, While Loops, Case Structures and functions. The different components are “wired” together and show the flow of data within the block diagram. Shift registers can be employed to store values from one iteration of a loop to the next.

The block diagram associated with the front panel presented in Figure B.2 is reproduced below (Figure B.3). The pull-down menu and the push buttons on the front panel (Figure B.2) have corresponding elements in the block diagram (Figure B.3). A more detailed description of the different features of a block diagram and its building elements is provided in Appendix C, where the developed Virtual Instrument for data acquisition and analysis is described in detail.

The power of LabVIEW lies in the hierarchical nature of VIs. After a VI is created, it can be used as a subVI in the block diagram of a higher level VI. One can have an essentially unlimited number of layers in the hierarchy.

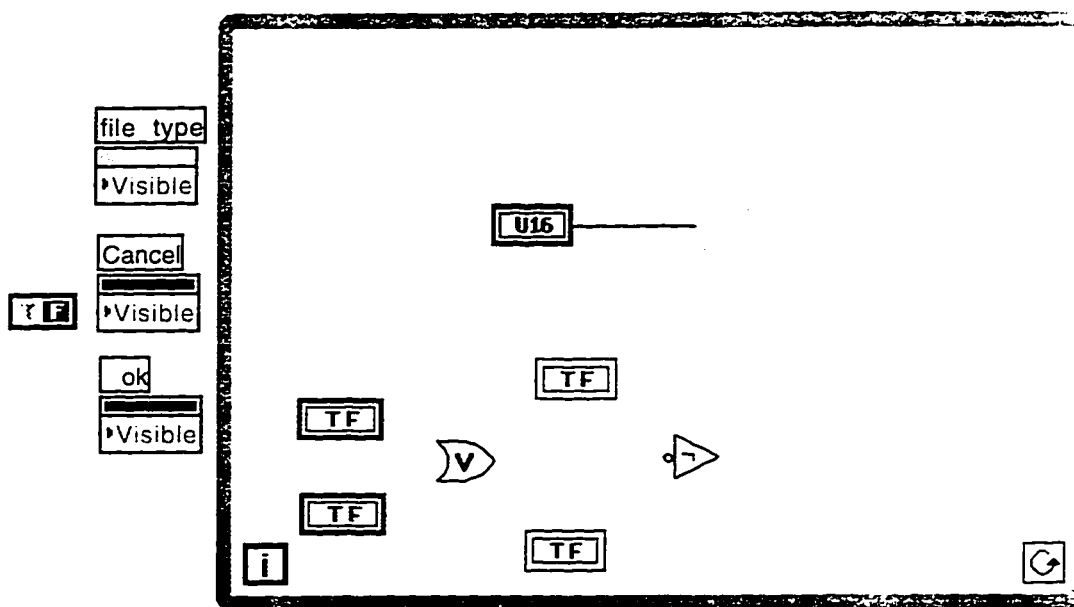


Figure B.3 Block diagram of ChooseFileType.VI.

Icon/Connector Pane

The icon/connector pane is used to turn a VI into an object that will be used in the block diagram of other VIs as subroutine or function. The icon and the connector

are located in the upper right corner of the VI's front panel. The icon graphically represents the VI in the block diagram of other VIs. The connector terminals determine where the inputs and outputs of the VI as a "building stone" have to be wired. The terminals are analogous to parameters of a subroutine or function; they correspond to the controls and indicators on the front panel of the VI. The icon hides the connector until the user chooses to view it.

The icon for ChooseFileType.VI is illustrated in Figure B.4. This subVI appears in the block diagram of the main program and can be converted to its connector pane for wiring purposes. (The connections in the block diagram are called wires; when a block diagram is built, the program elements are connected using the wiring tool).













Figure B.4 Icon of ChooseFileType.VI used as subroutine in the main program.

Tools Palette

LabVIEW 4.0 has a floating tools palette (Figure B.5) which is used to edit and debug VIs. A tool is a special operating mode of the mouse cursor that is used to perform specific functions.

The list of the tools provided is given bellow:

- 
 - operating tool - places Controls and Functions palette items on the front panel or block diagram.
- 
 - positioning tool - positions, resizes and selects objects.

-  • labeling tool - edits text and creates free labels.
-  • wiring tool - wires objects together in the block diagram.
-  • object pop - up menu tool - brings up on a pop-up menu for an object.
-  • scroll tool - scrolls through the windows without using the scroll-bars.
-  • breakpoint tool - sets breakpoints on VIs, functions, loops, cases and sequences.
-  • probe tool - creates probes on wires.
-  • color copy tool - copies colors for pasting with the color tool.
-  • color tool - sets foreground and background colors.

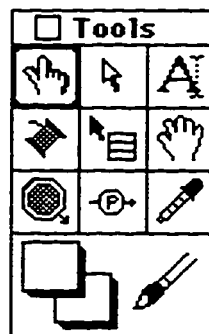


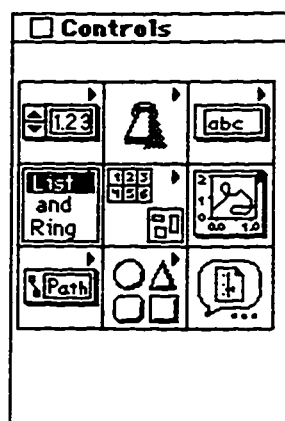
Figure B.5 LabVIEW 4.0 Tools Palette.

If the tool palette is not visible it can be opened by selecting **Windows>Show Tool Palette** from either the front panel menu or the block diagram menu.

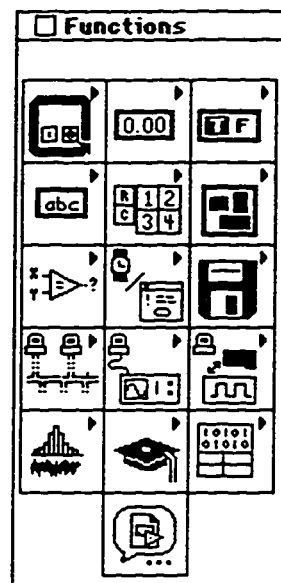
Controls Palette/ Functions Palette

The controls palette consists of a graphical, floating palette that automatically opens when LabVIEW is launched. This palette (Figure B.6 (a)) is used to place controls and indicators on the front panel of a VI. The controls and indicators can belong to one of the following categories: numeric, Boolean, string and table, list and ring, array and cluster, graph, path and refnum, decoration or customized type.

The functions palette (Figure B.6 (b)) consists of a graphical, floating palette that also is automatically opened when the user switches to the block diagram. This palette is used to place nodes (constants, indicators, VIs and so on) on the block diagram of a VI. Each top-level icon contains similarly subpalettes and an object of a block diagram can belong to one of the following categories: structures, numeric, Boolean, string, array, cluster, comparison, time and dialog, file I/O, communication, instrument I/O, data acquisition, analysis, advanced or customized type.



(a)



(b)

Figure B.6 LabVIEW floating palettes: (a) Controls Palette: (b) Functions Palette

When different objects are wired together, the color and the thickness of the connecting wire changes according to the data type flowing through that particular link making the block diagram easier to understand. When the data is integer, the wire in the block diagram is blue, for Boolean data the wire is green, for floating point it is orange etc.

Being a graphical programming language, LabVIEW is very different from the code based languages and in many cases easier to use.

Appedix C presents many programming techniques employed in the developing of the Virtual Instrument for DAQ and analysis for power electronic circuits.

Appendix C

Data Acquisition and Analysis Program

C.1 The Virtual Oscilloscope Front Panel

C.1.1. Multiple plot graph

The data acquisition part of the front panel features a graph or “screen” where the waveforms that have been read are plotted together with the corresponding legend indicating the color assigned to each channel (Figure C.1). The display looks exactly as it does on the oscilloscope. Probe scaling information is not reflected on the graph.

Any item on the front panel can be moved at will using the positioning tool from the tools palette, without affecting the data flow of the program. This is a desired feature when a new item has to be accommodated on the front panel. The graph or the push buttons can also be re-dimensioned using the resizing tool and their color can be changed with the coloring tool. All these actions are rather cosmetic and can bring advantages when the computer screen being used is changed (e.g. using a laptop instead of a desktop computer).

The graph, a library item, can be customized to match the data display requirements. From the many features available this chart has only its legend displayed. Other features include: a scroll-bar, a palette and a digital display. They can be activated by popping up on the chart and selecting the desired features [39],[40]. IEEE-519 Standard requires that 12 periods of the fundamental be acquired for obtaining reliable data for harmonic analysis [14]. For this reason, by default, the time axis is spanned over 0.2 s. However these limits can be changed using the labeling tool. If for example one wishes to view only one period of a 60 Hz voltage: double-click on (-1.00E-1) with

the Labeling tool, type 0 and press <return>; again with the Labeling tool the second number from the right extreme of the X axis can be set to 16.67E-3.

C.1.2 General Control Buttons

After the oscilloscope is turned on, a number of controls on the front panel give the user flexibility in acquiring and analyzing data. Figure C.2 shows the controls regarding the communication between the computer and the oscilloscope.

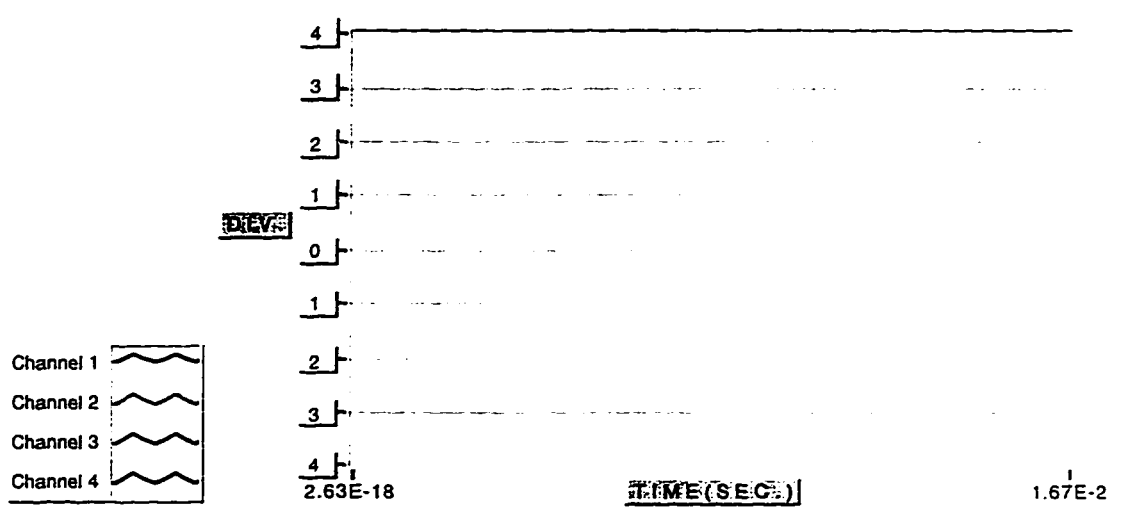


Figure C.1 The graph and its legend.

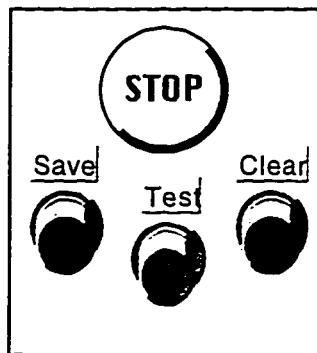


Figure C.2 Main front panel controls.

All push buttons are operated by mouse-click using the operation tool.

- the **Stop** button is pressed to end the communication session with the Tektronix oscilloscope.

- the **Test** control checks whether or not there is communication between the computer and the oscilloscope. If the communication is correct, the oscilloscope will emit an acoustic signal when the button is pressed. If no sound is heard, the computer and the oscilloscope are not communicating properly.

- the **Clean** button is pressed to clean the graph.

- the **Save** button is used to save the waveforms on the computer screen and on file. The user is prompted for a file format (either Matlab or Spreadsheet) and a file path name. The spreadsheet format saves the data in tab-delimited columns. The Matlab format saves the data in an array called TDS420. All four channels plus the time array are saved.

C.1.3 Data Acquisition Indicators

The two indicators provided on the front panel in connection with the data acquisition are shown in Figure C.3.

- $t(0)$ indicates the initial point for data acquisition.

- dt is the time increment value from one acquired point to the next.

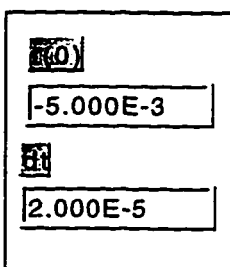


Figure C.3 Data acquisition indicators.

C.1.4 Channel Controls and Indicators

The controls and indicators associated with each channel of the virtual oscilloscope are presented in Figure C.4. All four channels are identical regarding the probe scales available. The functions performed by each control and indicator are as follows:

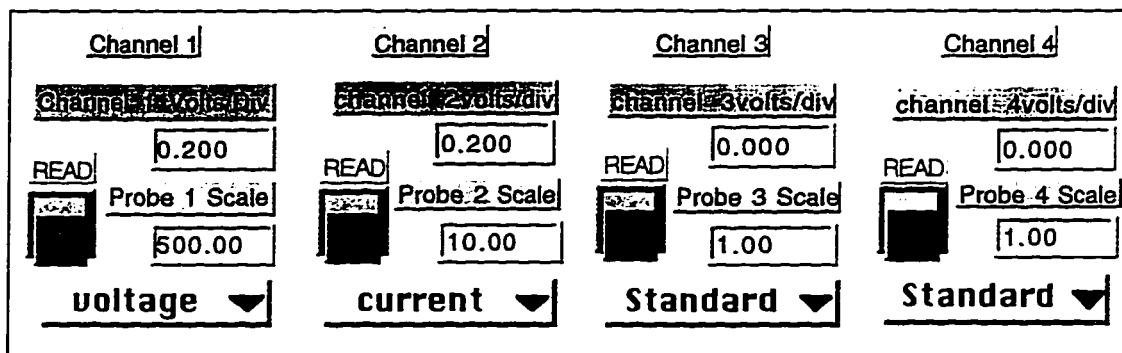


Figure C.4 Channels controls and indicators.

- **READ**: by pressing this push-button the corresponding channel is read. This will also prompt for scale information if anything other than a standard probe is being used.
- **Channel x Volt/Div** : displays the Volt/division for channel x. $x = 1, 2, 3$ or 4 .
- **Probe scale** : displays the scaling factor from the probe being used for channel x. A standard probe has a factor of 1. Choosing a probe other than standard (as shown in Figure C.4 for channel 1 and 2) will prompt the user for scale information. The front panels of the subVI corresponding to voltage probe and current probe are illustrated in Figure C.5 (a) and (b). If, for example, the acquired waveforms are two voltages and two currents -as in the case of three-phase power measurements, the user is prompted two times to select voltage probe constants and two times for current probe information. The numeric values associated with each probe is employed in calculations resulting in voltage and currents saved on file in Volts and Amps and power calculations displayed in VA and Watts.

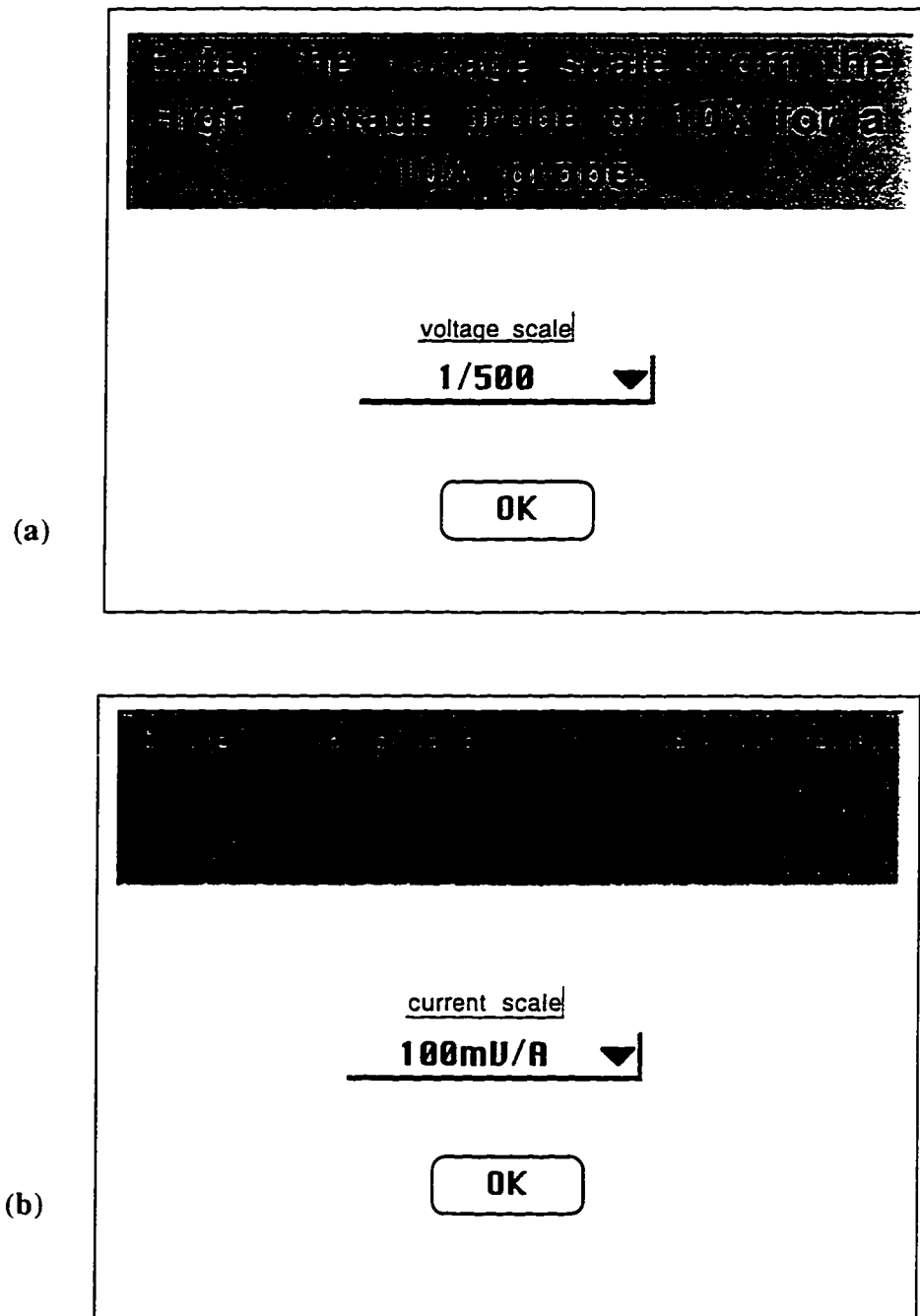


Figure C.5 Scale-prompt front panels: (a) Voltage Info.VI. (b) Current Info.VI.

C.2 Virtual Oscilloscope Block Diagram

C.2.1 Initialization

The initialization of the oscilloscope uses the InitializeVI from the Tektronix TDS 4xx library available in LabVIEW 4. This subVI concatenates a command string and sends it to the oscilloscope. The instrument can be reset by setting the reset control on the front panel of this VI. (To open the front panel of any subVI double-click on its icon in the block-diagram). Figure C.6 shows the connections of the InitializeVI in the virtual oscilloscope's block diagram. This VI is obtained from the Tektronix library delivered with the software. The instrument descriptor appears on the main front panel of the developed virtual instrument and the Boolean switches ID Query and Reset can be accessed on the front panel of the subVI.

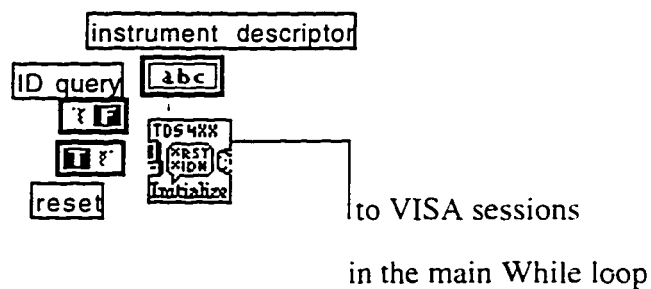


Figure C.6 Initialization subVI.

C.2.2 Data Acquisition block diagram

The main program is contained in a While Loop which is controlled by the Stop button on the front panel (see Figures 5.4 and C.2).

The virtual oscilloscope waveforms acquisition resides in a Sequence Structure, which performs like frames of film and executes the block diagram sequentially. In

conventional programming languages, the program statements execute in the order in which they appear. In data flow programming, a node executes when data is available at all of the node inputs. In this case it is necessary to execute certain nodes in a pre-defined order. LabVIEW places the diagram that the VI executes first inside the border of Frame 0, it places the diagram it executes second inside the border of Frame 1 and so on. Using this technique, the data acquisition consists of six frames of Sequence Structure that execute the different stages of the process as outlined in the following discussion.

Frame 0 contains two Case structures and the block diagram corresponding to the Boolean switches associated with the Clear and Test buttons on the front panel (see Figure C.2). The Case structure is by default a Boolean type and it has only two cases: true and false. In text-based programming languages the Case structure is analogous to an if-then-else statement. The Case structure controlled by the Test button, contains a library subVI named Tek TDS Audio Alert.VI which sends a BELL command to the instrument if the button is pushed (i.e. Boolean set on True). The Test button is used to confirm that communication exists between the computer and the instrument. The Frame 0 is shown in Figure C.7 with both Case structures set on True.

The upper Case structure in Figure C.7 is controlled by two Booleans through an OR gate. One Boolean is the Clear button on the front panel; the other Boolean is connected to the While loop containing the main VI. When on True, the Case writes zero in four global variables corresponding to the waveforms to be acquired from the four oscilloscope channels: Waveform 1, 2, 3 and 4.

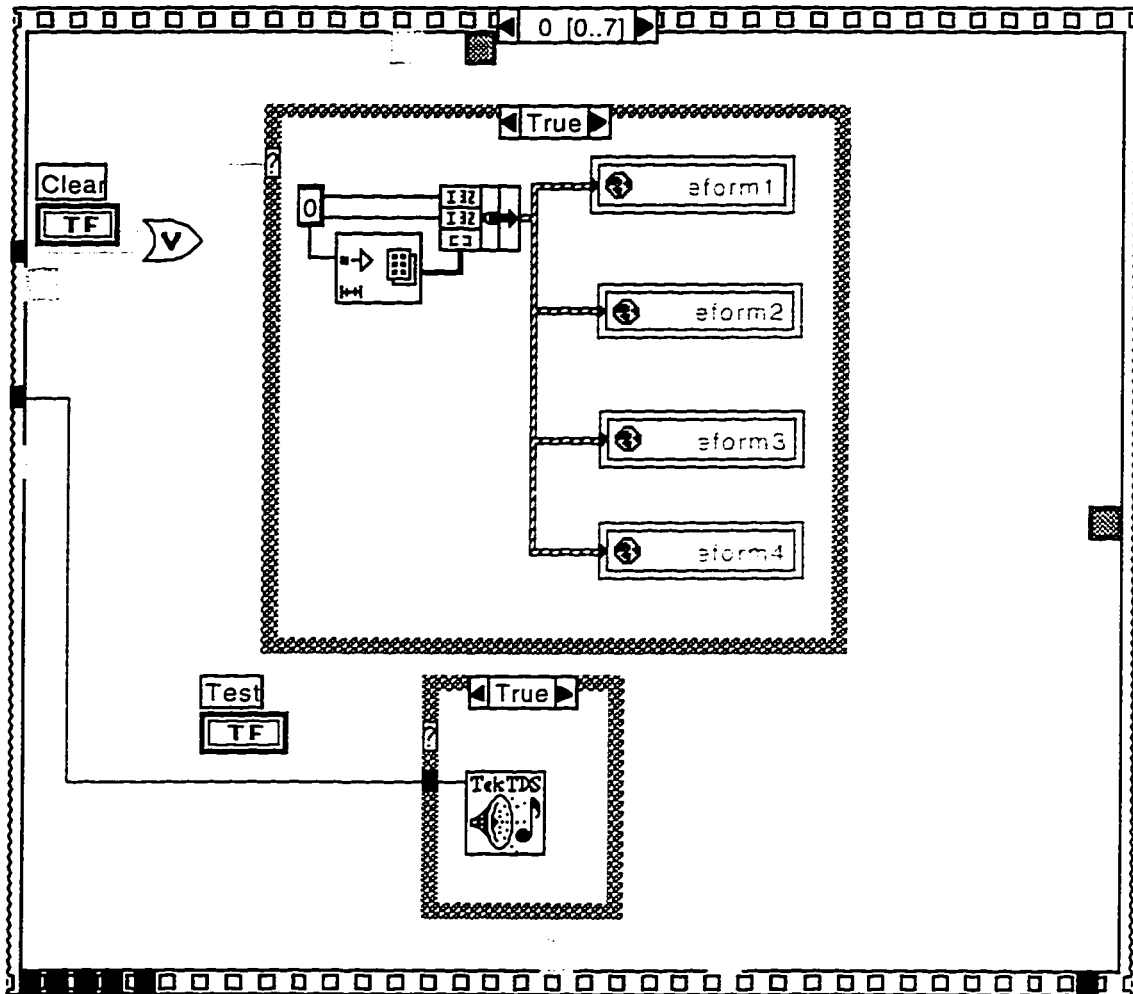


Figure C.7 Data Acquisition: Frame 0 with True set Case structures.

The first time the main VI is run, the True is passed into the loop and the case is executed which clears the front panel and the variables. At the end of the first execution of the While loop, on the right hand side (see Figure 5.4), a False Boolean is passed into the shift register. This makes the variable False so that the only way to execute the Case structure (i.e. to write 0 in all variables) is by pressing the Clear button on the

front panel by mouse-click. The shift register works as an auto-clear the first time the VI is run, to delete the data that was in the global variables (i.e. waveform 1 to 4) from the last time it was run. The shift register has to be set to False at the right side of the While loop, or else it would always pass a True back to the left side and always execute the clear. When these two Case structures are False, they are empty and no action takes place.

Frame 1 of the Sequence structure in the main VI is the part of the program responsible for the data acquisition from channel 1 of the oscilloscope. Again in the frame there are Case sequences executing subprograms according to the controllers wired to their frame. The largest Case structure in this Frame, as shown in Figure C.8, is controlled by the Channel 1 Boolean switch available on the front panel. If the Read button (see Figure C.2) is pushed, i.e. True on the block diagram, the Tek TDS Read Data.VI reads the entire waveform from the channel 1 of the oscilloscope. The Volts/div constant set for the oscilloscope is read and displayed on the front panel in the group of controls and indicators corresponding to channel 1. From the “waveform out” output of the subVI the initial time “t(0)” and the time step “delta t” are extracted by the function “Unbundle by name”, to be displayed on the front panel of the main VI. The Frame 1 is shown in Figure C.8 with the Boolean Case structures set on values corresponding to acquiring data. The second largest Case structure in Figure C.8 is controlled by the value of delta t. If delta t is non-zero, the Case structure executes which means writing the acquired array in the global variable “waveform 1”, displaying the initial time and the time step. Depending on the probe type employed and selected on the front panel, the user will choose a probe constant from a pop-up dialog box.

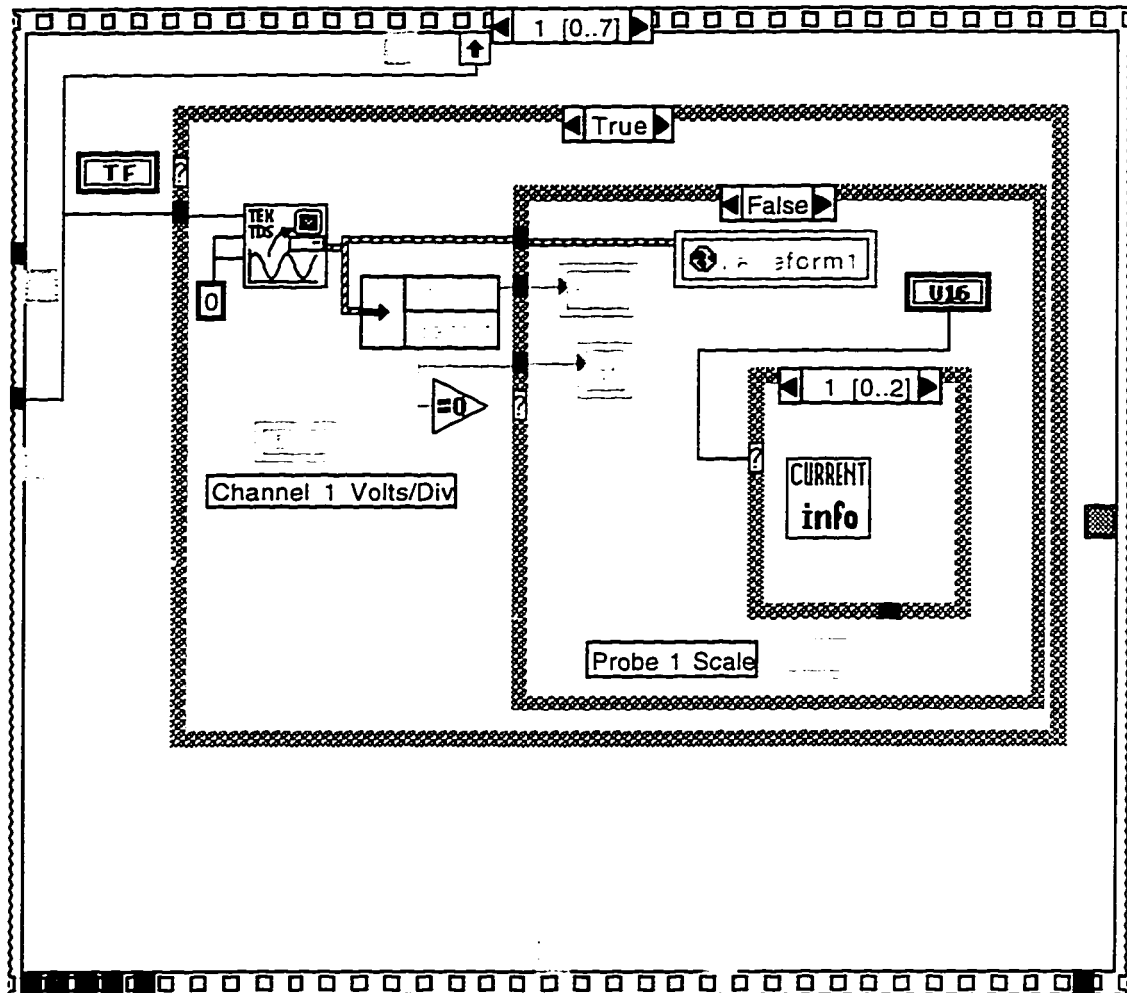


Figure C.8 Frame 1: channel 1 data acquisition and constants display.

An alternative to using Case structures occurs when numeric controls are used instead of Boolean controls. This is the case in choosing the probe type. The program provides three options: standard probe, when the probe scale is 1. current probe and voltage probe, each one with a number of probe-constant values to select from. as illustrated in the next few paragraphs.

When the control of the largest Case structure in Figure C.8 is set on False. i.e. the Read button for channel 1 was not pushed on the front panel, the Case is empty and no data is acquired. The same effect will have $\Delta t = 0$ for the smaller Boolean Case structure. Figure C.9 shows the “inner” numerical Case structure of Figure C.8 for the standard probe and the voltage probe selections.

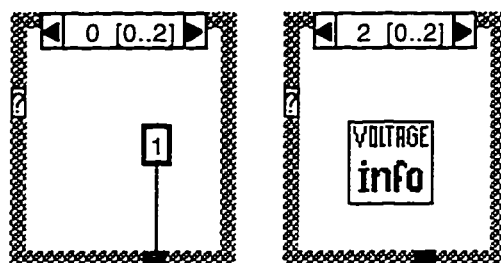


Figure C.9 Standard probe and voltage probe Case structure in Figure C.8.

Data acquisition from channel 2, 3 and 4 of the Tektronix TDS 420 oscilloscope is performed in a similar mode as presented above, with the difference that, at the waveform source input of the Tek TDS Read Data.VI the numerical value of 1, 2 respectively 3 are wired. The corresponding frames (Frame 1, Frame 2 and Frame 3) of the main program are very similar in appearance and functionality to Frame 0 and are not described separately. Appendix D contains the entire code with all the details regarding the block diagram of the of the virtual instrument.

Frame 5 contains the part of the program that sets the parameters for the Graph, plots the acquired waveforms on the front panel of the virtual instrument and selects the waveform for harmonic analysis. The block diagram is reproduced in Figure C.10 below.

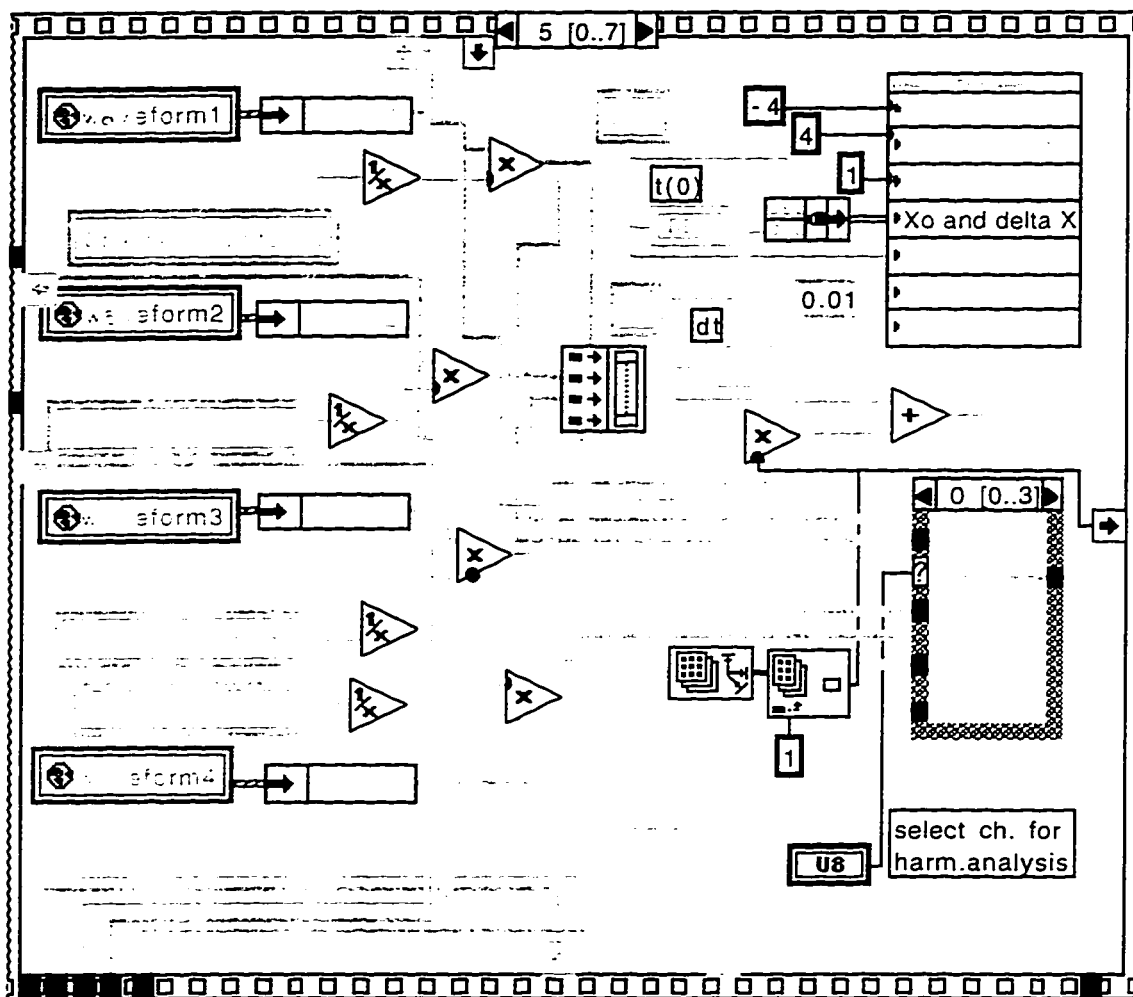


Figure C.10 Frame 5: Writing data to the Graph.

Considering the global variable Waveform 1 (Figure C.10). the array 1 is “extracted” using the function Unbundle by Name. After being divided by the Volts/div scale, the array becomes one of the inputs of the central node of the frame. This is a Bundle Array function which has also array 2, array 3 and array 4 as inputs.

corresponding to the other three channels of the oscilloscope. The Bundle Array function concatenates the inputs in top-to-bottom order and applies the resulting array to the Graph which is represented in the block diagram by the node [EXT] (see Figure C.10, center-bottom). The same resulting array containing all acquired waveforms is used for obtaining the dimension of the arrays.

The Graph's parameters are defined by its Attribute Node (Figure C.10, upper right-hand side). This node sets the maximum, the minimum and the increment values for the vertical axis --Y as well as the horizontal (time) axis --X, the initial time and the time increment. There is no visible link between the attribute node and the graph on the block diagram. However, the link is highlighted when one selects the "show attribute node" option from the pop-up menu of the graph in the block diagram. The numerical case structure in the Frame 5 selects one channel for harmonic analysis. The control associated with this structure resides on the front panel of the harmonic analyzer (see next section).

The arrows at the edge of the frame in Figure C.10 are connectors linking variables to other frames. The sense of the arrows indicate the data flow direction. In Frame 5 the arrays corresponding to all acquired waveforms are passed to Frame 6 for data saving. Current and voltage data points are also passed to the power calculation program.

Frame 6 contains the main Boolean case structure controlled by the Save button on the front panel (see Figures C.2). When this button is pushed (i.e. True in the block diagram of Figure C.11), the waveform arrays are multiplied by the probe constants and a new array is built and passed to the "inner" Sequence Structure. As

emphasized in the discussion above, this type of structure is used to impose a certain order in the data flow (i.e. to sequence the program execution).

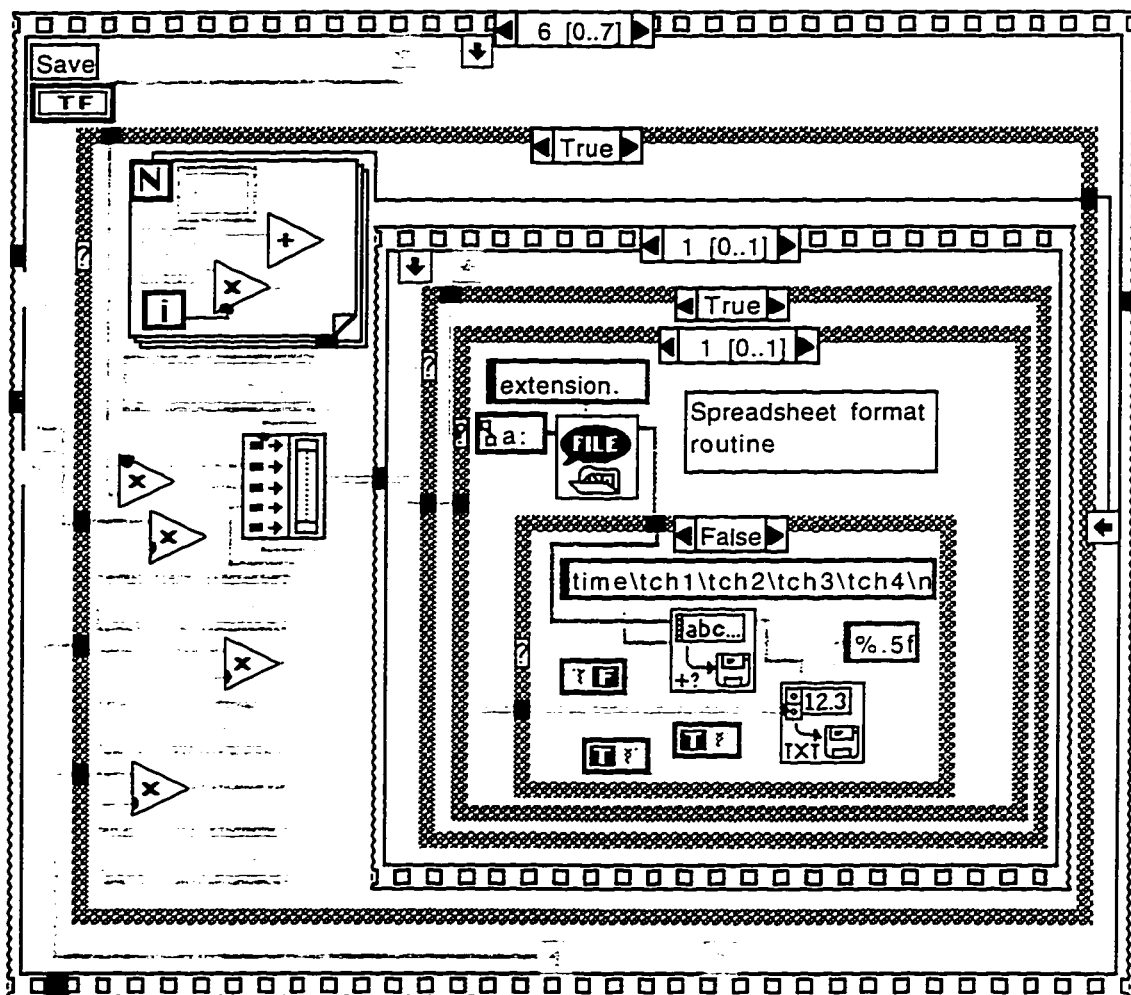


Figure C.11 Frame 6: Save Data subroutine- Spreadsheet format.

The first frame of the sequence contains a subVI which prompts the user to select a type of file for data saving. Figure C.12 illustrates the front panel for this

routine. The option presented saves data in spreadsheet format. The block diagram of the Choose File Type.VI and the subVI seen as a building block in the main program are given in Figure C.13 . The file type and the OK control signals are passed to the Sequence 1 as illustrated in Figure C.11.

As long as the OK command is not given, the Case is empty and no action occurs regarding data saving. When OK is selected, the Boolean is set on True and the outermost Case structure is executed. First the user is prompted for file name and file path and if the choice is not canceled (i.e. a Boolean on False is sent by the File Dialog function), the data is written to file. When the innermost Case structure executes, a file is created, the data is written and the file is closed. The data stored on disk can be used for analysis using other software applications.

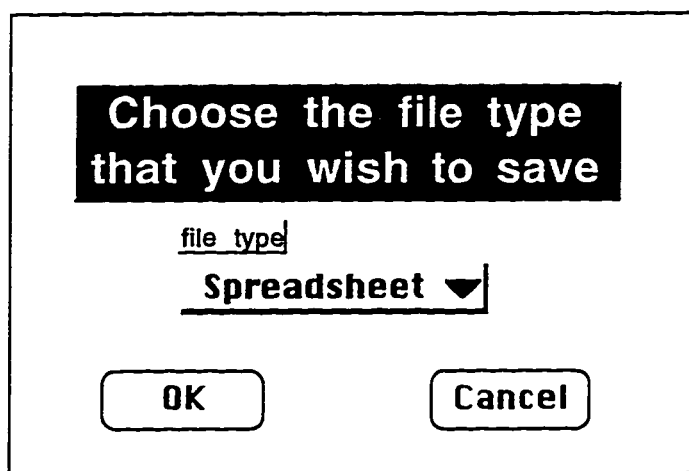
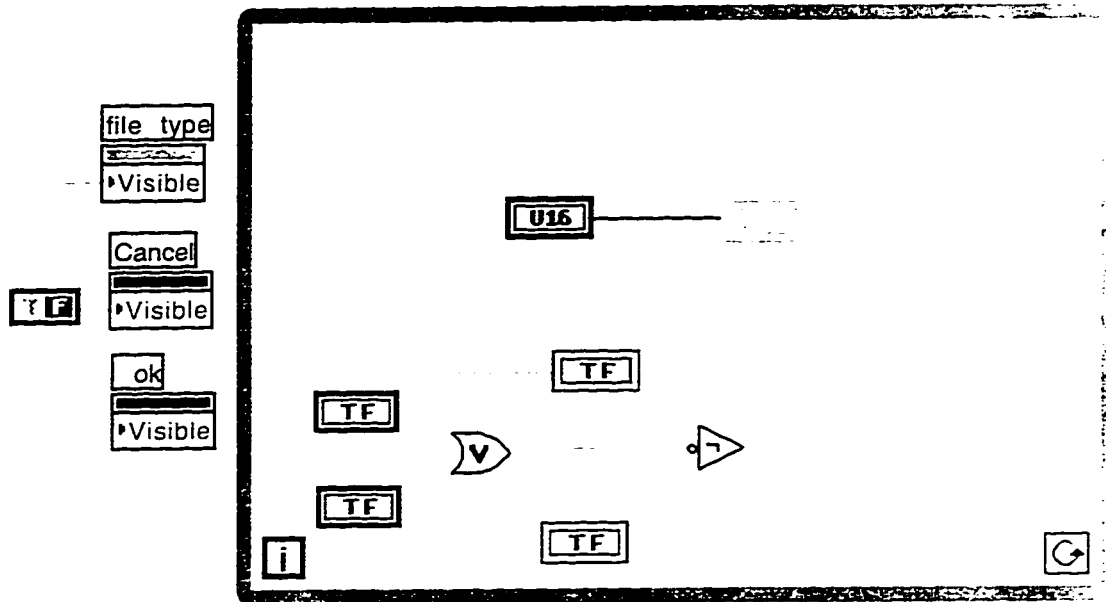
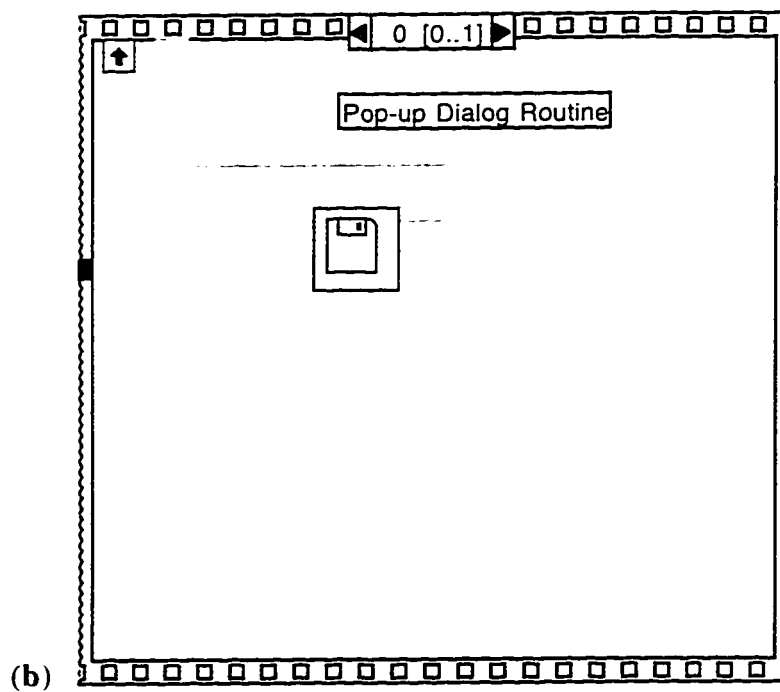


Figure C.12 Front panel for ChooseFileType.VI



(a)



(b)

Figure C.13 Choose File Type.VI : (a) block diagram. (b) subroutine in the main program.

Additional sequences (frames) can be added to the main program for other operations such as a printing subroutine.

C.3 Harmonic Analyzer Front Panel

The harmonic analyzer is a distinctive part of the main virtual instrument developed in this thesis. On the front panel, a numerical ring allows the user to select one of the four acquired signals for harmonic analysis. The analysis subVI plots the harmonic spectrum on the chart and indicators give calculated values for the total harmonic distortion factor relative to the fundamental (THD-F) and relative to the total rms (THD-R). Other front-panel indicators give the calculated value of the current distortion factor (CDF) as well as the power calculations and the quality factors (Figure C.14). The harmonic amplitudes of the signal are listed in the ring indicator beside the chart. This list is resizable with the sizing tool from the tool palette. The index in LabVIEW starts from zero and consequently to view, for example, the 5th harmonic at the top of the harmonic amplitude list, the index has to be set on 4.

The oscilloscope, set to acquire 5000 data points in 100 divisions in 0.2s. sets the time increment to $\delta t=40\mu s$. This causes the harmonics spectrum to be plotted for a frequency of 12.5 kHz. The circuits investigated in the next chapters have low frequency harmonics which are not relevant for frequencies larger than 1.2 kHz. For this reason, using the labeling tool, the frequency range of the harmonic spectrum display is set to 1.2 kHz in most cases. This covers the first 20 harmonics of a 60 Hz signal. Calculation requirements are written as warning labels on the front panel using the labeling tool.

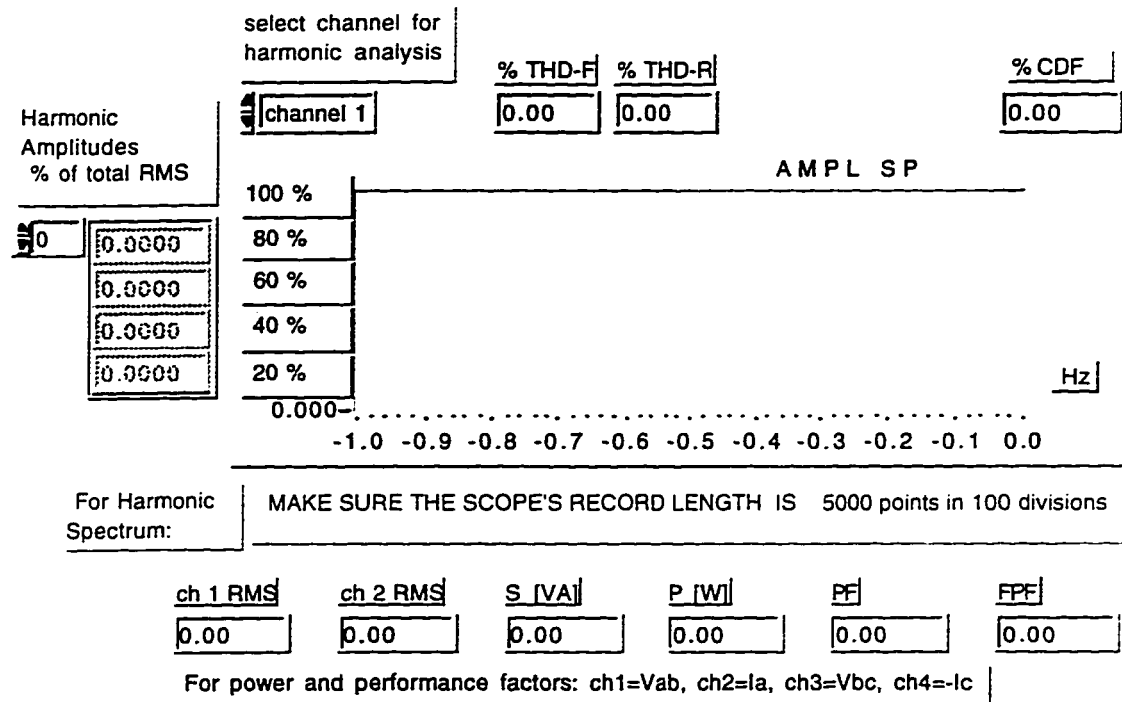


Figure C.14 Front panel: Harmonic analyzer, power calculations and performance factors.

C.4 Harmonic Analyzer Block Diagram

The code of the harmonic analyzer is included in the same main While Loop with the data acquisition block diagram. The array containing the data from a selected channel is the input for the Amplitude Spectrum.VI. This VI, available as a library function in LabVIEW 4, computes the Real Fast Fourier Transform (FFT) or the

Discrete Fast Fourier Transform. If the size of the sequence is a multiple of 2, the VI performs a FFT, otherwise the DFT is performed. The Amplitude Spectrum.VI is provided in the library: Measurement<Analysis<Functions accessible from the function palette. The amplitude spectrum is plotted in frequency domain on the front panel. The entire block diagram of the harmonic analyzer is shown in Figure C.15. This particular subprogram was created for a fixed setup of the Tektronix TDS 420 oscilloscope as described in the previous section. A more flexible virtual instrument could not be implemented at this stage because of memory management limitations of the Power Macintosh computer and bugs in the THD.VI provided in the above mentioned library (in the Advanced Measurements sub-palette). Recommendations for further developments are given in the last chapter of this work.

The Total Harmonic Distortion (THD) is calculated regarding both the total rms (THD-R) and relative to the fundamental (THD-F). The program also calculates the Current Distortion Factor (CDF).

A useful property of LabVIEW is the possibility to write mathematical formulas in a Formula Node. The Formula Node is a resizable box similar to the four structures (Sequence Structure, Case Structure, For Loop and While Loop). Instead of containing a subdiagram, the Formula Node contains one or more formula statements delimited by semicolon. Formula statements use a syntax similar to the most text-based programming languages for arithmetic expressions. The expression of the CDF is written in the formula node case in a Case structure (Figure C.15) [39],[40],[41].

and placing the editing tool on the block (function) in the program. In many cases the Simple Help offers examples of function implementation for more clarity.

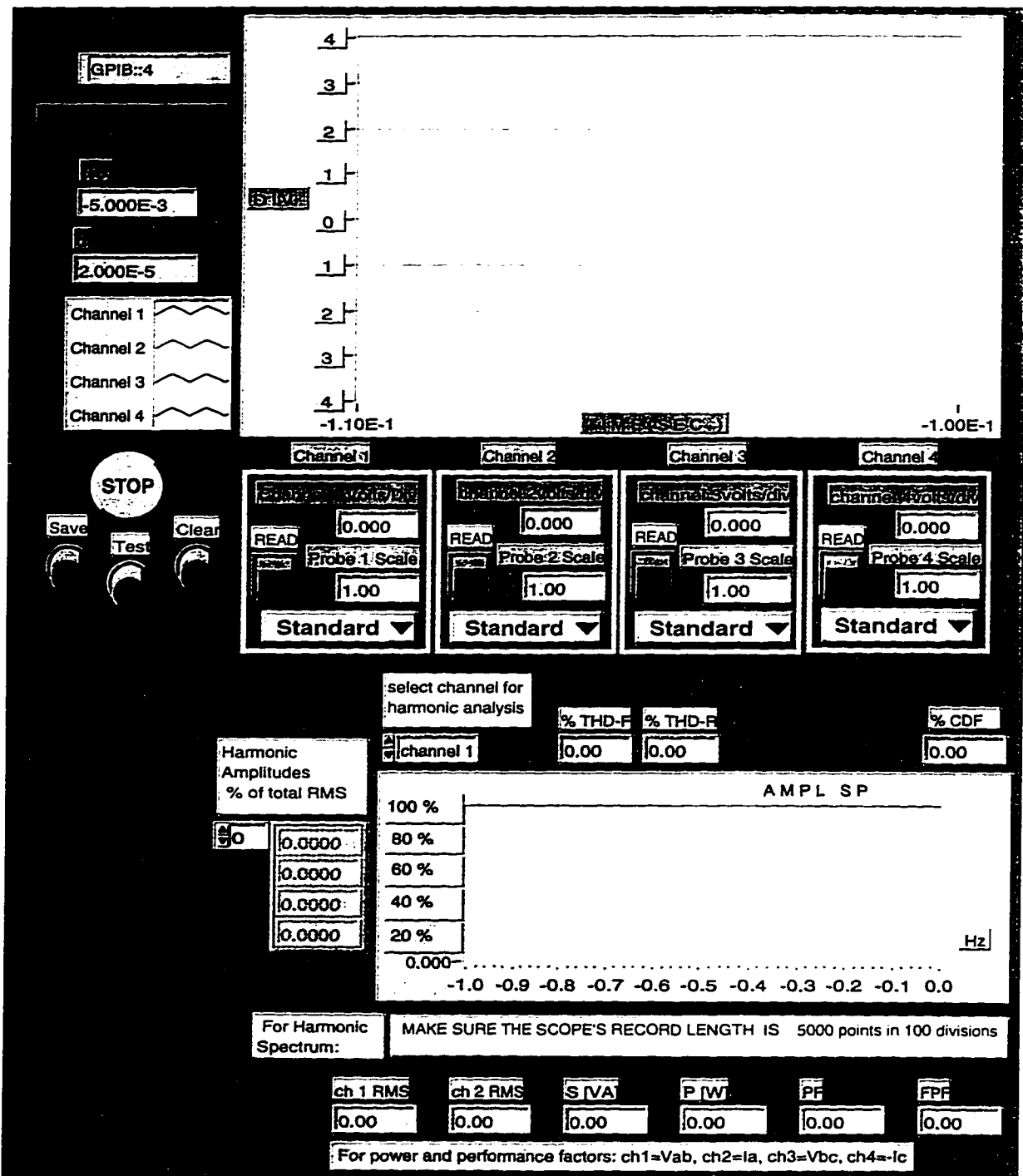
The power and power factors calculations are performed for a given set-up of the acquired signals. The method of two wattmeters for three phase power calculations employs two currents and two voltages (see Chapter 5). The virtual instrument performs correct calculations under the following conditions: the oscilloscope channels have to be assigned as ch1: v_{ab} , ch2: i_a , ch3: v_{bc} and ch4: $-i_c$ considering the three phases labeled a, b and c, and positive current entering the circuit. The oscilloscope acquired signals are in mV and, prior to calculations, each array is multiplied by the corresponding probe scale constant which is a local variable in the acquisition subprogram. The line current and line-line voltage rms calculations as well as power and power factors calculations are suggestively depicted in the general block diagram (see Figure 5.4).

This Appendix described in detail the LabVIEW program for data acquisition and analysis. The features provided on the front panel of the virtual instrument (the user interface) were explained in correlation with their role in the block-diagram (the actual code). The discussion outlined the data flow character of the LabVIEW program and the sequence structure employed for data flow control. The performance of the developed DAQ system is illustrated in Chapters 6,7 and 8. Waveform acquisitions, harmonic analysis, power and performance factors calculations are performed from a selected number of power electronic circuits including rectifiers, induction motor variable speed drives and research level circuits for harmonic control. Appendix D lists the entire LabVIEW program developed in this work.

Appendix D

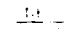


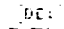

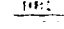
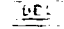
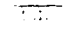
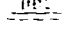
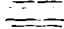
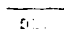
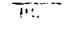

Virtual Instrument documentation

Front Panel

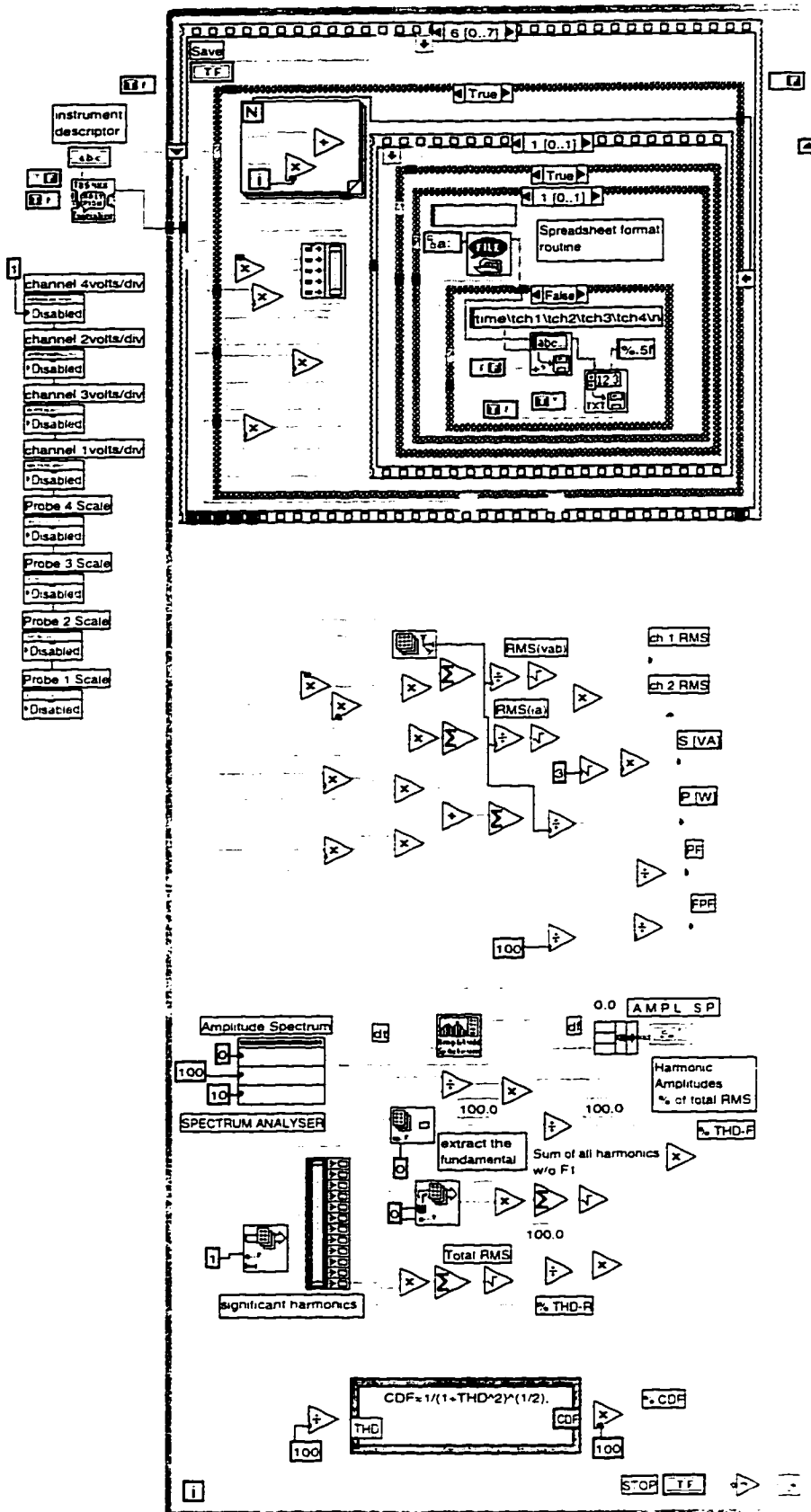


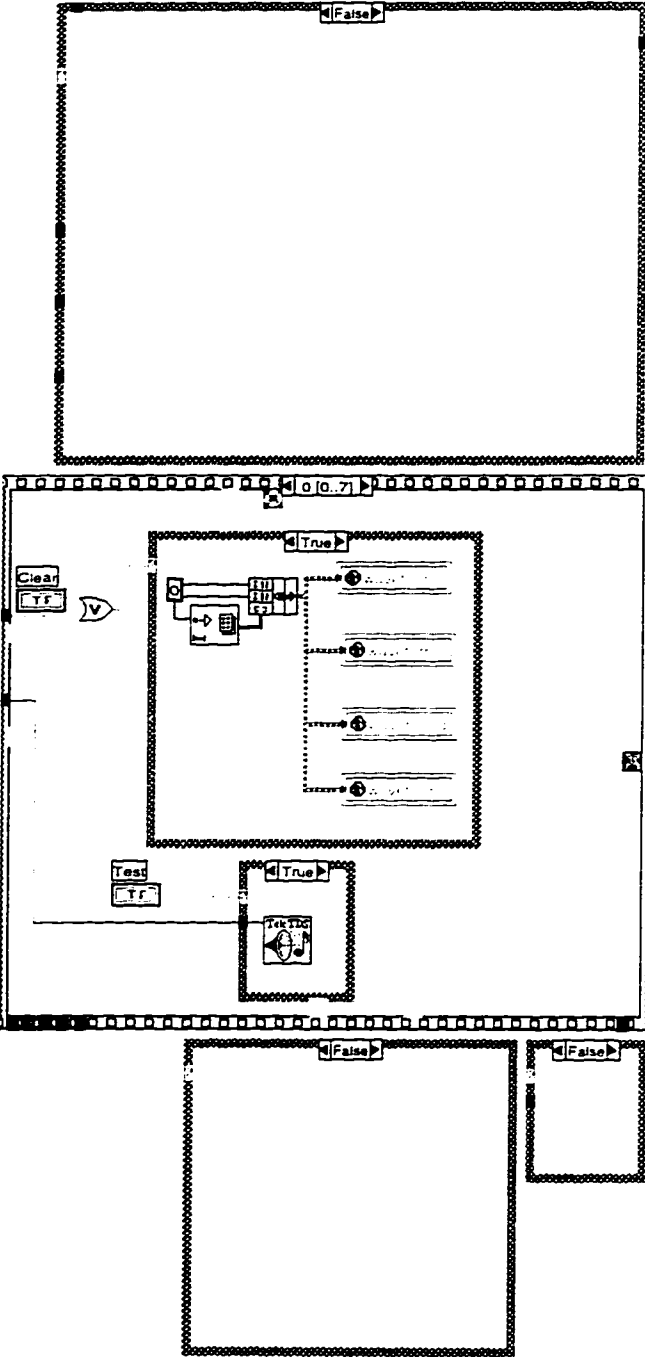
Controls and Indicators

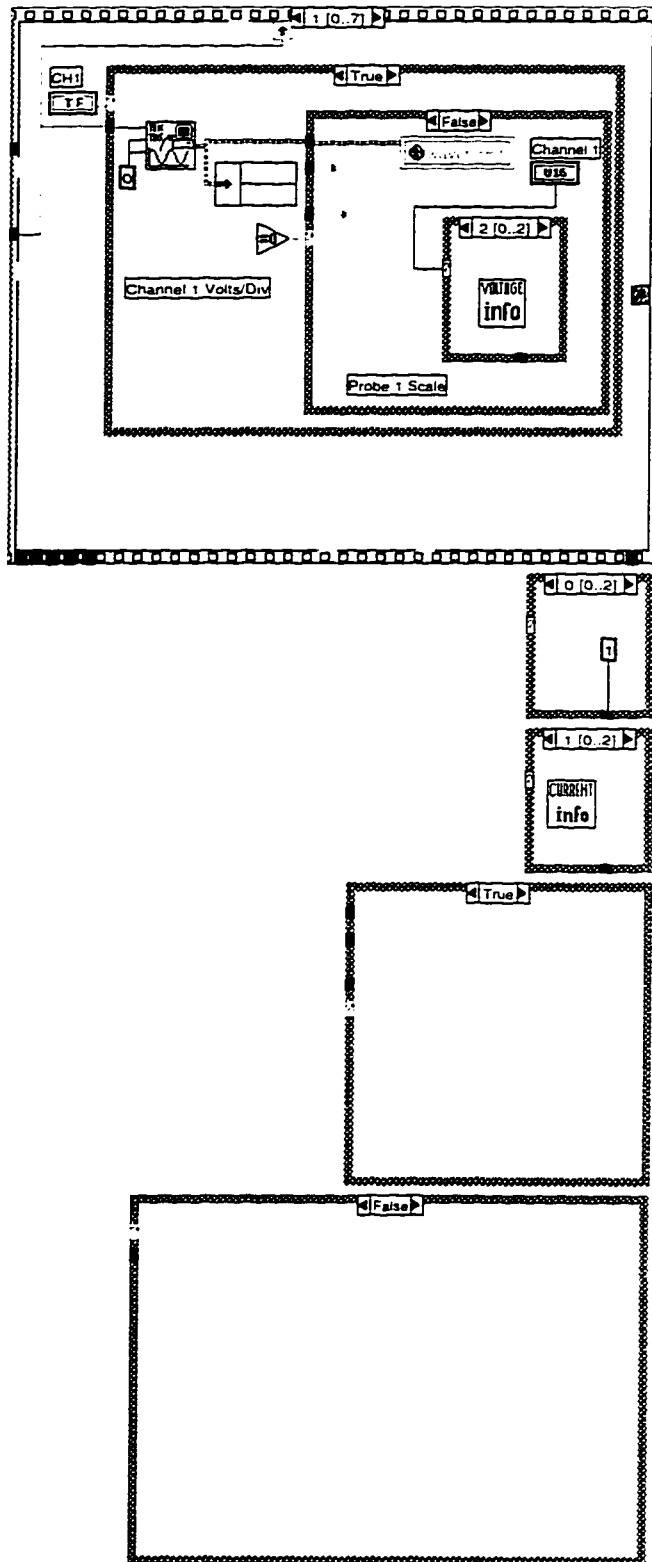
- TF** CH1
Press to READ Channel 1. This will also cause prompt for scale information if anything other than a standard probe is being used
- TF** CH 2
Press to READ Channel 2. This will also cause prompt for scale information if anything other than a standard probe is being used
- TF** CH 3
Press to READ Channel 3. This will also cause prompt for scale information if anything other than a standard probe is being used
- TF** CH 4
Press to READ Channel 4. This will also cause prompt for scale information if anything other than a standard probe is being used
- TF** stop
Press this button to end the communication session with the Tektronix Oscilloscope.
- TF** Clear
Press this button to clear the graph.
- TF** Save
Press this button to save the waveforms on the computer screen. You will be prompted for a file format (either Matlab or Spreadsheet) and a file path and name. The spreadsheet format saves the data in tab-delimited columns. The Matlab format saves the data in an array called TDS420A. All four channels plus the time array are saved.
- U16** Channel 1
Choose the type of probe being used on Channel 1. A 10X probe is considered a standard probe. A current probe measures current only, and the voltage probe is for high voltage only.
- U16** Channel 2
Choose the type of probe being used on Channel 2. A 10X probe is considered a standard probe. A current probe measures current only, and the voltage probe is for high voltage only.
- U16** Channel 3
Choose the type of probe being used on Channel 3. A 10X probe is considered a standard probe. A current probe measures current only, and the voltage probe is for high voltage only.
- U16** Channel 4
Choose the type of probe being used on Channel 4. A 10X probe is considered a standard probe. A current probe measures current only, and the voltage probe is for high voltage only.
- TF** Test
This button will tests whether or not there is communication between the computer and oscilloscope. If the connection is correct, the oscilloscope will beep when the button is pressed. If no sound is heard, then the computer and oscilloscope are not communicating properly.
- abc** instrument descriptor
- U5** select channel for harmonic analysis
This ring sets the oscilloscope channel for harmonic analysis.
- This graph will plot the channels that have been read. The display should look exactly as it does on the oscilloscope. Probe scaling information is not reflected on the graph, but only when data is saved to file.
- Channel 1 Volts/Div
This displays the Volts/Div for Channel 1.
- channel 2volts/div
This displays the Volts/Div for Channel 2.
- channel 3volts/div
This displays the Volts/Div for Channel 3.
- channel 4volts/div
This displays the Volts/Div for Channel 4.
- t(O)
This value is the intial acquired point t(0)
- dt
This is the time increment value from one point to the next.
- Probe 1 Scale
This displays the scaling factor from the probe being used for Channel 1. A standard probe has a factor of 1. Choosing a probe other than standard will prompt the user for scale information.
- Probe 2 Scale
This displays the scaling factor from the probe being used for Channel 2. A standard probe has a factor of 1. Choosing a probe other than standard will prompt the user for scale information.
- Probe 3 Scale
This displays the scaling factor from the probe being used for Channel 3. A standard probe has a factor of 1. Choosing a probe other than standard will prompt the user for scale information.

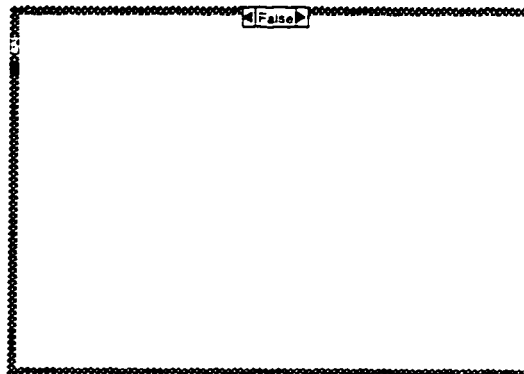
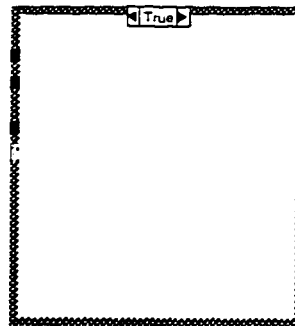
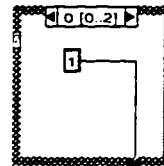
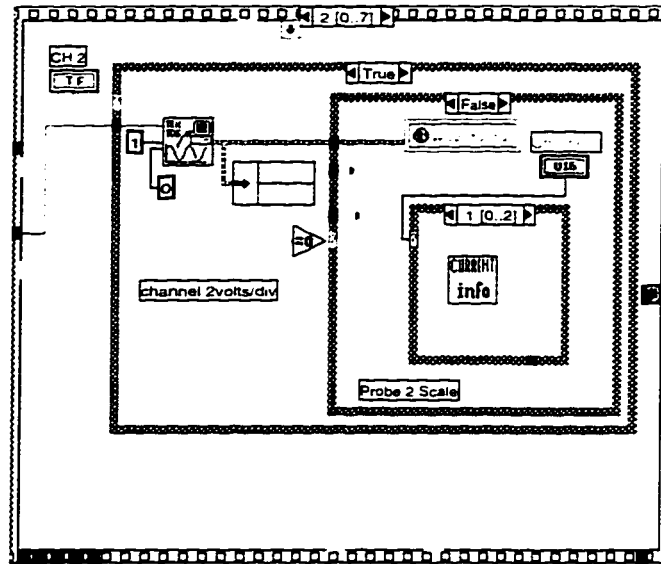
	Probe 4 Scale This displays the scaling factor from the probe being used for Channel 4. A standard probe has a factor of 1. Choosing a probe other than standard will prompt the user for scale information.
	A M P L S P This plot gives the harmonic spectrum of the chosen signal. The frequency range can be changed with the Labeling tool
	% THD-F % THD-F is the percent Total Harmonic Distortion relative to the fundamental.
	Harmonic Amplitudes % of total RMS Ring indicator of harmonic amplitudes. Index=0 : fundamental Index=1 : 2nd harmonic etc.
	Harmonic Ampe's
	% CDF indicates the CDF-R or CDF-F, function of the selection switch.
	% THD-R gives the Total Harmonic Distortion relative to the total RMS.
	PF
	P [W]
	S [VA]
	ch 2 RMS
	ch 1 RMS
	FPF

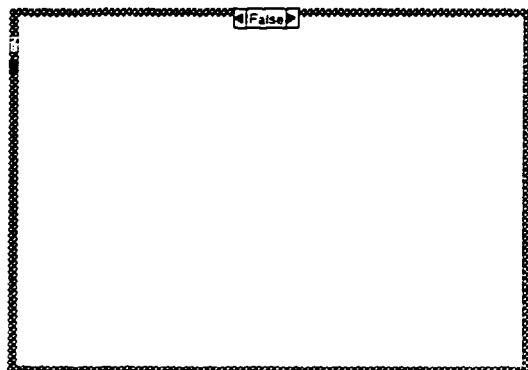
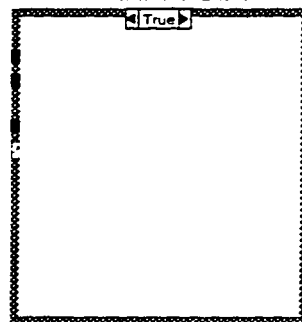
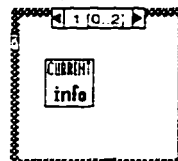
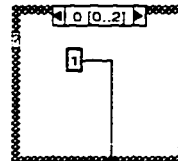
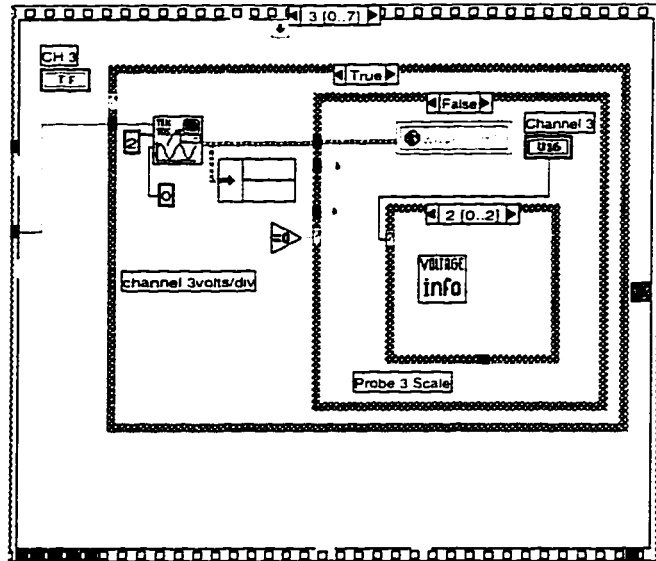
Block Diagram

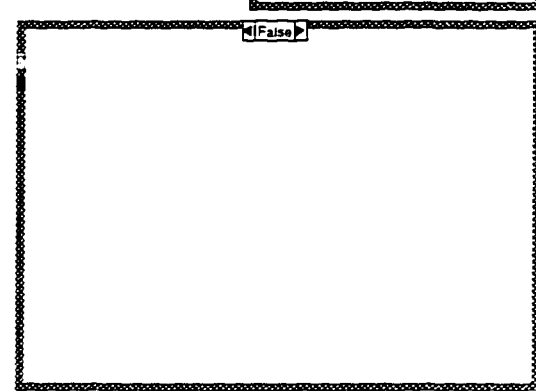
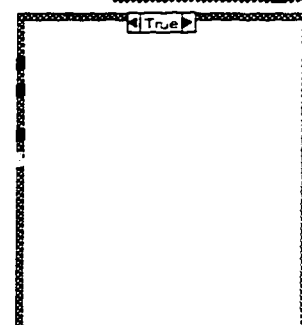
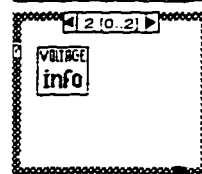
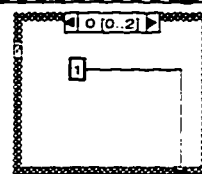
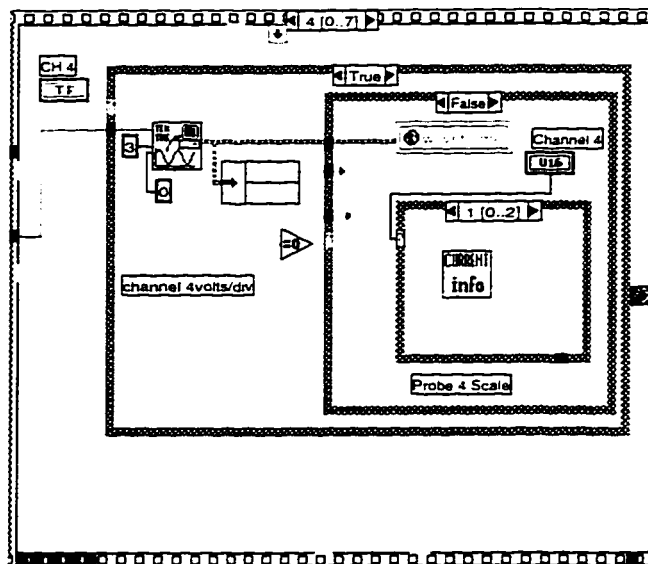


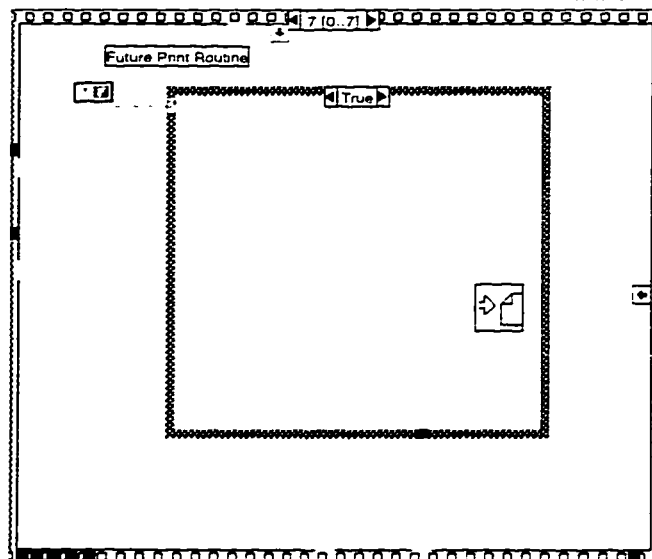
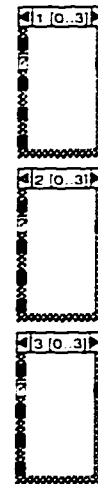
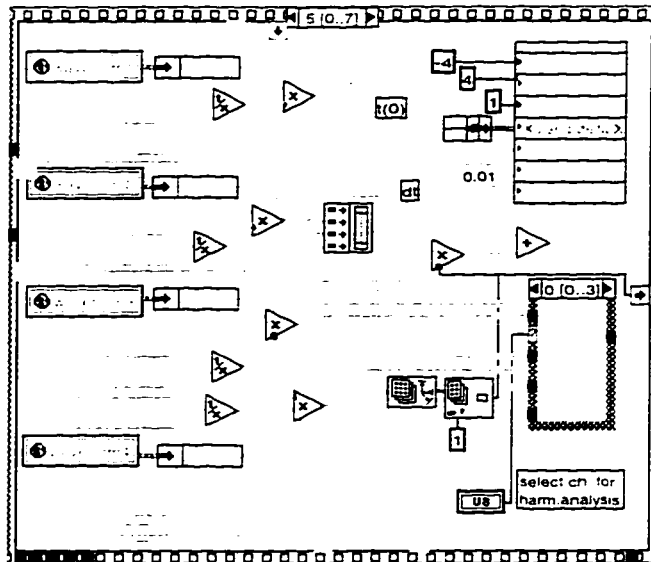


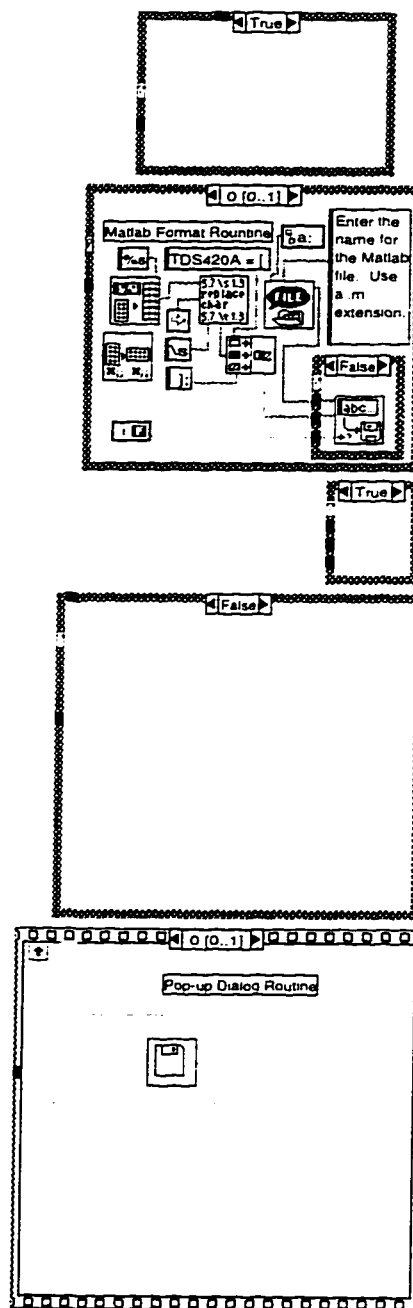


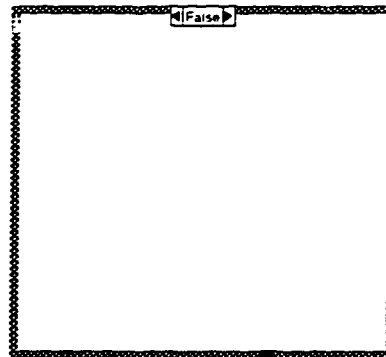






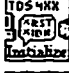

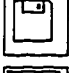
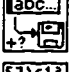














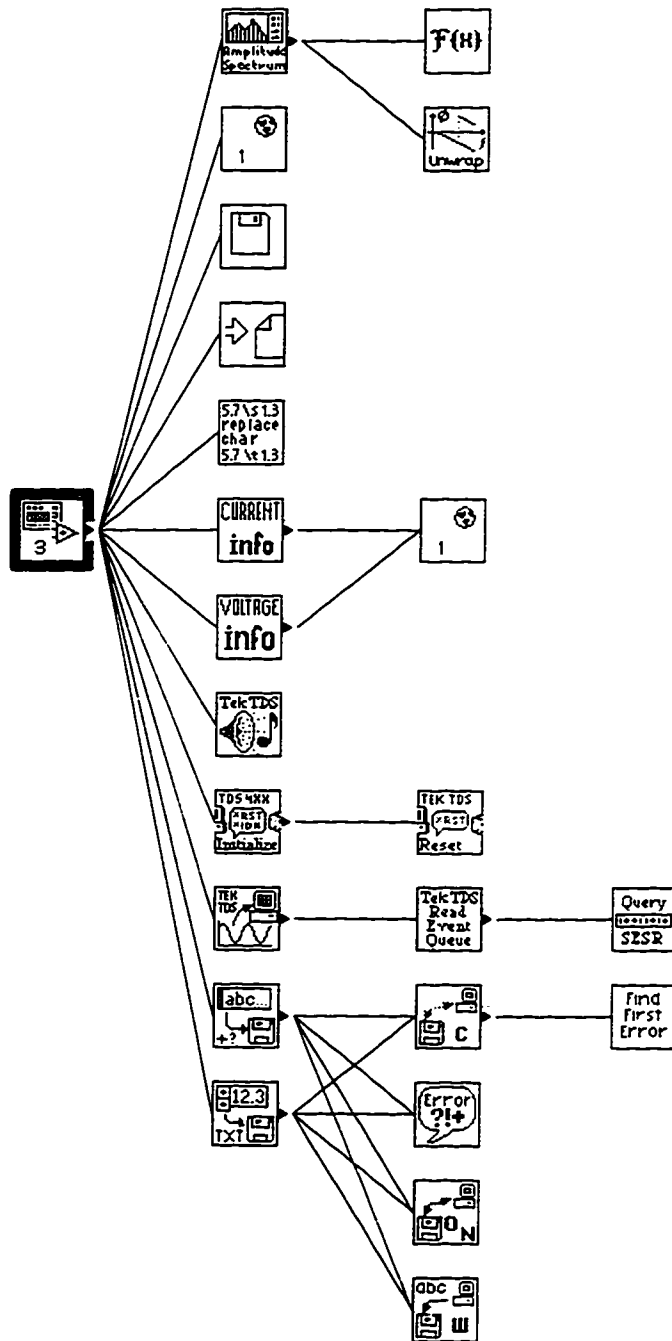
 List of SubVIs

	Tek TDS Read data.vi Babylon 5:applications:LabVIEW4:user.lib:Tek TDS Read data.vi
	array.glb Babylon 5:applications:LabVIEW4:user.lib:array.glb
	Tek TDS 4XX Initialize.vi Babylon 5:applications:LabVIEW4:project:TKTDS4XX.LLB:Tek TDS 4XX Initialize.vi
	Voltage Probe Babylon 5:applications:LabVIEW4:user.lib:Voltage Probe
	Choose File Type Babylon 5:applications:LabVIEW4:user.lib:Choose File Type
	Write Characters To File.vi Babylon 5:applications:LabVIEW4:vi.lib:UTILITY:FILE.LLB:Write Characters To File.vi
	Search String and Replace.vi Babylon 5:applications:LabVIEW4:examples:general:strings.lib:Search String and Replace.vi
	Tek TDS Audio Alert.vi Babylon 5:applications:LabVIEW4:project:TKTDS4XX.LLB:Tek TDS Audio Alert.vi
	print waveforms.vi Babylon 5:applications:LabVIEW4:user.lib:print waveforms.vi
	Write To Spreadsheet File.vi Babylon 5:applications:LabVIEW4:vi.lib:UTILITY:FILE.LLB:Write To Spreadsheet File.vi
	Amplitude and Phase Spectrum.vi Babylon 5:applications:LabVIEW4:vi.lib:Analysis:0measdsp.lib:Amplitude and Phase Spectrum.vi
	Hall Current Probe.vi Babylon 5:applications:LabVIEW4:project:Hall Current Probe.vi

 Connector Pane


TDS420/SpAn/THD/P/S/PF/FPF

Position in Hierarchy



Appendix E

Electrical Machines Nameplate Data:

1) Squirrel Cage Induction Machine:

Power:	7.5 HP
Speed:	1170 rpm
Nominal Voltage:	208 V
Nominal Current:	22 A
Number of phases:	3
Supply Frequency:	60 Hz

2) Direct Current Machine:

Power:	24 HP
Speed:	1725 rpm
Nominal Voltage:	230 V
Nominal Current:	13.5 A